CHARACTERIZATION OF RODESSA FORMATION RESERVOIR (LOWER CRETACEOUS) IN VAN FIELD, VAN ZANDT COUNTY, TEXAS

A Thesis

by

YANYAN TRIYANA

Submitted to the Office of Graduate Studies of
Texas A&M University
in partial fulfillment of the requirements for the degree of

MASTER OF SCIENCE

May 2003

Major Subject: Geology

CHARACTERIZATION OF RODESSA FORMATION RESERVOIR

(LOWER CRETACEOUS) IN VAN FIELD, VAN ZANDT COUNTY, TEXAS

A Thesis

by

YANYAN TRIYANA

Submitted to Texas A&M University
in partial fulfillment of the requirements
for the degree of

MASTER OF SCIENCE

Approved as to style and content by:

Wayne M. Ahr (Chair of Committee)	Jerry L. Jensen (Member)
Robert R. Berg (Member)	Andrew Hajash Jr (Head of Department)

May 2003

Major Subject: Geology

ABSTRACT

Characterization of Rodessa Formation Reservoir (Lower Cretaceous)

in Van Field, Van Zandt County, Texas. (May 2003)

Yanyan Triyana, B.S., Padjadjaran University, Bandung, Indonesia

Chair of Advisory Committee: Dr. Wayne M. Ahr

The Rodessa Formation is one of the major oil and gas reservoirs in the East Texas Basin. In Van Field, the upper Rodessa Formation consists of interbedded biotic and abiotic mudstones to grainstones. The lower Rodessa is composed of interbedded sandstones, shales, and limestones called the Carlisle Member. Based on core and well log interpretation, the Rodessa Formation was deposited on a broad, restricted, shallow marine platform interpreted to be lagoonal, subtidal, and intertidal.

Both Rodessa limestone and sandstone have been altered significantly by diagenetic processes that include micritization, cementation, dissolution, neomorphism and compaction. Dissolution is the main factor that resulted in enhanced porosity and permeability while cementation adversely affected porosity. Diagenesis is interpreted to have begun in the marine phreatic environment and continued through the freshwater phreatic and shallow burial environments.

Two reservoir units have been identified from core and well log interpretations. The potential reservoir within the Rodessa Formation occurs in the Carlisle Member

which is composed mainly of medium to coarse grained sandstone with porosities and permeabilities in ranges of 8 to 11 percent and 46 to 896 millidarcies, respectively. The water saturation analysis has also shown the reservoir to be hydrocarbon bearing, having water saturation below 46 percent.

This thesis is dedicated to my mom in heaven,

Mom, you always be here in my heart

ACKNOWLEDGEMENTS

I would like to express my sincere appreciation and gratitude to Dr. Wayne M. Ahr, chair of my advisory committee, for his support, patience, guidance, constructive criticism, and aggressive encouragement. I would also like to thank my committee members Dr. Jerry L. Jensen and Dr. Robert R. Berg, for their assistance and comments.

I am deeply indebted to the Unocal Gulf Region Team, especially Coleen C. Shannon, Art Saller, Vic J. Rosato, David C. Watso, Mark Andreason, and Semion Kopelev for their willingness to assist me with my data. I also want to thank the people in Unocal Indonesia, especially Yoseph J. Partono, Hans F. Schwing, Dan Maguire, Sena Reksalegora, Eko Lumadyo, and Sigit Sutiono, for their assistance in helping me obtain a scholarship.

I wish to thank my fellow graduate students, especially the “soft rock” team Matthew D. Gentry, Dylan Morgan, Mychal Murray, Femi Esan, Michael Sturdy, Tiffany L. Hopkins and Karine Schepers, for the discussions and inputs. I also want to express my deep appreciation to my friends Iwan, Munji, Maria, Fitrix, Tomo, Mursal, Ridha, Darmo, and Sigit who have made my stay in USA very enjoyable. A special thanks goes to my family members, Mamah (almh), Apa, Ade, Ida, and Aang, for their patience and understanding. A special thanks goes to someone who has always supported me. Finally, all of this could not have happened without the mercy of Allah.

TABLE OF CONTENTS

Page

Page

LIST OF TABLES

LIST OF FIGURES

Figure Page

Figure Page

Figure Page

Figure Page

INTRODUCTION

The Rodessa Formation in East Texas mainly consists of fossiliferous-fragmental to coquinoid limestone, oolitic limestone, sandy limestone, and gray shale with thin beds of anhydrite, which are confined to the upper part of the formation (Forgotson, 1957). The lower part of the formation consists of interbedded limestone and sandstone, the latter of which, according to Roberts and Lock (1988), is the main reservoir in Rodessa Field, Caddo Parish, Louisiana. Rodessa field is located near Van Field, where some operators use the name "Carlisle" as the local name of the sandstone.

Carbonate reservoirs are inherently heterogeneous because they contain a variety of textures, bedding types, and stratal architecture. Carbonate reservoirs have unique characteristics that reflect combinations of depositional and diagenetic processes. Depositional processes establish the initial pore size, porosity distribution and the geometry of individual depositional facies. Diagenetic processes modify both pore size and geometry, which in turn influence permeability. Both of them influence reservoir quality; therefore, information about depositional and diagenetic characteristics is valuable for reservoir development.

This thesis follows the style and format of the AAPG Bulletin.

Objectives

The objectives of this study are to identify, describe, map, and interpret the principal reservoir zones that produce from the Rodessa Formations in Van Field. These objectives will be accomplished using the following methods:

1. Constructing a depositional model for the Rodessa Formation based on core descriptions and borehole log interpretation
2. Determining the nature and distribution of depositional and diagenetic porosity in the reservoir
3. Characterizing the Carlisle, which is considered to be the main reservoir within the Rodessa Formation, in terms of porosity, permeability, and flow unit quality

Location

Van Field is located near the town of Van in the southeastern part of Van Zandt County, Texas, along the northwest flank of the East Texas Basin. It is located about 55 miles northeast of Powell Field in Navarro County and 45 miles northwest of Boggy Creek Field in Cherokee and Anderson counties. The location of the study area is shown in Figure 1.

Field History

Pure Oil Company discovered the Van Field area in 1929 after drilling the Jarman No. 1 discovery well (Sellers and Phillips, 1979). In January, 1929, core drilling was begun on the Van structure; the location of the tests being governed by the control

established from geological and geophysical work. The Jarman No. 1 well encountered many oil and gas shows and was completed as a commercial well in the Woodbine Formation (Upper Cretaceous) at depth of 2,710 feet on October, 1929. Van Field had produced half of billion barrels from the Woodbine before the Rodessa and Carlisle Formations were developed during the 1970's. By June, 1989, Van had produced an additional 500 million barrels of oil.

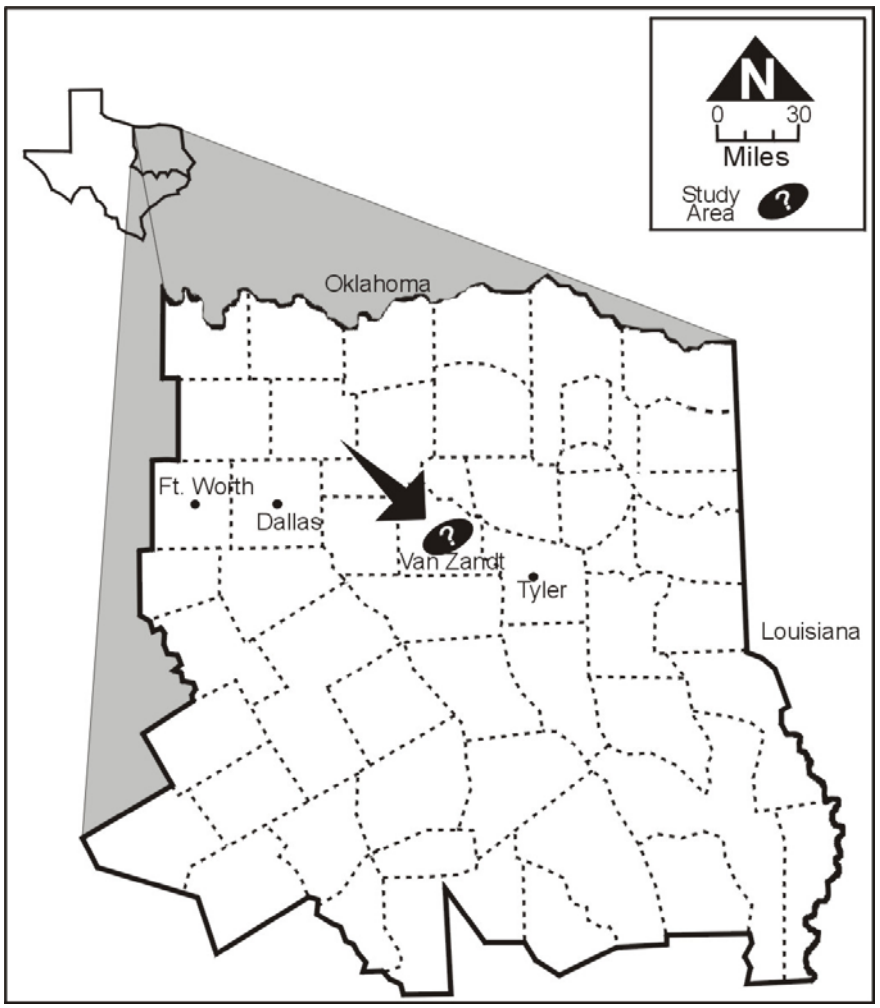

Figure 1. Location of the study area in Van Field, Van Zandt County, Texas.

Regional Geology

Regional Tectonic Framework

Van Field is located in The East Texas Basin, which formed as a failed rift during Late Triassic-Early Jurassic times (Jackson and Seni, 1983). During Middle Jurassic time, basin subsidence set the stage for a widespread restricted marine environment to develop. The Jurassic Louann salt developed in this hypersaline restricted basin and lies unconformably on Triasic rift sediments and Paleozoic basement rock. Salt thickness ranges from zero to more than 4,000 feet (Turner, 1993).

Plastic deformation of the Louann Salt was caused most of the structures to form in the study area. Jackson and Seni, 1983, stated that the Louann had developed structures that ranged from pillow to piercement domes. This process followed three stages of growth: pillow, diapir, and post diapir (Jackson and Seni, 1983). The deep-seated salt uplift formed the four-way closure in the Van Field (Lowe and Carington, 1990). The present day distribution of salt structures in the East Texas Basin is shown in Figure 2.

The East Texas Basin is bounded by the Mexia-Talco fault zone on the north and west, by the Angelina – Caldwell flexure on the south, and by the Sabine Uplift on the east (Figure 3). The Mexia – Talco fault zone consists of a series of normal faults and grabens. The northeast trending Edgewood graben fault system lies westward from the area. Faulting within the East Texas Basin has a parallel trending with those systems and the deep - seated salt feature radial fault pattern.

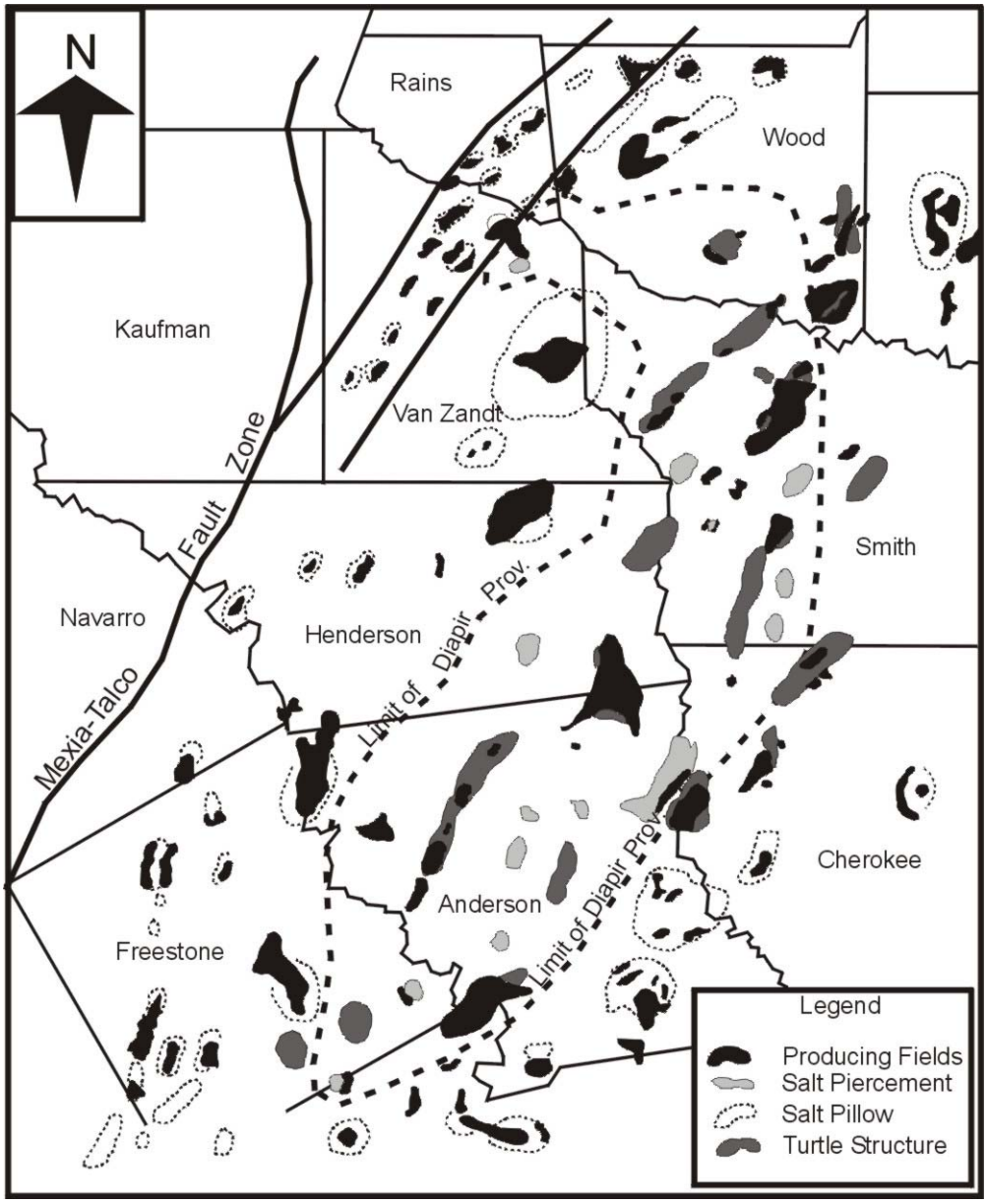

Figure 2. Map showing the distribution of salt structures and the major producing fields in the East Texas Basin (modified from Wescott and Hood, 1994, and Lowe and Carington, 1990).

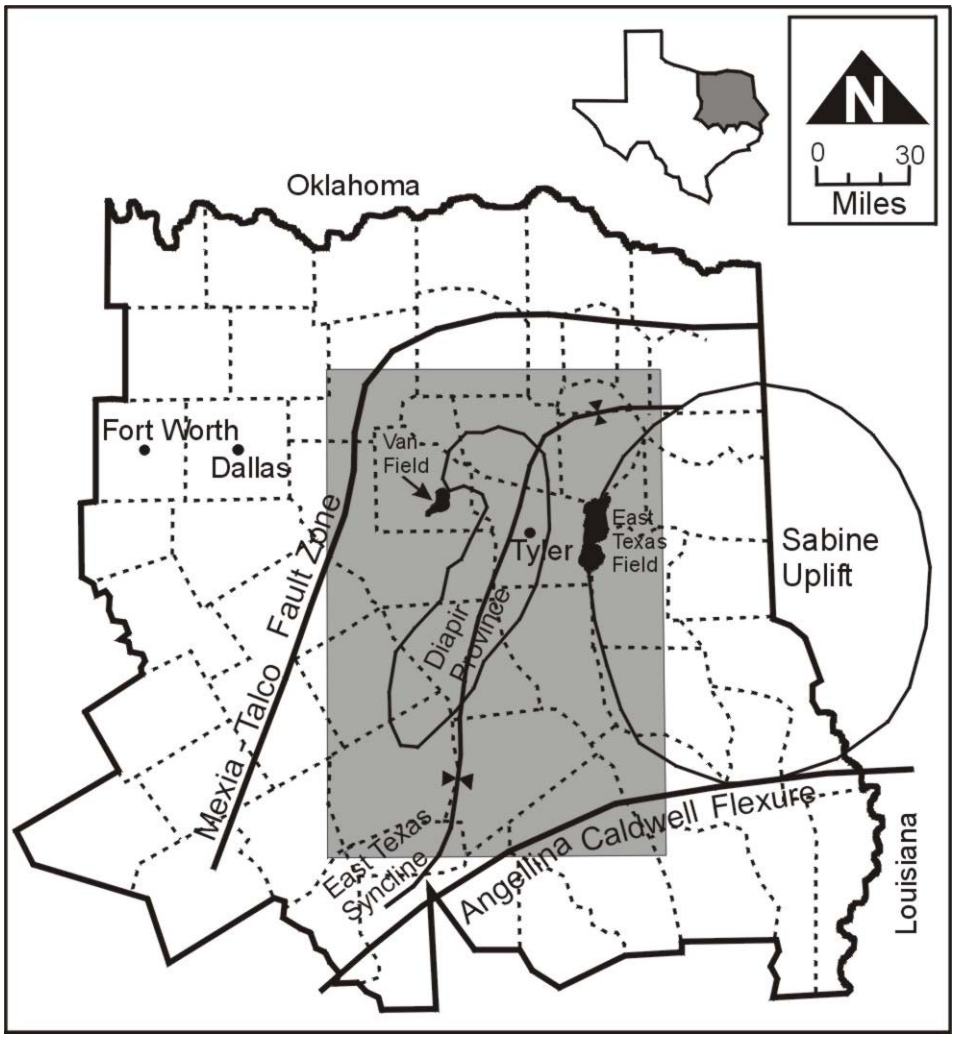

Figure 3. Map showing the East Texas Basin bounded on the north and west by the Mexia-Talco fault zone and on the east by Sabine Uplift. The Basin extends into the Upper Gulf Coast province south of the Angelina-Cadwell Flexure (modified from Wescott and Hood, 1994).

Stratigraphic Setting

The regional stratigraphy of the East Texas Basin started with the deposition of Louann salt during the Middle Jurassic time. By Late Jurrasic time, subsidence had allowed unrestricted marine circulation to inundate the region. In this setting, the open

marine carbonate ramp deposits of the Smackover and Cotton Valley Formation were deposited. Pindell and Dewey (1982) stated that during the latest Jurassic time the basin margins were breached by major drainage systems and terrigenous clastics of the Bossier, Cotton Valley, and Lower Cretaceous Travis Peak Formations prograded across the shelf of the newly formed Gulf of Mexico. After Travis Peak deposition, mainly marine shales and carbonates of the upper Trinity, Fredericksburg, and Washita group were deposited. The Trinity group consists of Ferry Lake Anhydrite, Rodessa, James, and Pine Island Formations (Turner, 1993).

The Lower Cretaceous section of the East Texas Basin is composed of alternating transgressive and regressive sediments. Travis Peak sandstones were deposited in deltaic and oxidizing coastal plain environments (Rainwater, 1970). This formation overlapped the Upper Jurassic Cotton Valley shales and sands. Travis Peak deposition ended when the supply of land-derived sediment diminished, basin subsidence continued and the shoreline advanced. In the shallow sea, Sligo-Pettet limestones and shales were deposited during periods when there was little or no terrigenous sediment influx. The Pearsall sub-group consists of Pine Island, James limestone, and Bexar shale, which had a similar depositional history to the underlying Sligo-Pettet.

The Rodessa Formation was deposited mainly during regressive periods when the influx of sand and clay exceeded subsidence. Porous and permeable sands were deposited in deltaic depocenters and on the flanks of deltas. Organic-rich lagoonal muds, tidal flat clays, and restricted-marine, near-shore lime muds were deposited over the

deltaic and lagoonal siliciclastics. The deltaic sandstones of the type exhibited by the Rodessa Formation are similar to many other sandstones in the East Texas Basin that produce extensive amounts of oil and gas. The Ferry Lake Anhydrite was deposited in the central and eastern Gulf Coast when a barrier restricted oceanic circulation and there was little influx of terrigenous sediment (Rainwater, 1970). Figures 4 and 5 show the summary of stratigraphy of the East Texas Basin.

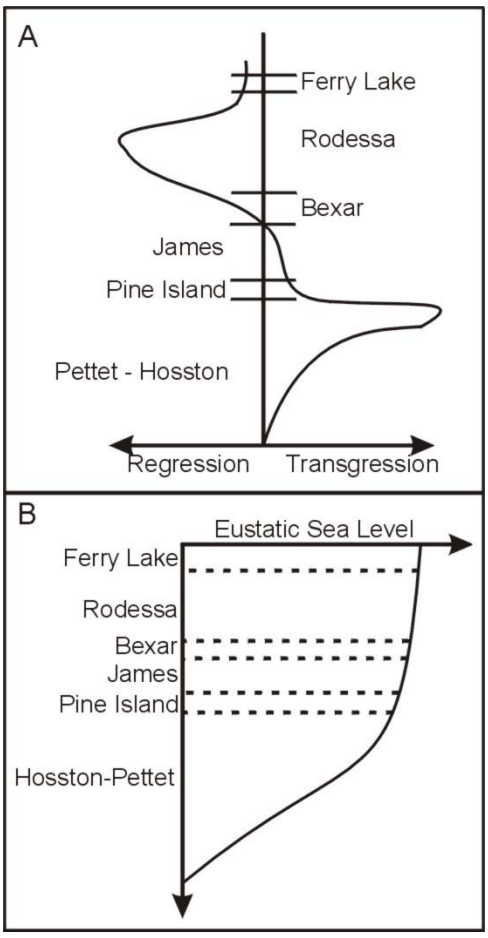

Figure 4. A. Diagram showing the facies shifts during the Lower Cretaceous Time. B. Diagram showing eustatic sea level change during the Lower Cretaceous Time (modified from Bushaw, 1968).

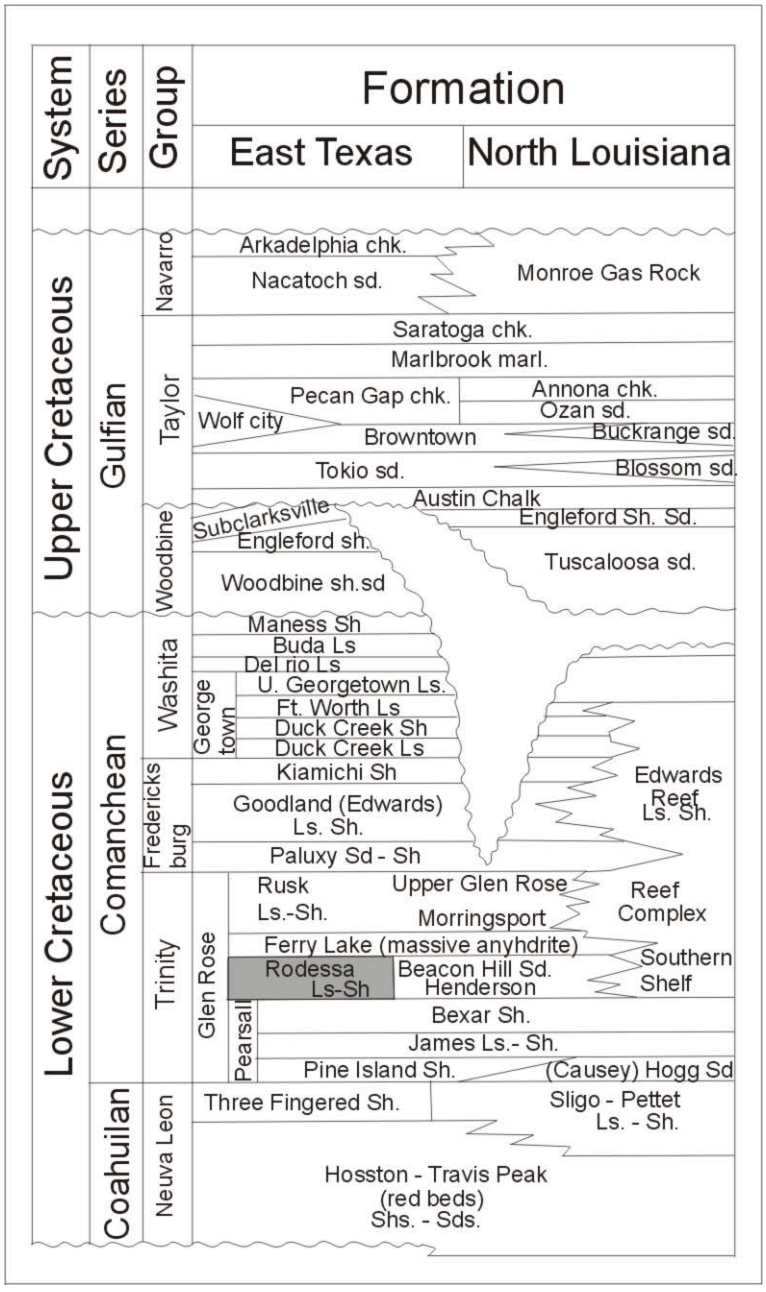

Figure 5. Stratigraphic column for the East Texas Basin showing the Rodessa as a part of the Lower Cretaceous System (modified from Wescott and Hood, 1994).

Previous Work

Much of the early work on the Rodessa limestone was done by Keith and Pittman (1983), who studied Running Duke Field in Houston County, Texas. Their work revealed that the Lower Cretaceous depositional setting in the region was characterized by a broad, shallow water carbonate shelf with admixed terrigenous clastics. The Rodessa sequence at Running Duke field is interpreted by the writers to be a local carbonate biohermal buildup that developed on the older Glen Rose carbonate platform. Those authors recognized six Rodessa lithofacies in cores. Each facies is characterized by distinctive diagenetic histories that were linked to different pore systems that can be identified and mapped across the field as reservoir flow units. A grainstone facies is the principal reservoir in the field and it exhibits two different diagenetic modifications. First was an episode of marine isopachous cementation followed by a later partial infilling by burial calcite that produced intergranular porosity with a unimodal pore-size distribution. The later sequence is represented by a patchy distribution of meteoric phreatic calcite cement followed by a second generation of burial calcspar that resulted in a bimodal pore size distribution consisting of intergranular macropores and intercrystalline micropores within pelloids and micritized ooids.

In the same field, Asquith and Jacka (1992) studied the petrophysics of bimodal porosity of Rodessa limestone. Within this Rodessa limestone, they found that the microporosity associated with high capillary pressure caused the difficulties of hydrocarbon to enter the pores, because the pores were saturated with immovable water. The presence of the irreducible water in the intragranular microporosity (micritize ooids)

caused the grains to conduct an electric current. When this occurs the path of electric current is less tortuous because the current is flowing through the grains and also through the formation water around the grain. The less tortuous electric flow path resulted in an abnormally low resistivity recorded by the resistivity logs. This situation caused unusually high S_w to be calculated. In Running Duke Field the Rodessa ooid grainstone had a total water saturation (S_{wt}) range from 54.8 to 86.5 percent. After it was corrected due to the presence of water-filled microporosity the effective water saturation ranged from 14.3 to 58.4 percent.

Distribution of Hydrocarbons

Structures formed by the Louann Salt exerted the major control on the occurrence and distribution of hydrocarbons in the East Texas Basin (Wescott and Hood, 1994). Those authors also stated that the hydrocarbons in the Rodessa Formation and other Lower Cretaceous formations are typical of oil identified to have originated in Jurassic source rocks owing to their carbon isotopic and sulfur–to-nitrogen ratio analysis. Oil to source rock correlation suggests that much of Smackover oil was sourced by Jurassic rocks.

The most reasonable way to bring Jurassic oil into a Cretaceous reservoir is by vertical migration along the faults (Burgess, 1990). This conclusion was supported by several hypotheses. First, most of the field in which Jurassic oil has been identified is fault related, with faults forming the trap or the field being a highly faulted dome or anticlinal closure. Also, there are demonstrable relationships between faulting and

hydrocarbon production, particularly if faults exhibited enough interconnected porosity (non-sealing faults) to allow migration. The seal within this system is the Ferry Lake anhydrite that overlies the Rodessa Formation.

METHODOLOGY

Data

Data for the study were provided by Unocal Corporation and include the following types of material:

1. Base maps and other supporting maps.
2. Digital and hard copy log data from 32 wells in Van field and surrounding fields (Table 1). Some of them have a complete log of the interval of interest. The field base map is illustrated in Figure 6.
3. Conventional cores from the Brawner 10-22.
4. Thin sections of the cored interval.

The study was conducted at Texas A&M University using the facilities of Department of Geology and Geophysics and also using some laboratory facilities of the Petroleum Engineering Department. Petrophysical analyses were done by using PC-based Geographix^{TM} software.

Petrographic, Petrophysical, and Petrological Methods

Core and Thin Section Analysis

Basic rock properties, such as permeability, porosity, and fluid saturation were obtained by direct measurement on core. Only one conventional core was available for this study; it is a core of the reservoir interval in the Brawner 10-22 well. This core

penetrated the Rodessa Formation and provides an almost complete record of deposition and diagenesis. Core descriptions and core analysis provide a basic reference for subsequent interpretation of borehole log responses and for petrophysical calculations on wells where cores were not available. Core descriptions in this thesis include identification of rock type, depositional texture, grain composition, visible porosity, sedimentary structures, and stratigraphic contact. Carbonate rocks were classified using the Dunham classification scheme, and siliciclastics were described using Wentworth scale of grain size measurement. Thin sections were examined under the petrographic microscope to measure pore size and abundance, to determine pore origin, and to establish correspondence between pore characteristics and depositional – diagenetic history as it has impacted reservoir quality.

Borehole Log Analysis

Core descriptions provided a baseline for lithological characteristics of the Rodessa Formation in the study area. Borehole log characteristics were compared and correlated with lithological and petrographic features to establish relationships between rock and log properties that were applied across the field, where cores were not present. Core porosity was also calculated and compared with log porosity in order to evaluate petrophysical characteristics of the entire reservoir at field scale. Finally, after core porosity and log porosity were compared and a relationship established, core permeability and core porosity were also compared to determine an empirical relationship that was used to estimate pseudo-permeability from log-derived porosity.

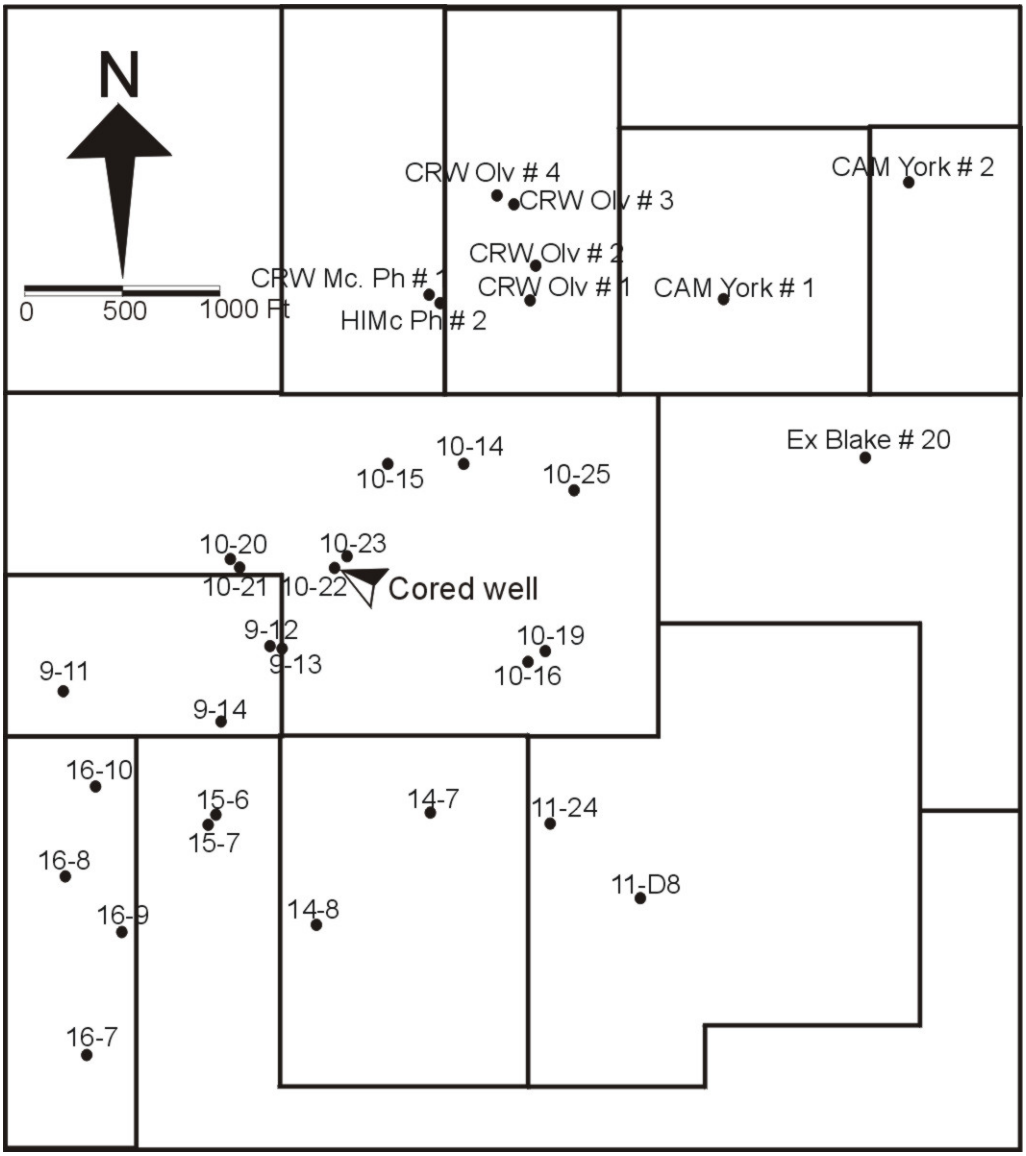

Figure 6. The base map of the study area including all well locations and lease blocks.

Table 1. List of wells names, API numbers and logs

No	Well Name	API	Correlation	Resistivity	Porosity
1	9-11	42467004420000	GR, SP, SPIND	SFL, ILM, ILD	NPHI, DPHI
2	9-12	42467309830000	GR, SP	AO10, AO30, AO90	NPHI, DPHZ
3	9-13	42467309860000	GR, SP	DFL, HMRS, HDRS	
4	9-14	42467310240000	GR_TC		
5	10-14	42467309760000	GR, SP	SFL, ILM, ILD	NPHI, DPHI
6	10-15	42467309790000	GR, SP	SFLU, ILM, ILD	NPHI, DPHI
7	10-16	42467309810000	GR, SP	DFL, HMRS, HDRS	
8	10-19	42467309900000	GR		NT
9	10-20	42467309940000	GR, SP	AHO10, AHO30, AHO90	NPHI, DPHZ
10	10-21	42467310000000	GR, SP	AO10, AO30, AO90	NPHI, DPHZ
11	10-22 (cored)	42467310060000	GR		NT, DPHI
12	10-23	42467310050000	GR, SP	SFL, ILD	NPHI, DPHI
13	10-25	42467310340000	GR, SP	AO10, AO30, AO90	DPHI
14	11-24	42467310350000	GR, SP	AHO10, AHO30, AHO90	NPHI, DPHZ
15	11-D8	42467005070000	GR, SP	AM16, AM64	
16	14-7	42467309920000	GR, SP	AHO20, AHO90	NPHI, DPHZ
17	14-8	42467310230000	GR, SP	AHF10, AHF90	NPHI, RHOB
18	15-6	42467309960000	GR, SP	AT10, AO90	NPHI, DPHZ
19	15-7	42467310010000	GR, SP	AO10, AO60, AO90	NPHI, DPHZ
20	16-7	42467300480000	GR, SP	SN, ILD	DPHI
21	16-8	42467309820000	GR, SP	AHO10, AHO30, AHO90	NPHI, DPHZ
22	16-9	42467309970000	GR, SP	AHO10, AHO30, AHO90	NPHI, DPHZ
23	16-10	42467310040000	GR, SP	AO10, AO30, AO90	NPHI, DPHZ
24	CAM York # 1	42467310300000	GR, SP	SN, ILD	NPHI, DPHI
25	CAM York # 2	42467310310000	GR, SP	SN, ILD	NPHI, DPHI
26	CRWMc. Ph # 1	42467309800000	GR, SP	AT10, AT90	NPHI, DPHZ
27	CRW Olv # 1	42467309710000	GR, SP	SFL, ILD	NPHI, DPHI
28	CRW Olv # 2	42467309750000	GR, SP	SFL, ILD	NPHI, DPHI
29	CRW Olv # 3	42467309850000	GR, SP	SFL, ILD	NPHI, DPHI
30	CRW Olv # 4	42467309840000	GR, SP	SFL, ILD	NPHI, DPHI
31	EX Blake # 20	42467301110000	GR, SP	SFL, ILD	NPHI, RHOBFDC
32	HI Mc. Ph # 2	42467309950000	GR, SP	AT10, AT90	NPHI, DPHZ

Due to the high percentage of shale in the formation, the water saturation (S_w) was calculated using the Simandoux equation (Asquith, 1982, after Simandoux, 1963), Eq. 1. The Simandoux equation requires shale volume (Vsh), effective porosity ($ø_e$) and resistivity (Rt). Shale volume is estimated from equations 2 and 3. The effective porosity (Eq. 4) was estimated from the porosity logs and shale volume.

$$SwSM = \left(\frac{0.4 \times R_w}{\phi_e^{\,2}} \right) \times \left[-\frac{V_{sh}}{R_{sh}} + \sqrt{\left(\frac{V_{sh}}{R_{sh}} \right)^2 + \frac{5\phi_e^{\,2}}{R_t \times R_w}} \right] \quad \ldots\ldots \quad 1$$

$$Vsh = \left(\frac{GR - GRclean}{GRshale - GRclean} \right) \quad \ldots\ldots \quad 2$$

$$Vsh = \left(\frac{SP - SPclean}{SPshale - SPclean} \right) \quad \ldots\ldots \quad 3$$

$$\phi_e = \phi \times (1 - Vsh) \quad \ldots\ldots \quad 4$$

Where SwSM : water saturation (Simandoux)

R_w : formation water resistivity

$Ø_e$: effective porosity

V_{sh} : volume of shale

R_{sh} : resistivity of shale

R_t : true formation resistivity

GR : gamma ray value

SP : spontaneous potential value

RODESSA LITHOFACIES AND DEPOSITIONAL ENVIRONMENT

Rodessa Lithofacies

Based on the full Rodessa section in the Brawner 10-22 well, five carbonate and two siliciclastic lithofacies were identified on grain composition and depositional texture. The carbonate lithofacies are: oolitic mudstones to grainstones, skeletal mudstones to packstones, oolitic packstones to grainstones, mollusks packstones, and pelloid-lithoclast packstones to grainstones. The siliciclastic lithofacies are fine to medium carbonaceous sandstones and medium to coarse sandstones.

Oolitic Mudstone to Grainstone Lithofacies

The oolitic mudstone to grainstone lithofacies consist of gray to dark gray limestones with ooids as the main constituent (Figure 7 and 8). The skeletal constituents in this lithofacies are dominated by mollusks (bivalves) followed by foraminifera and ostracods. Beside ooid, some non-skeletal constituents such as pelloid, pellet, and lithoclast are also present. This lithofacies is cemented mostly by sparry calcite. Anhydrite cements is moderately common in the lower part.

Sedimentary structures are mostly massive for the entire interval, but a few small-scale discontinuous, wavy, non-parallel beds also are present. Burrow is abundant especially in the lower part. The stylolites and grain breakage are present in some parts as a clue of mechanical compactions. This lithofacies has relatively high effective

porosity and permeability averaging about 7.6 percent and 16.18 millidarcies. The porosity is mostly interparticle, intraparticle, vuggy, and moldic porosity.

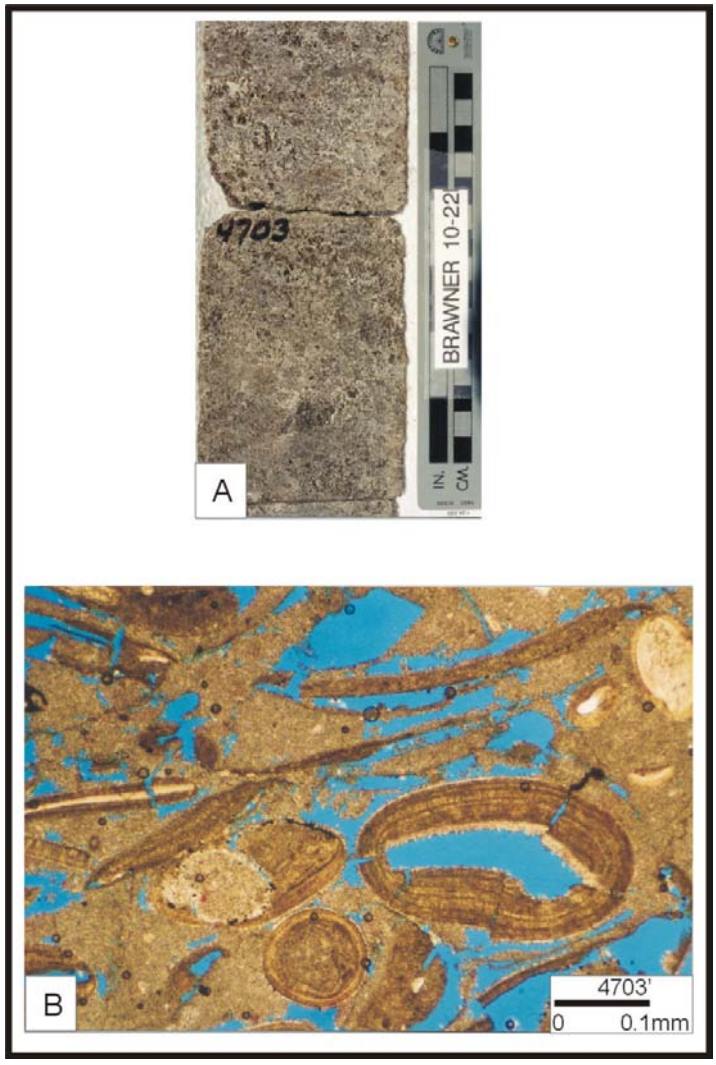

Figure 7. A. The core samples for the oolitic mudstone to grainstone lithofacies from the depth of 4703 feet of Brawner 10-22. B. The blue stained thin section from the depth of 4703 feet showing oolite as the main non-skeletal constituent in this lithofacies.

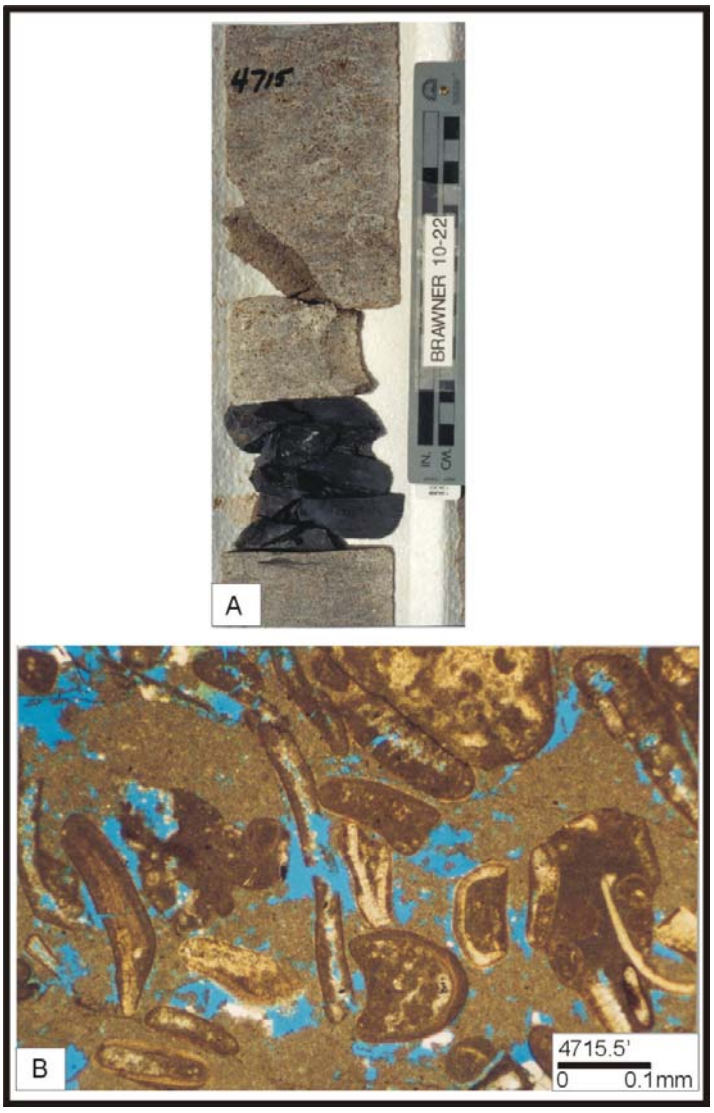

Figure 8. A. Photo illustrating the lower part of the oolitic mudstone to grainstone lithofacies at a depth of 4715 feet. A thin layer of lignite also is present in this lithofacies. B. The blue stained thin section showing skeletal constituents within the rock.

Skeletal Mudstone to Packstone Lithofacies

The skeletal mudstone to packstone lithofacies consists of dark gray to dark yellow limestones with poorly sorted constituents, commonly in a mud matrix. Based on the Dunham classification of carbonate rocks (1960), this lithofacies consists of mudstones to packstones. Skeletal constituents include bivalves, foraminifera, brachipods, and ostracods. Bivalves are the dominant constituent in this mixture. Non-skeletal constituents are dominated by ooids and followed by pisoids and lithoclasts. Sparry calcite is the main cement followed by anhydrite. From the depths of 4749 through 4750.5 feet, a thick 1.5 feet zone of bedded anhydrite with chicken wire fabric is present.

Sedimentary structures include small-scale discontinuous, wavy, non-parallel, and parallel lamina. Burrows and other forms of bioturbation are common. This lithofacies has relatively low porosity and permeability due to high percentage of lime mud matrix and anhydrite cement. The pores are mainly interparticle and intraparticle with average porosity of about 3.56 percent and average permeability of about 0.02 millidarcies

Oolitic Packstone to Grainstone Lithofacies

The oolitic packstone to grainstone lithofacies consists of gray to yellow limestones with up to 60 percent of all constituents being ooids (Figure 9). Skeletal constituents include mainly mollusks (bivalves) followed by foraminifera. Beside ooid, other non-skeletal constituents including lithoclast and peloids also are present. In the

lower part, allochems have been altered so that they are not easy to recognize. Cement includes mainly sparry calcite and anhydrite.

A few small scales, discontinuous wavy non-parallel laminae are present in some zones. Stylolites and grain breakage are present. This lithofacies has relatively low effective porosity and permeability averaging about 5.6 percent and 1.57 millidarcies, respectively. Most of the pores are interparticle-depositional.

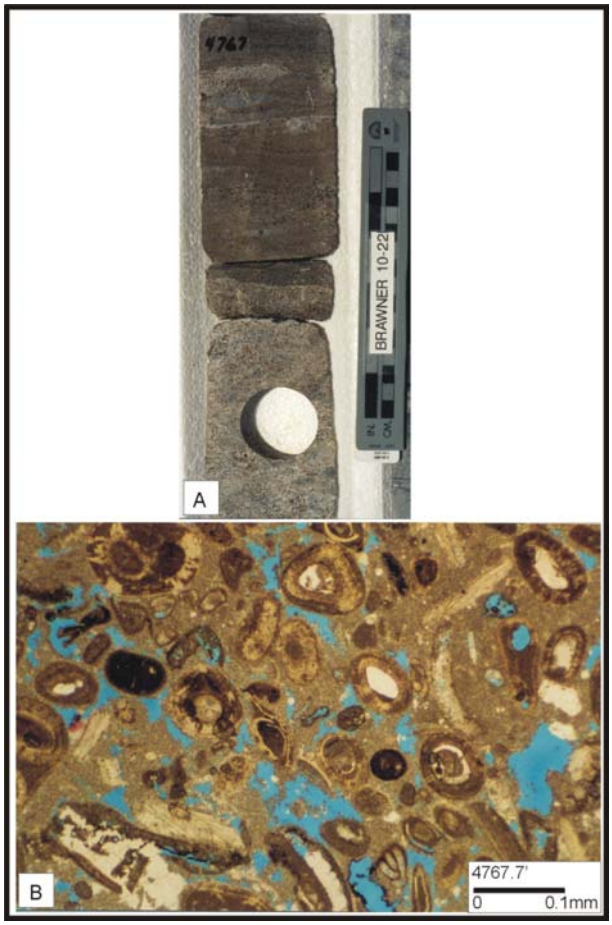

Figure 9. A. Core samples taken from the Brawner 10-22 well at a depth of 4763 feet showing the oolitic packstone to grainstone lithofacies. B. Note that ooids constitute almost 60 percent of the total constituents.

Mollusks Packstone Lithofacies

The mollusks packstone lithofacies consists of gray lime packstone composed mainly of well preserved bivalves and bivalve fragments (Figure 10). Pellets, peloids and lithoclasts are present and cements consist mainly of anhydrite. Sedimentary structures consist of small-scale, discontinuous, wavy, non-parallel lamina and extensive burrowing. Compaction is indicated by the abundance of broken mollusk shells. Porosity effective averages about 4.75 percent and permeability averages is about 3.62 millidarcies.

Figure 10. Core sample taken from the Brawner 10-22 well at a depth of 4791 feet showing well preserved bivalves.

Carbonaceous Sandstone Lithofacies

The carbonaceous sandstone lithofacies consist of interbedded fine sandstones and thin layers of limestones. Hydrocarbon staining has modified the typical gray to yellow rock color (Figure 11). Sand grains are angular to sub-rounded and moderately sorted. Quartz makes up almost 80 percent of the grainy constituents. Pyrite is present as minor constituent, along with scattered foraminiferal skeletal remains.

Sedimentary structures include wavy, parallel, continuous, parallel lamina, cross lamina, and fine ripple beds. Coal and lignite are present in some intervals. This lithofacies has a low effective porosity and permeability, averaging about 6.65 percent intergranular porosity and 1.83 millidarcies permeability.

Peloid-Lithoclast Packstone to Grainstone Lithofacies

The peloid - lithoclast packstone to grainstone lithofacies consists of gray to yellow limestones with abundant lithoclast. The skeletal constituents include mainly foraminifera and mollusks. Non-skeletal constituents are dominated by lithoclasts, detrital quartz, and peloids. Scattered cementation by sparry calcite is present.

Porosity is mainly interparticle, intraparticle, and intercrystalline, and average values for effective porosity and permeability are 5.77 percent and 17.8 millidarcies, respectively.

Sandstone Lithofacies

The sandstone lithofacies consists of interbedded, medium to coarse grained sandstones, along with limestone and shale interbeds. Dominant rocks colors are yellowish brown to green (Figure 12). Sand textures are sub angular to rounded and well sorted. Skeletal constituents in limestones beds include foraminifera. The sandstone sections are hydrocarbon stained.

Sedimentary structures developed are inclined, planar, and wavy, parallel, continuous beds. This lithofacies is probably the best reservoir in Van field because its average effective porosity is about 10.24 percent and its permeability averages about 56.85 millidarcies.

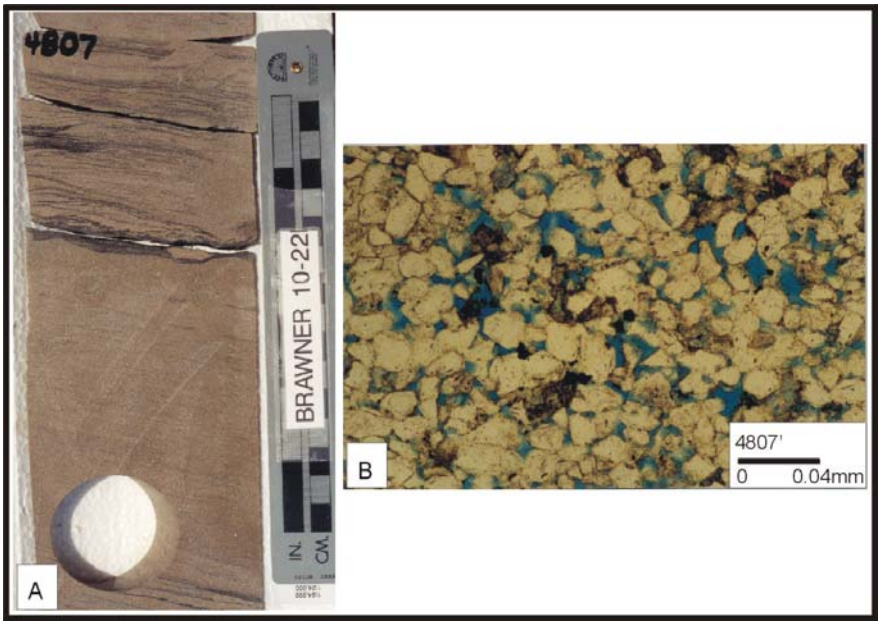

Figure 11. A. Photo of a core sample from the Brawner 10-22 well at a depth of 4807 feet illustrating the carbonaceous sandstone lithofacies. Note the wavy and inclined beds. B. A thin section view showing fine quartz and oil stains in depositional pores.

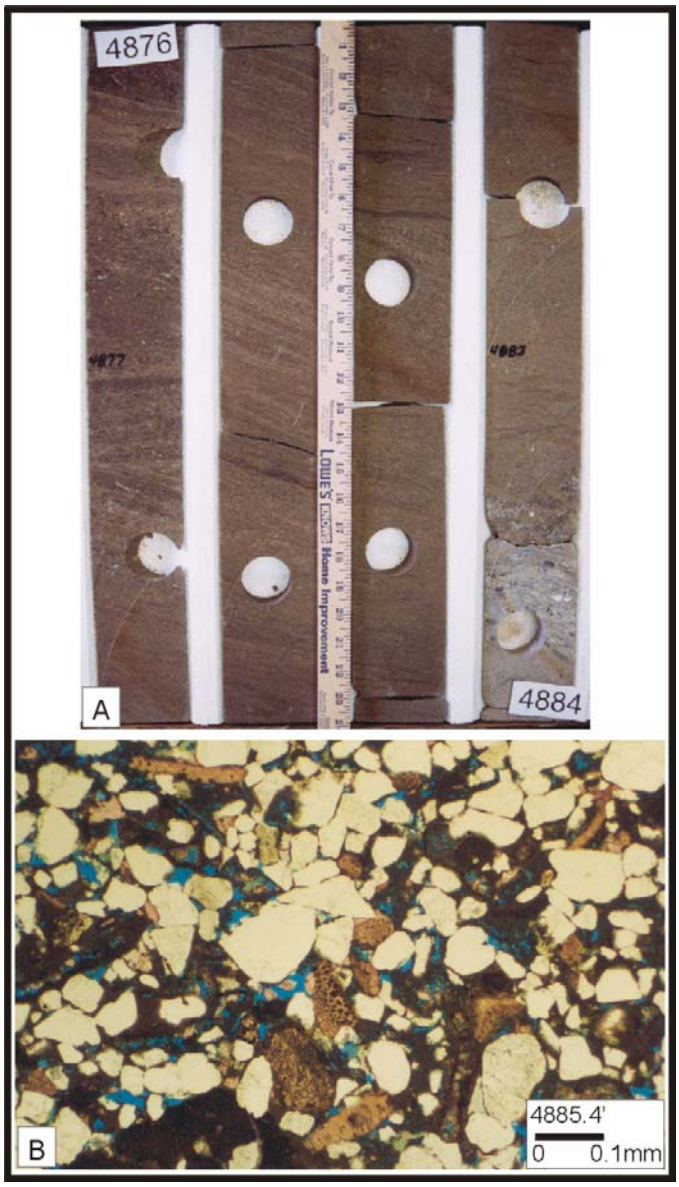

Figure 12. A. A core from the Brawner 10-22 well at a depth of 4876 to 4884 feet showing the sandstone lithofacies that make up the main reservoir in the study area. B. Thin section photomicrograph of the facies showing sandstone texture and

Rodessa Depositional Environment

The Rodessa Formation includes the Rodessa Limestones and the Carlisle Sandstones (Figure 13). The name Rodessa was first used by Forgotson (1956) to define the stratigraphic unit that deposited between the base of the Ferry Lake Anhydrite and the top of Bexar Shale members of the Pearsall Formation. Rainwater (1970) noted that the Rodessa Formation was deposited mainly during regressive periods when the influx of sand and clay exceeded subsidence.

Depending on what depositional dip position one considers, Rodessa rocks could have been deposited from coastal, deltaic and lagoonal environments to restricted, shallow subtidal marine settings.

The Bexar shale is black calcareous shale that is easily identified on electrical logs, which makes it a good stratigraphic marker. Most workers agree that the Bexar Shale was deposited in a shallow neritic, restricted marine or lagoonal environment. The ferry lake anhydrite is the only widespread evaporite deposit in the Lower Cretaceous of the ancestral gulf region (Rainwater, 1970). It was deposited in a broad platform characterized by a very shallow and highly restricted marine environment.

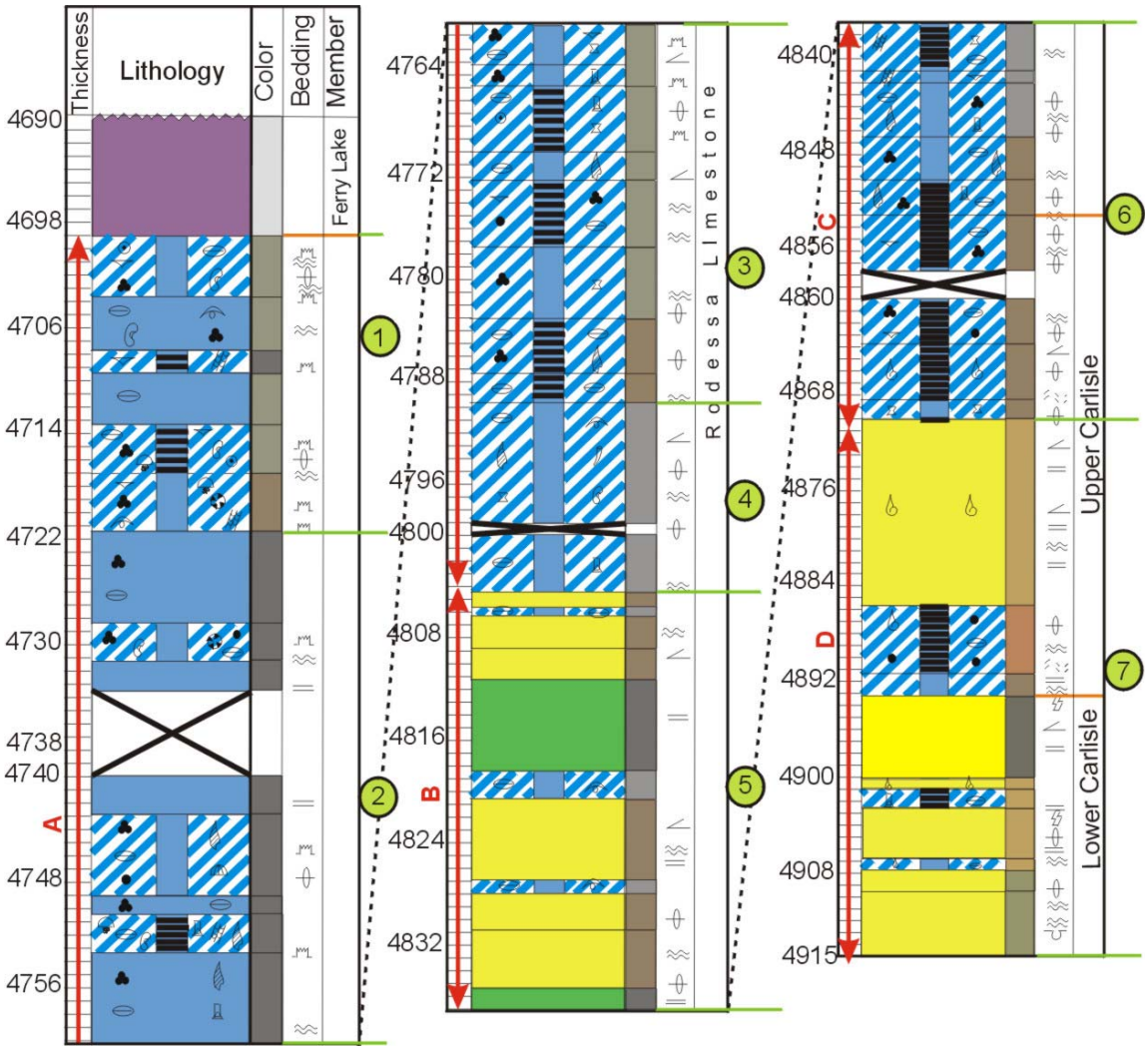

Legend:
1. Oolitic mudstone to grainstone lithofacies
2. Skeletal mudstones to packstones lithofacies
3. Oolitic packstone to grainstone lithofacies
4. Mollusk packstone lithofacies
5. Carbonaceous sandstone lithofacies
6. Peloid-lithoclast packstone to grainstone lithofacies
7. Sandstone lithofacies

Figure 13. Stratigraphic column illustrating the subdivision of the Rodessa Formation. The Rodessa formation is bounded at the top by Ferry Lake Anhydrite and at the bottom by Bexar Shale.

The Brawner 10-22 Core

Interval A

The Brawner 10-22 core (Figure 13) is representative of the stratigraphy in the study area. The interval A consists of the oolitic mudstone to grainstone lithofacies, skeletal mudstones to packstones lithofacies, oolitic packstone to grainstone lithofacies, and mollusk packstone lithofacies (lithofacies 1 to 4). This interval is 104 feet thick and consists of massive, and wavy, non-parallel, continuous beds. Burrowing and bioturbation are abundant. Constituents include mollusk, foraminifera, and interspersed beds of lignite. Chicken wire anhydrite is present at depth of 4748 – 4750 feet. The textures, composition, and sedimentary structures indicate that this interval represent a shallow, restricted marine environment, probably a lagoonal to distal flat setting.

Interval B

Interval B is 45 feet thick, it consist of interbedded fine, poor to moderately sorted, sub angular to rounded sandstones with thin bedded limestones and shales (carbonaceous sandstone lithofacies). Sedimentary structures are wavy, parallel, continuous, parallel lamina, and fine ripple beds. Clay-rich sediments at the top are poorly bedded. The sand-shale interbedded, parallel laminations, and fine ripple beds, indicate deposition by weak, fluctuating currents, probably it deposited within the tidal flat setting.

Interval C

Interval C consists of the peloid-lithoclast packstone to grainstone lithofacies (lithofacies 6). The total thickness of interval B is 31 feet. The limestones exhibit wavy, non-parallel, discontinuous beds. Burrowing and bioturbation are common, suggesting an open marine setting. The abundance of mollusks in the upper part also indicates a marine or brackish water environment. Peloids and lithoclast, along with siliciclastic sand interpreted to indicate proximity to the shoreline. The absence of large scale sedimentary structures, the higher matrix content in sandstones, the interbedded character of limestones and siliciclastics, all suggest that this interval was probably deposited in a lagoonal or distal deltaic setting.

Interval D

Interval D which includes the sandstone lithofacies, consists of yellowish brown to green, interbedded medium-coarse quartzarenites sandstones. The total thickness of interval D is 45 feet. Sandstones exhibit good sorting and rounded to sub-angular grain shapes. Sedimentary structure includes inclined, planar, and wavy, parallel, continuous beds. The clean, well sorted, and inclined beds indicate that interval D was deposited in a high energy setting, probably a tidal channel deposits.

Field-Scale Depositional Setting of the Rodessa Formation

Because only one core was available for study, the field scale depositional model was created from wireline log characteristics, which had first been calibrated to

lithological characteristics in the cored well. For example, grain supported carbonates generally tend to have lower gamma ray readings than mud supported rock (Figure 14). However, in some carbonates especially dolostones, the gamma ray log character could not be used to discriminate between depositional textures.

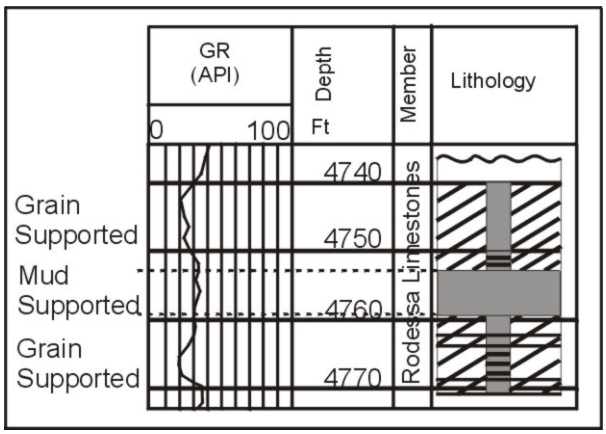

Figure 14. A gamma ray reading of Brawner 10-22 well at a depth of 4740 to 4770 feet showing the contrast of GR values on grain supported and mud supported carbonates.

Rodessa Limestones

Because the wireline log signature are similar across Van Field, because field well logs were carefully compared with the Brawner 10-22 cored well, and because the area occupied by Van Field is comparatively small and elongate more or less parallel to paleodepositional dip, it is probable that the environment of deposition for the Rodessa limestones in the Brawner well is the same for the field wells. That is, lagoonal to distal flat setting.

Rodessa Sandstones (the Carlisle Member)

In contrast to carbonates, sandstone depositional environments can commonly be interpreted from the shape of the gamma ray trace. This is accomplished assuming that the gamma ray trace is indicative of textural trend such as fining and coarsening upward. Fining-upward trends are indicated by increasing gamma ray counts and the reverse is true for coarsening-upward trends. In the case of Carlisle sandstones, a funnel shape (decreasing gamma ray counts upward) is present that is interpreted as coarsening upward sequence, probably a delta or shelf deposit. A few wells have a cylinder shaped gamma ray trace that probably represents delta-destructional bar deposits on the side of the Carlisle deltaic sequences that faced incoming waves. The maps of depositional environments within the field are shown in Figures 15 and 16 for the Upper Carlisle and Lower Carlisle sandy interval.

Depositional Model of the Rodessa Formation

The Rodessa formation was deposited in a broad, shallow-water environment ranging from shallow subtidal marine (including offshore bar builds up), delta, and highly restricted lagoon. Figure 17 shows the depositional model of the Rodessa Formation.

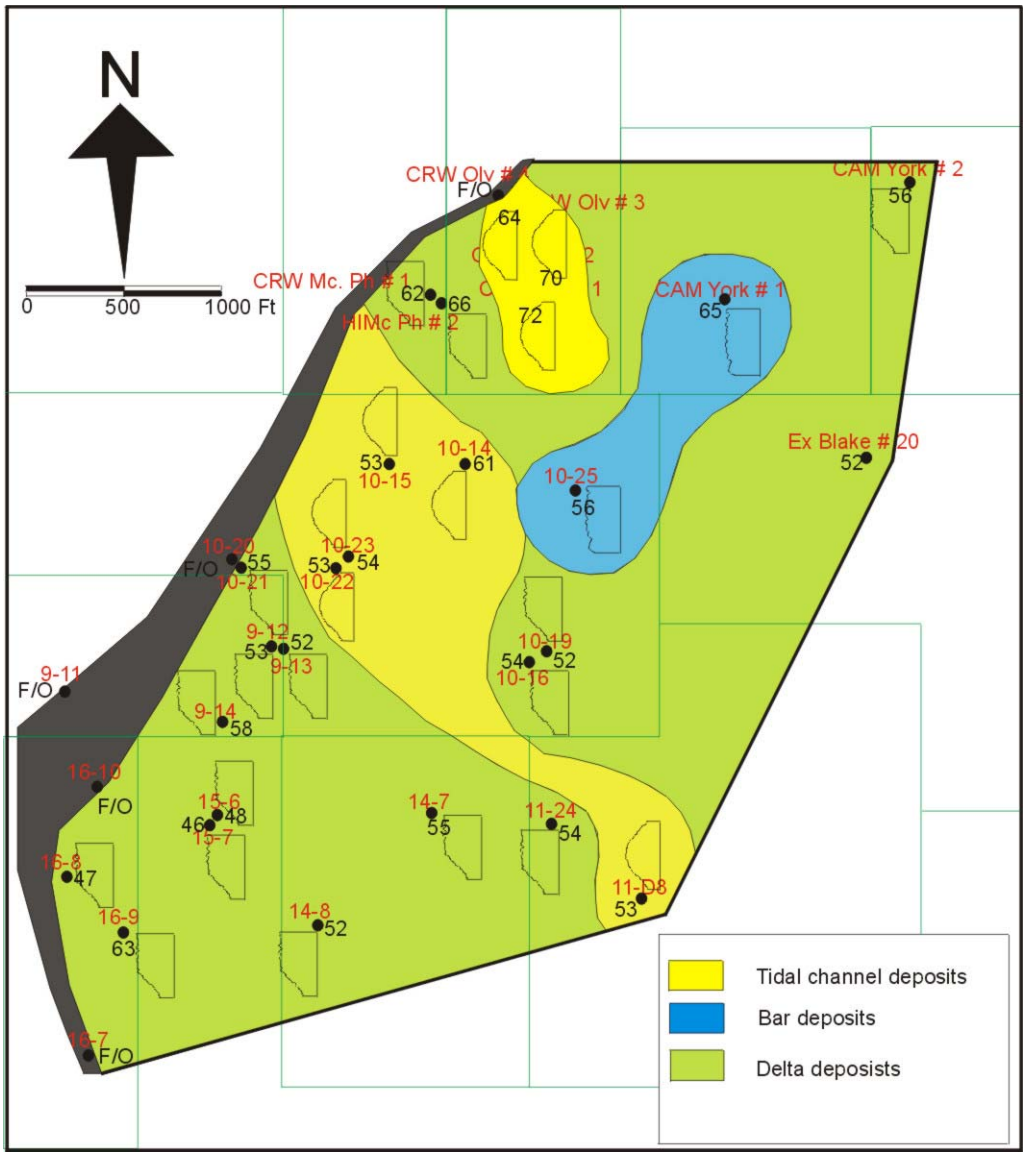

Figure 15. Depositional environment of the Upper Carlisle sandy interval throughout the field based on well log interpretation.

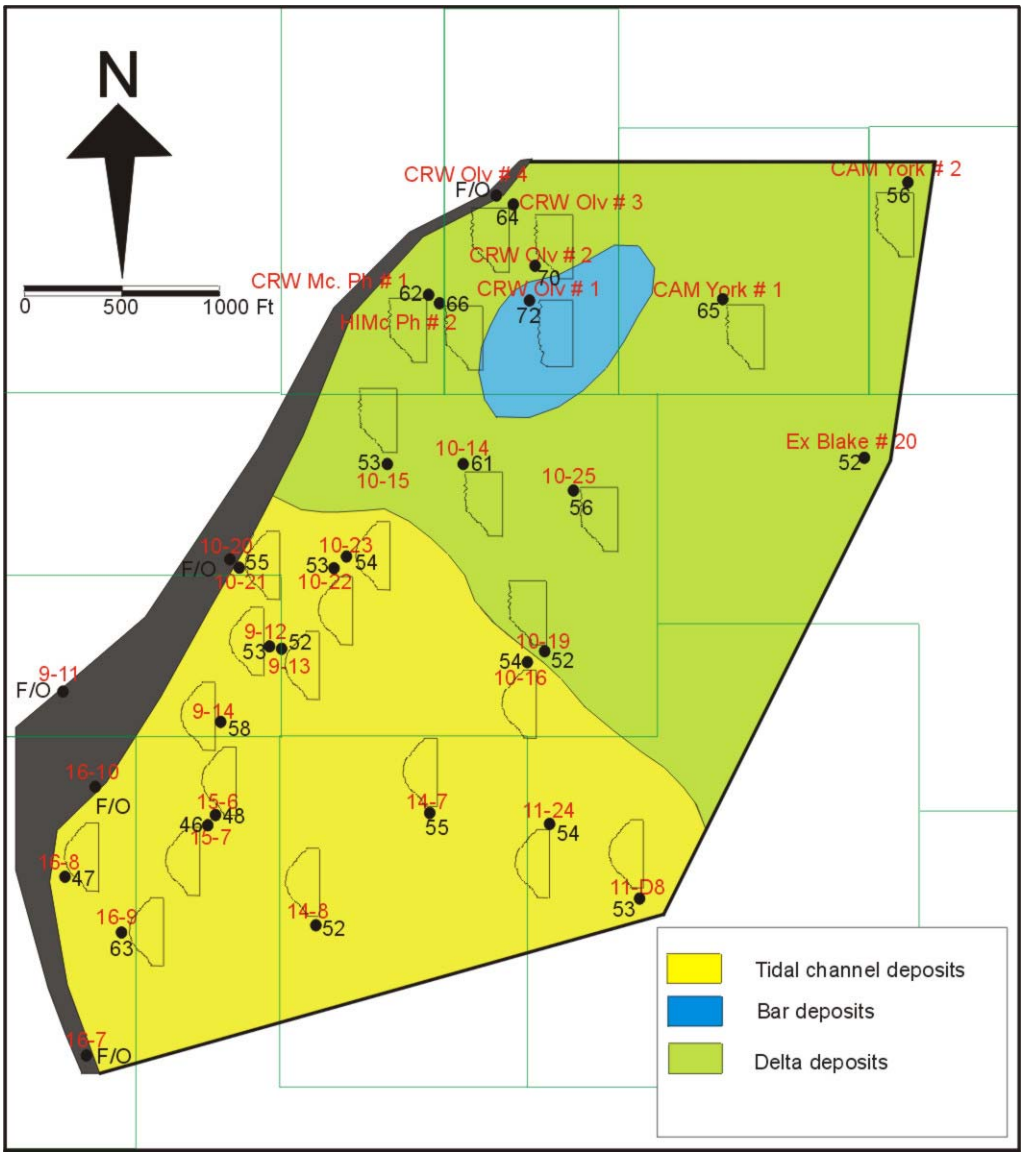

Figure 16. Depositional environment of the Lower Carlisle sandy interval throughout the field based on well log interpretation.

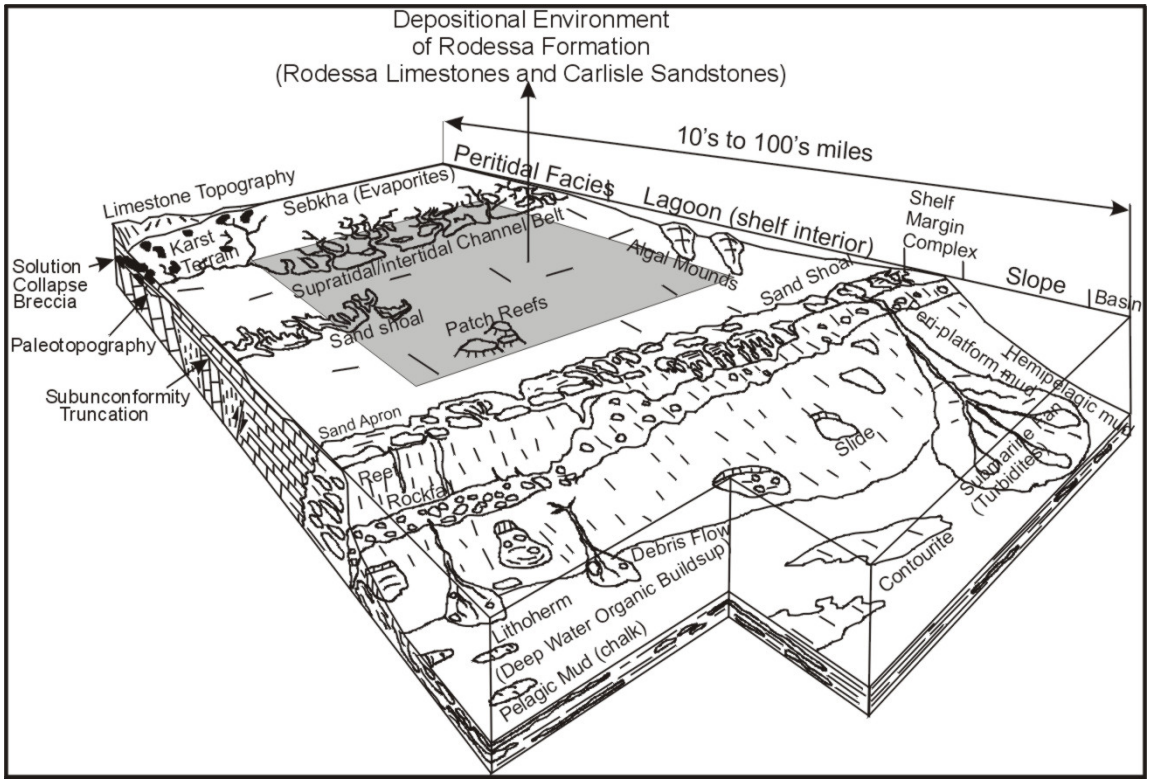

Figure 17. Depositional model of the Rodessa Formation (modified from Lucia, 1992).

DIAGENESIS

Because reservoir quality is influenced by diagenetic processes, it is important to understand the processes and their product. Rodessa rocks in Van Field are generally showed the following types of diagenetic alteration. Relative timing of diagenetic changes and their impact into reservoir quality will be discussed afterwards.

Micritization

Micritization is the process by which the margins of carbonate grains are replaced by micrite (Adams and MacKenzie, 1998). Micritization appeared in a few thin sections of Rodessa limestones; an example of which is shown in Figure 18A. In this case, micrite envelopes coated the original, aragonitic bivalves. The aragonite was selectively dissolved during early diagenesis, leaving only micrite envelope showing the original shell outline.

Cementation

Cementation result when minerals are precipitated in pore space. Most of the cement in Rodessa limestones is isopachous rim cement, bladed or blocky calcite cement, and large blocky calcite cement. Blocky calcite is the most abundant cement type and this type of cement is typical for fresh water phreatic zones (Longman, 1980). This type of cement is immediately touching the acicular marine rim cement. The

isopachous rim cement is very rare due to the extensive leaching and replacement of aragonite by calcite. It is a radial fibrous form of aragonite or mg-calcite, both of which are typical marine phreatic cements (Longman, 1980). Examples of isopachous rim, blocky calcite, and large blocky calcite cement are shown in Figure 18B and 18C. For the sandstones interval the main cements are silica.

Dissolution

Dissolution, or leaching, is the diagenetic process in which the cement, mineral, or grains are dissolved to enlarge or even create pore space. Dissolution is the main type of diagenesis in the Rodessa Limestones. In those cases, it has enhanced porosity. The evidence of leaching is the presence of moldic porosity and enlarged intergranular porosity in almost all intervals of limestones. Both skeletal and non-skeletal grains have been leached to form mold, some of which were later partially filled with calcite cements. Moldic pores are shown in Figure 18C.

Neomorphism

Neomorphism is a form of recrystallization in which an original texture or fabric is replaced by a new one without changing mineralogical composition (Adams and MacKenzie, 1998). In the Rodessa Limestones, neomorphism is represented by calcitized skeletal or non-skeletal constituents that were formerly aragonite

Compaction

Simple compaction is a mechanical process caused by loading stresses due to overburden. Compaction typically occurs soon after deposition and result in a significant change in the petrophysical properties of the reservoir rock. Compaction in the Rodessa Formation is indicated by the presence of thin, wispy laminae, stylolites, and microstylolites (pressure solutions), grain breakage, and increased number of contacts per grain. Figures 18B and 18D illustrate compaction in Rodessa rocks.

Influence of Diagenesis on Porosity and Permeability

Originally, the porosity in the Rodessa reservoir was depositional only. Subsequently, diagenetic overprints have modified it. For the limestones (interval A and C), almost all the diagenetic processes (micritization, cementation, neomorphism, and compaction), have resulted in the destruction or reduction of the original porosity and permeability.

Cementation is the dominant process that has reduced original porosity. On the other hand, leaching is the principal diagenetic process that has enhanced porosity and permeability, as indicated by the presence of moldic and vuggy porosity in the Rodessa Limestones. Although compaction initially decreased porosity and permeability, it also induced grain breakage and formed stylolites, which in rare case are beneficial to porosity and permeability.

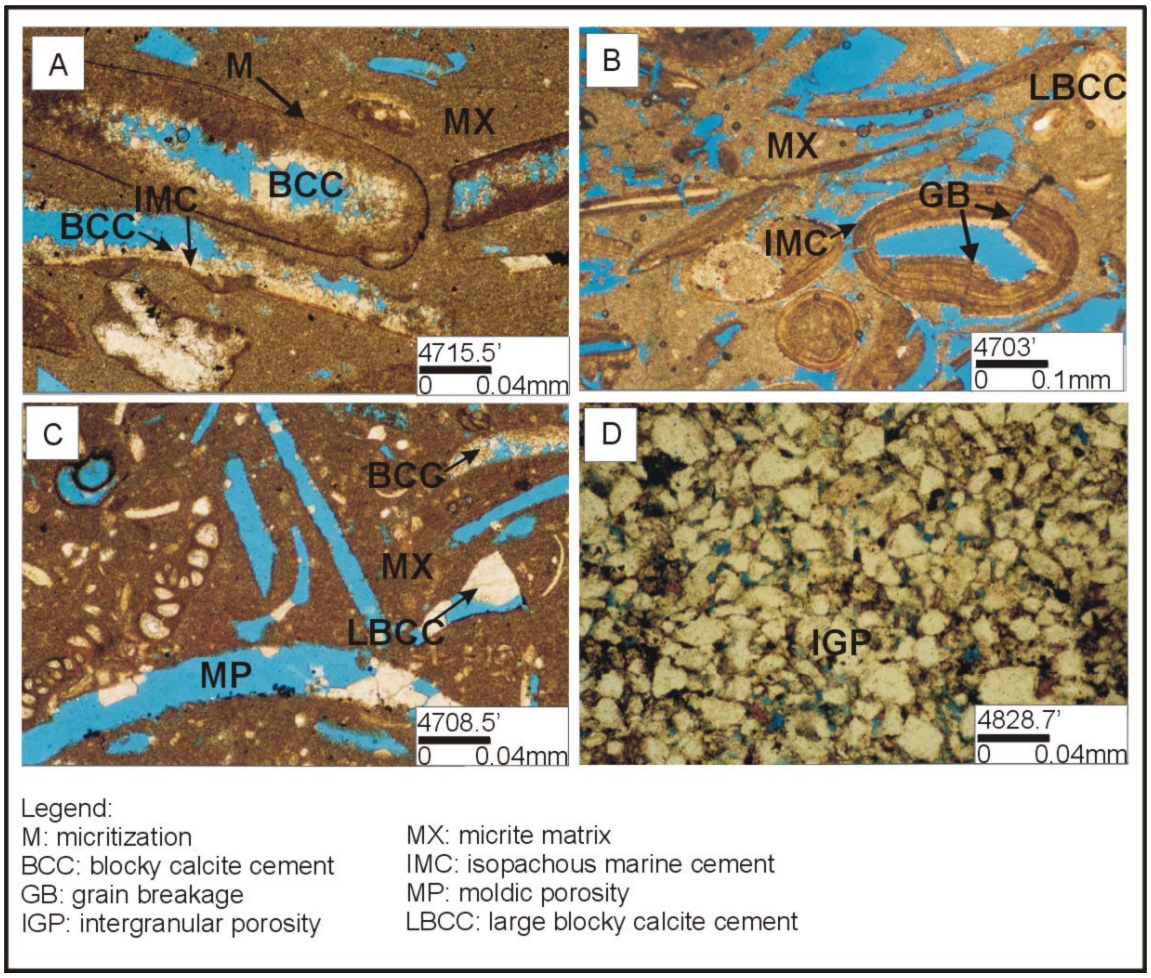

Figure 18. A. Photomicrograph of stained thin sections from the Brawner 10-22 well showing micritization (M) and extensive development of the micrite matrix (MX). B. Cementations and grain breakage (GB). C. Moldic porosity (MP) produced by leaching. D. Intergranular porosity (IGP) and compaction in sandstone interval.

For the Carlisle sandstones (interval B and D), simple intergranular porosity has been reduced by cementation and compaction. Dissolution of calcite cements has enhanced porosity in the sandstones section.

Diagenetic History

The diagenetic sequence in the Rodessa Formation is complex because the rocks have been exposed to several episodes of diagenesis from the surface to burial depths. Cross-cutting relationships in thin section have revealed the following sequences.

The Rodessa Formation began its diagenetic history in the marine phreatic zone as evidenced by the presence of isopachous marine rim cements that cover both skeletal and non-skeletal constituents. This type of cement is very rarely preserved due to the extensive dissolution.

Subsequent sea level fluctuations produced packages of shallowing-upward depositional sequences, or parasequences. Those nearest the subaerial environment were subjected to fresh water diagenesis soon after deposition. Bladed and blocky calcite cements were formed during this exposure to saturated, fresh water in the phreatic zone. Cementation, compaction, and neomorphism occurred early in the burial history of the Rodessa Formation. The diagenetic sequence is shown in Figure 19 and 20.

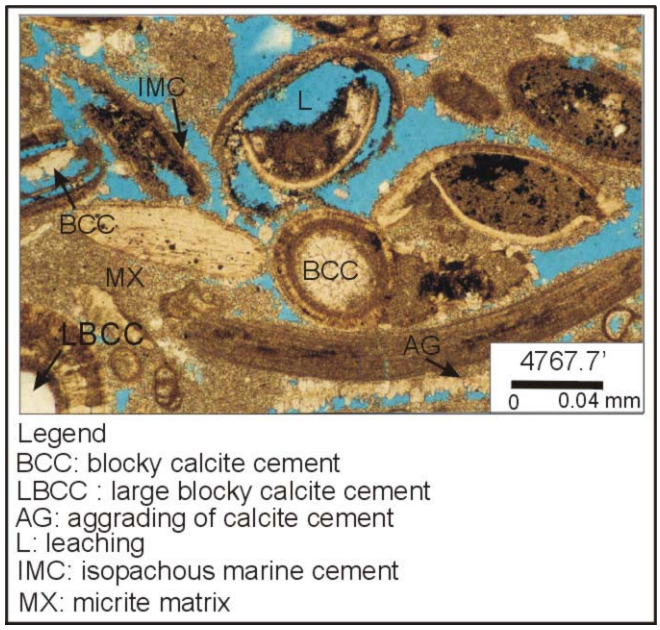

Figure 19. Photomicrograph of a stained thin section from a depth of 4767.7 feet in the Brawner 10-22 well. Several episodes of cementation are illustrated, beginning with isopachous marine rim cements (IMC) followed by leaching (L), and finally followed by blocky calcite cementation and aggrading.

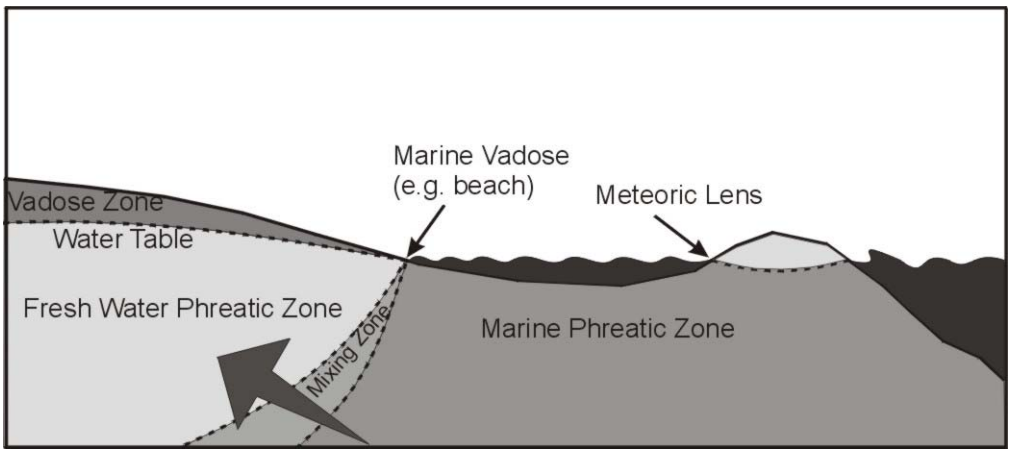

Figure 20. Four principal diagenetic environments. The Rodessa Formation began its diagenetic history in the marine phreatic zone and then evolved to the fresh water phreatic zone (modified from Adams and MacKenzie, 1998).

RESERVOIR ARCHITECTURE

The study area is about 7 percent of the entire Van Field covering about 31 acres or equal to 0.125 square km. It extends approximately 1.3 km from southwest to northeast, and 0.88 km from northwest to southeast. It is bounded in the northwestern part by a southwest to northeast fault that is interpreted to be part of the regional Mexia-Talco fault system.

A structural map of the area is shown in Figures 21 and 22. The top and bottom of the Rodessa Formation are typically high, structurally, in the western part of Van Field and dip gradually toward the east except where faults have influenced regional dip. An isopach of the Rodessa Formation is illustrated in Figure 23 and it illustrates two paleostructural highs on the top of the Rodessa Formation in the northern and southern parts of Van Field. The thickest Rodessa section in this area is about 228 feet thick in well 9-14; the thinnest is about 175 feet in well 11-D8.

The author divides the Rodessa Formation into two members; the Rodessa Limestone and the Carlisle Sandstone. The Carlisle Sandstone is, however, only a local name used by oilfield operators and is not acknowledged in the general stratigraphic literature. Carlisle Sandstone consist sandstones and some interbedded limestones and shales. The isopach maps for each member are shown in Figures 24 and 25 and cross sections are given in Figures 26, 27, and 28.

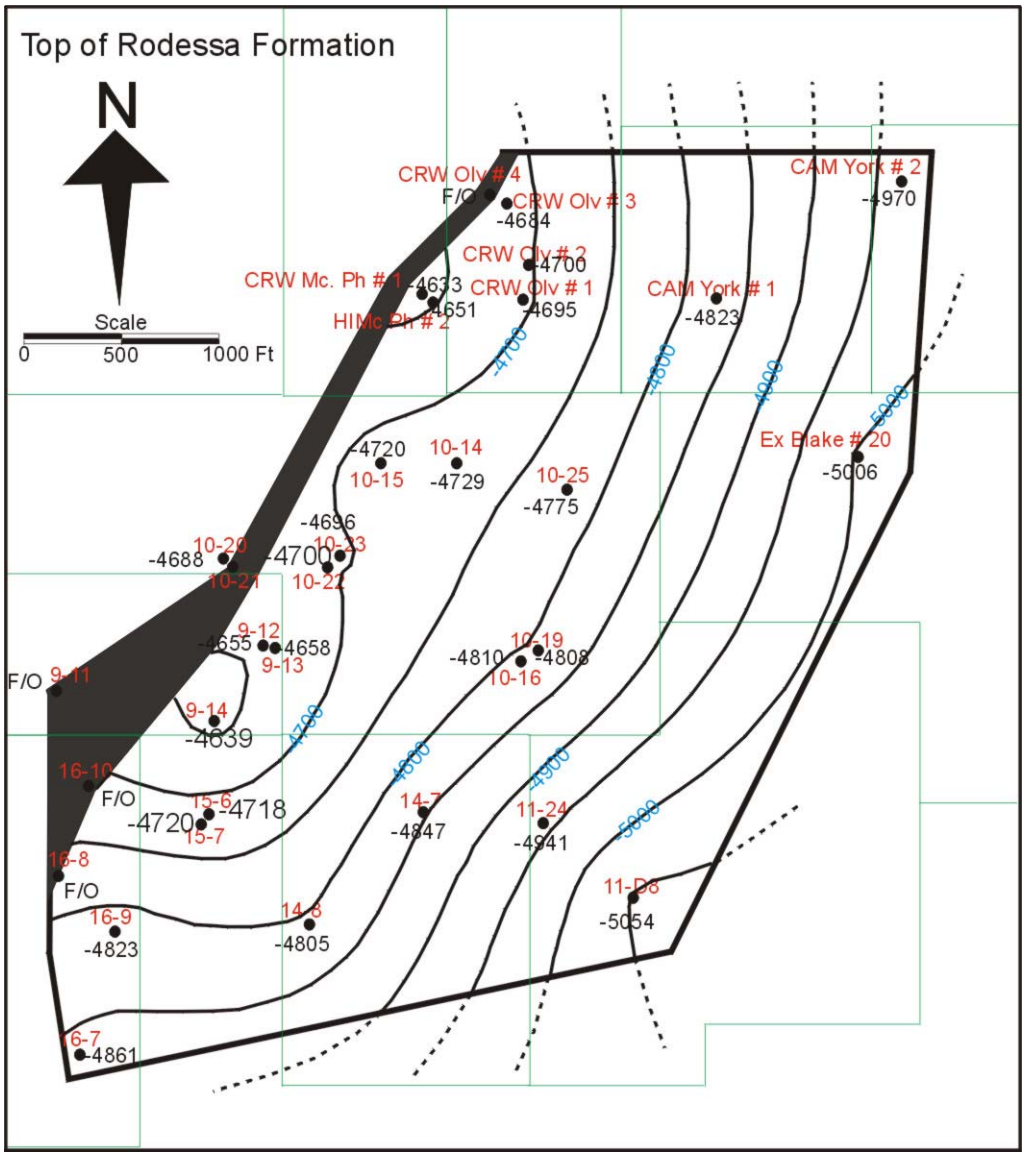

Figure 21. Structure map of the top of the Rodessa Formation.

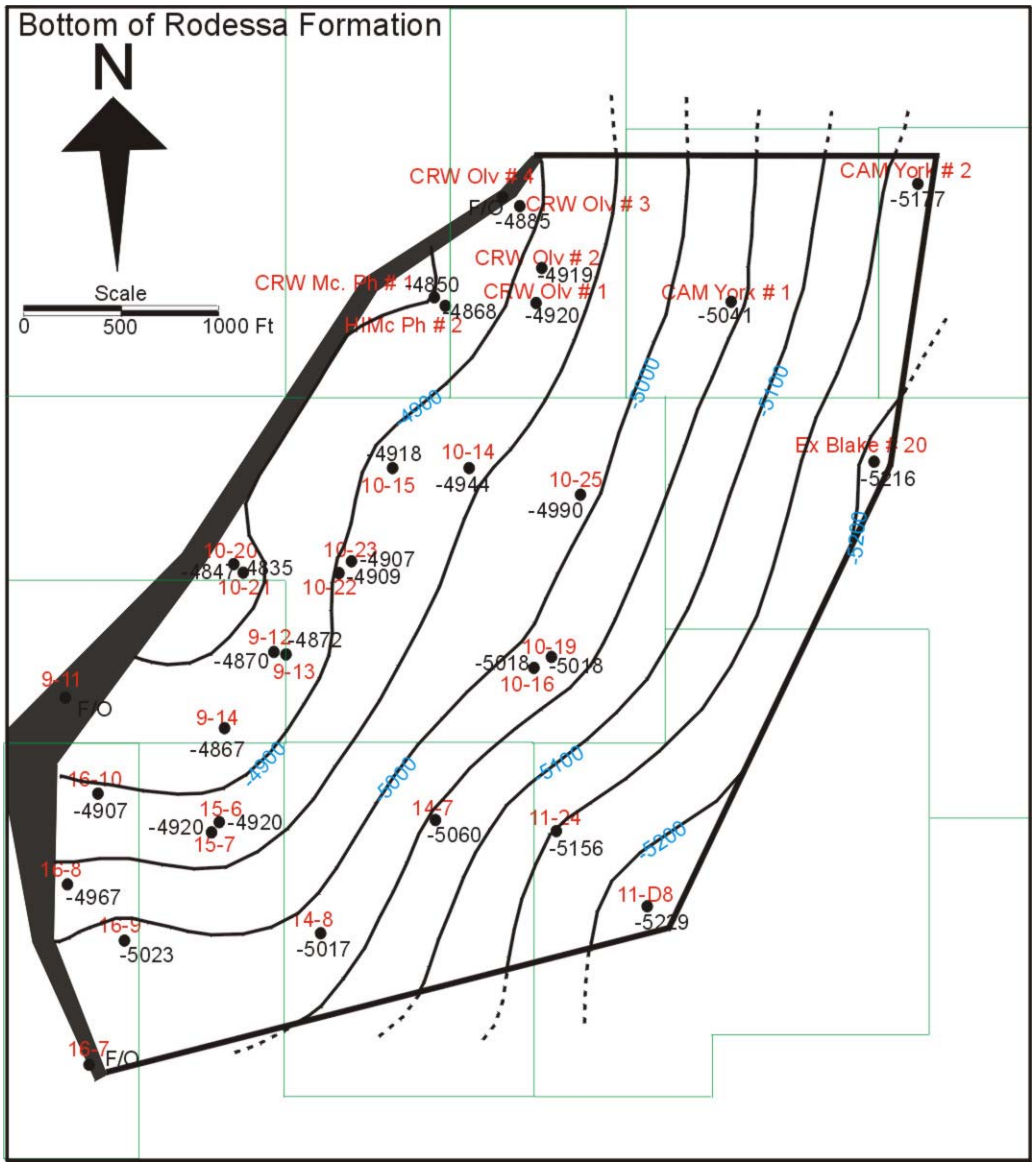

Figure 22. Structure map of the base of the Rodessa Formation.

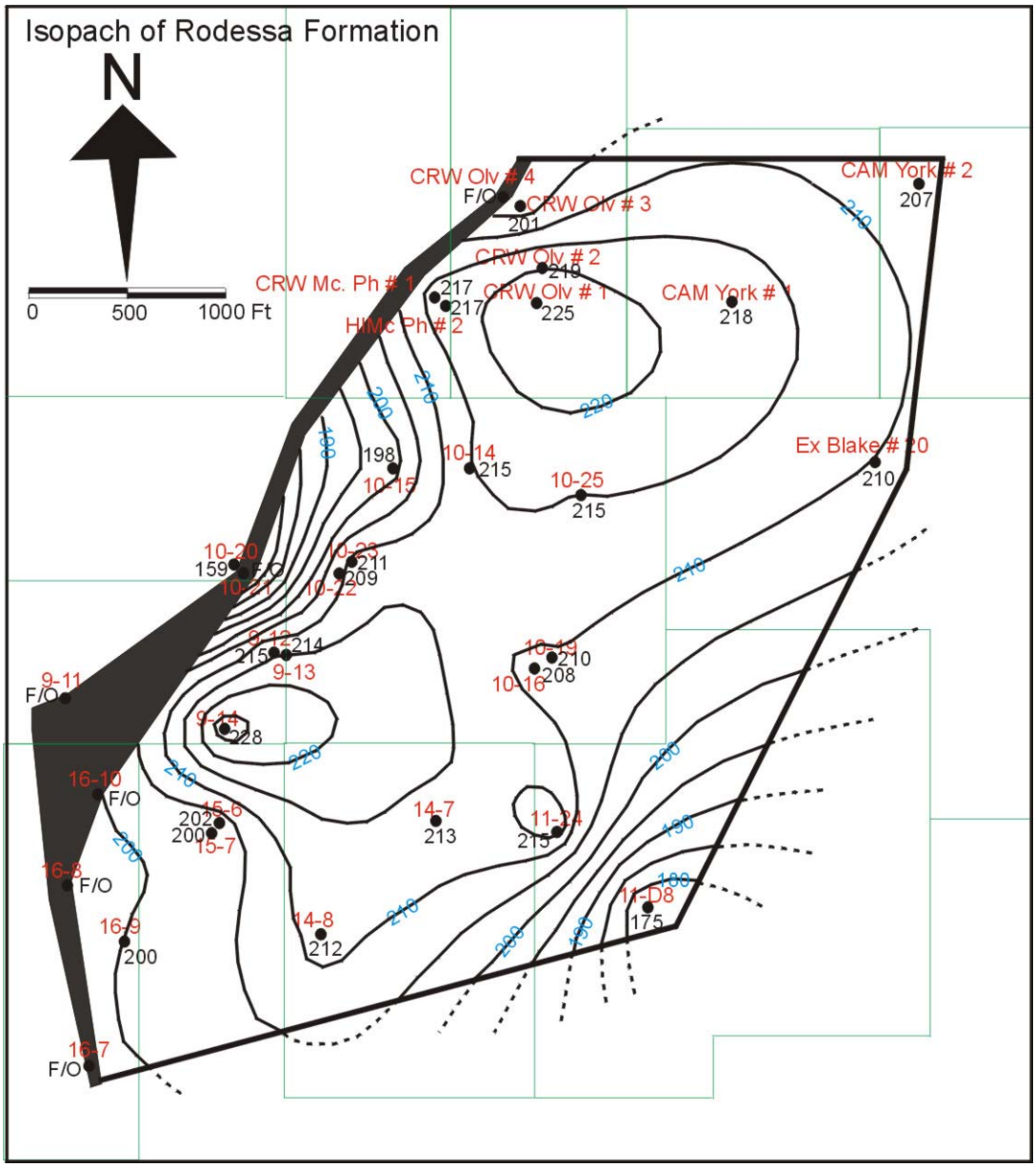

Figure 23. Isopach map of the Rodessa Formation.

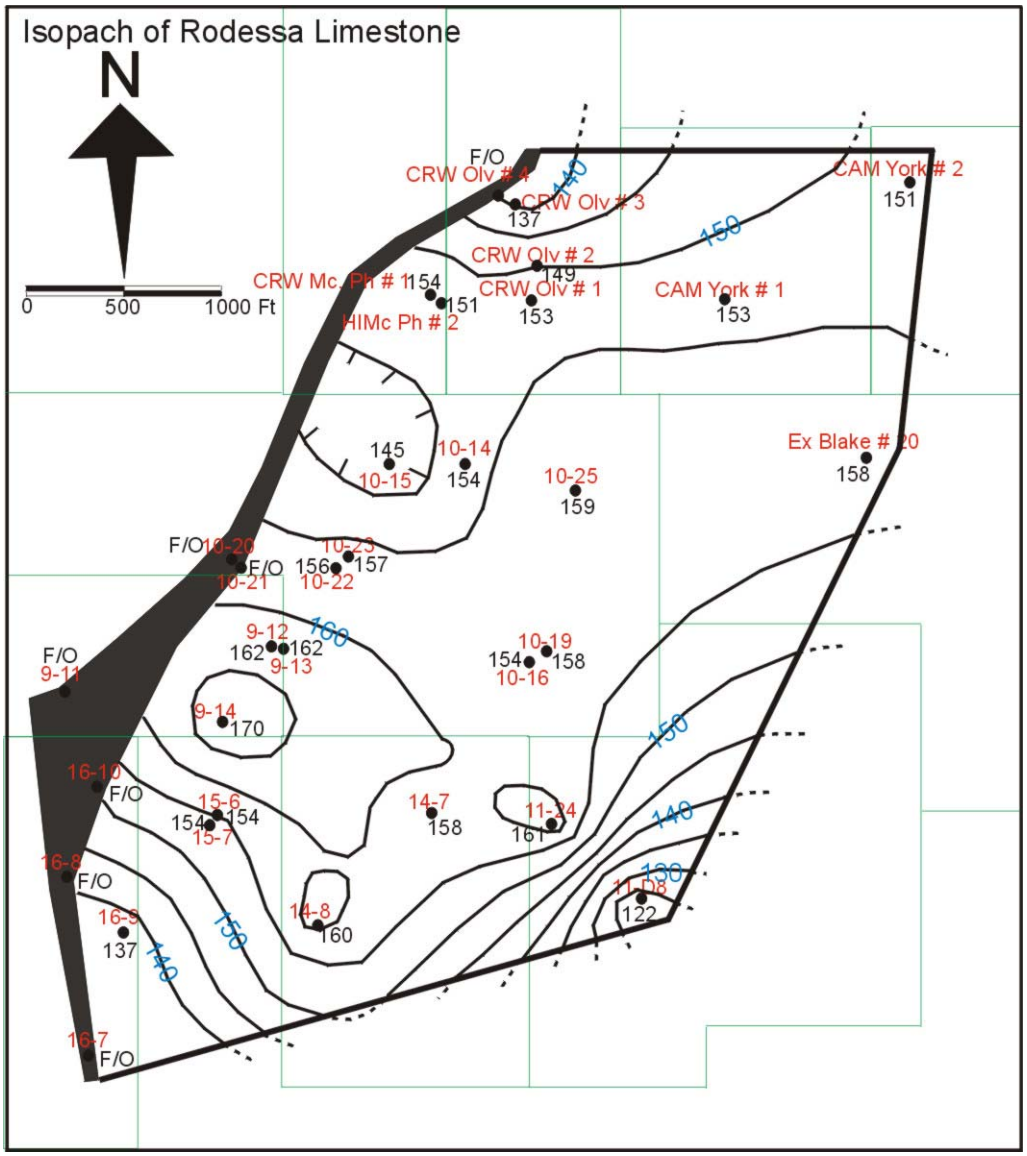

Figure 24. Isopach map of the Rodessa Limestone.

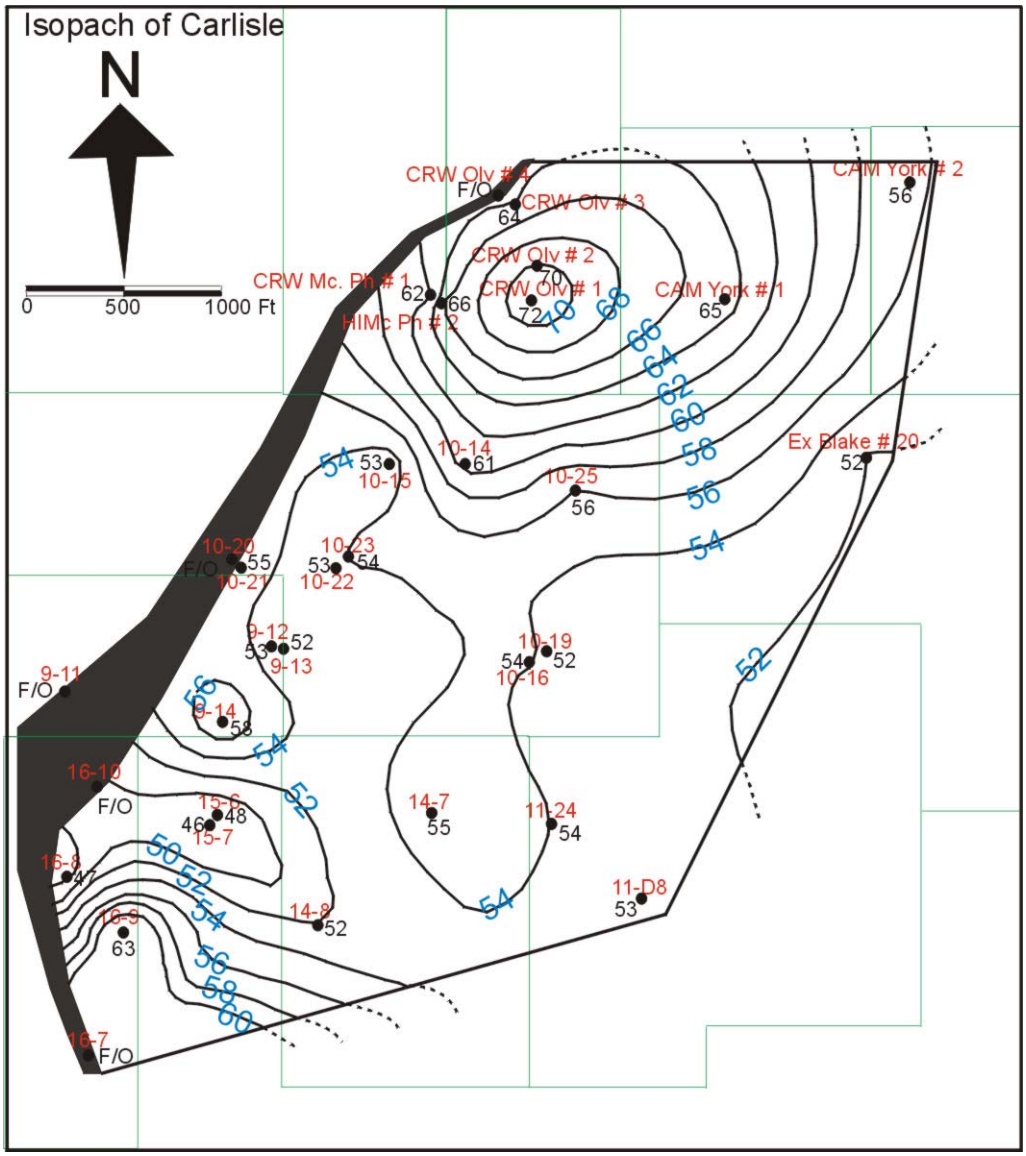

Figure 25. Isopach map of the Carlisle Sandstone.

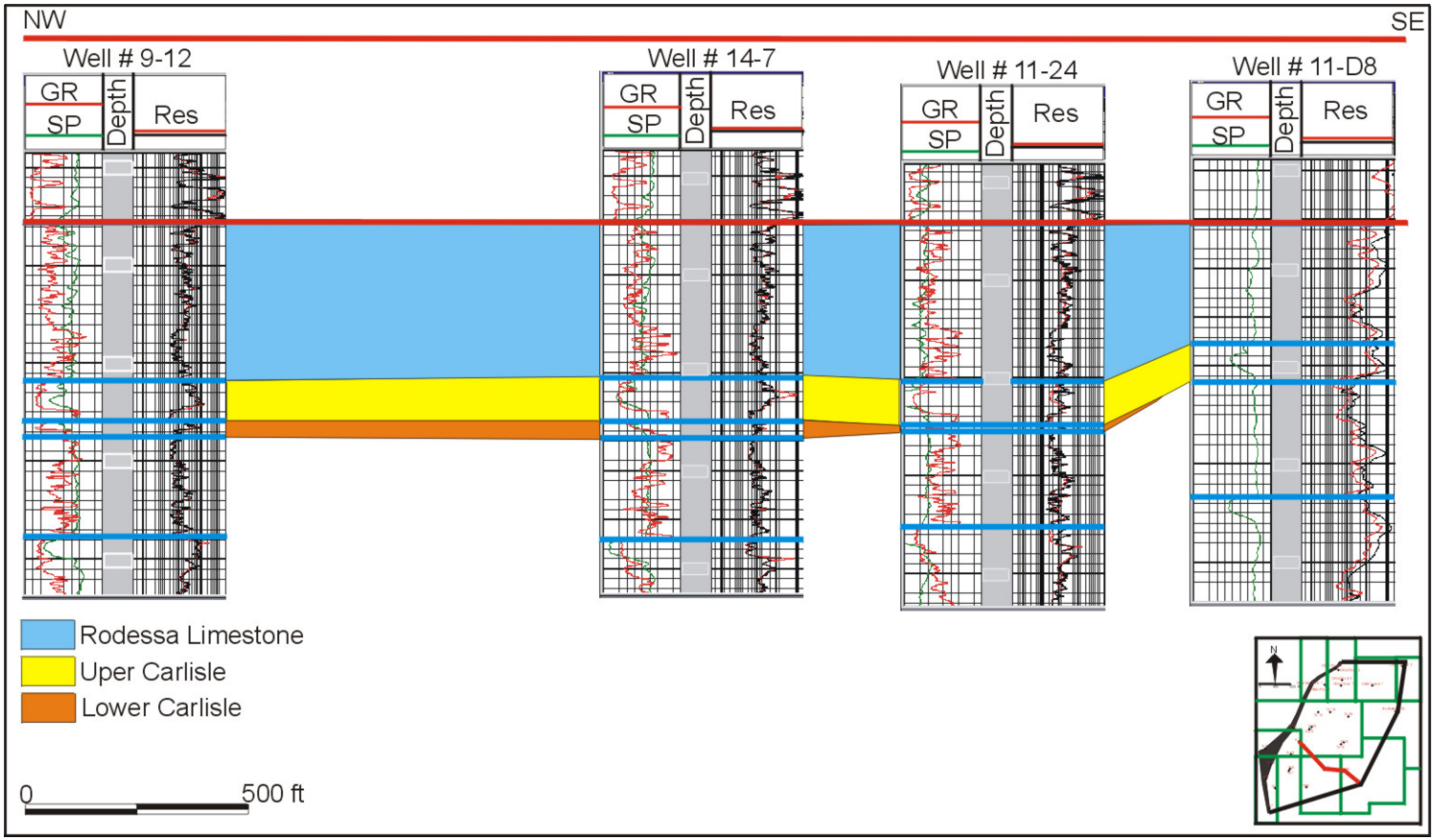

Figure 26. A northwest – southeast stratigraphic cross section in the southern part of the field illustrating the distribution of the Rodessa Limestone and the Carlisle Sandstone (datum is the base of the Ferry Lake Anhydrite).

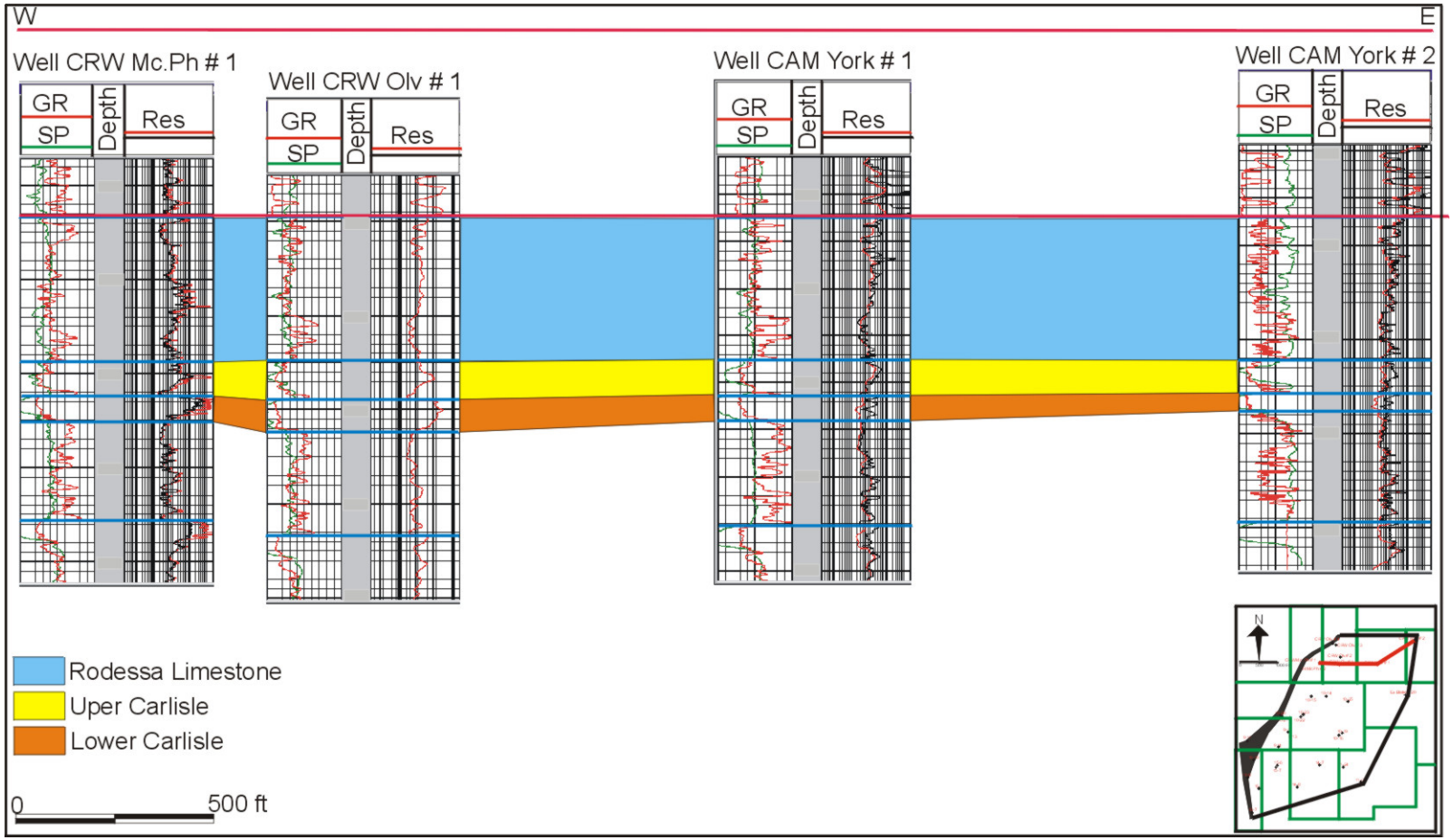

Figure 27. A west – east stratigraphic cross section in the northern part of the field illustrating the distribution of the Rodessa Limestone and the Carlisle Sandstone (datum is the base of the Ferry Lake Anhydrite).

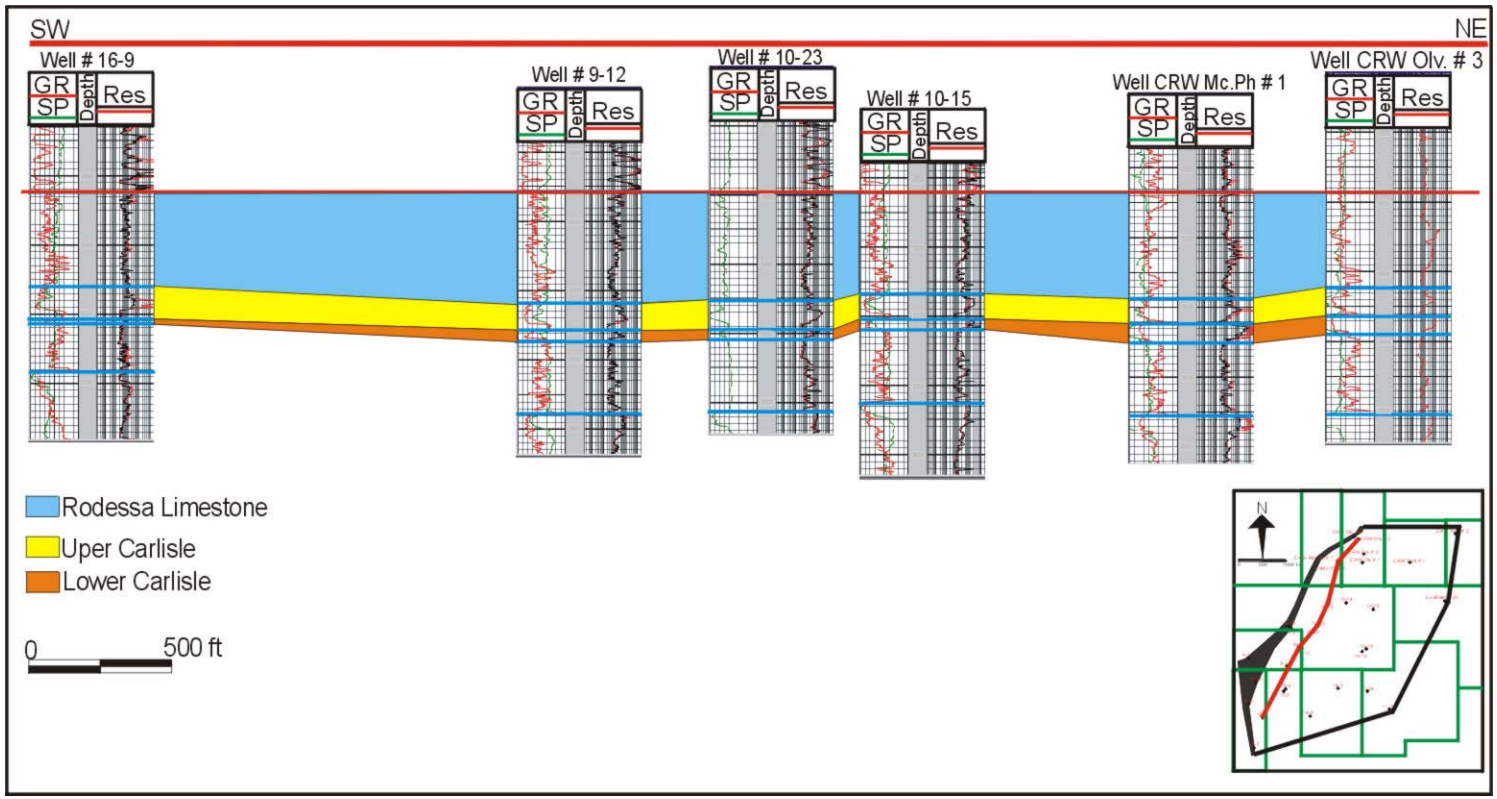

Figure 28. A southwest – northeast stratigraphic cross section illustrating the distribution of the Rodessa Limestone and the Carlisle Sandstone (datum is the base of the Ferry Lake Anhydrite).

RESERVOIR PROPERTIES

The reservoir properties such as porosity, permeability, and water saturation (Sw) were measured from the Brawner 10-22 core. In cases where core measurements were not available, these values estimated with wireline log calculations.

Reservoir Rocks and Pore Types

The reservoir rocks in this study were first identified in the cored well. Variations in facies along with general lithologies were calibrated against the suite of logs available for the cored well. For the remainder of the field, reservoir rocks and porosity were estimated from calibrated log signatures and from calculations to estimate permeability and saturation. Cross sections for the reservoir units in the field are shown in Figures 29 - 31.

Based on the core sample description, reservoir unit 1 is mainly composed of peloidal grainstones and siliciclastic sandstones (lithofacies 6 and 7). It has an average effective porosity of about 9 percent and 27 millidarcies of permeability. Reservoir unit 2 is composed mainly of siliciclastic sandstones (lithofacies 7), which have average porosity and permeability values of about 11 percent and 53 millidarcies.

For the carbonate rock types, the porosity classification used in this study was developed by Ahr (1995). This classification describes pore type along with processes that formed them, for example, depositional, diagenetic, and fracture porosity.

Depositional pore types relate to original texture and fabric and they include intergranular, intragranular, fenestral, and shelter porosity. Diagenetic pore types are those formed by diagenetic processes such as dissolution, neomorphism, and replacement. Diagenetically enhanced pores include moldic, vuggy, intercrystalline, and solution enhanced porosity. Fracture pore types are those formed by fracture or fault. The porosity classification of designed by Ahr (1995) is shown in Figure 32.

Rodessa pore types can be grouped as depositional, diagenetic, fracture, and as a combination of more then one type. The depositional pore types are dominant (more than 60 percent). Almost the entire interval displays a combination of intergranular and intraganular porosity except in sandstones. The sandstones exhibit purely intergranular porosity. The diagenetic pore types such us moldic, vuggy, intercrystalline, and solution enhanced porosity are the next most abundant type. Those porosity types can be observed in some places mainly in skeletal limestones. Based on that classification, the Rodessa Formation in the Van Field is fabric/facies selective. In other words, the porosity in this formation within the field generally was developed during deposition and then increased or decreased by diagenetic processes.

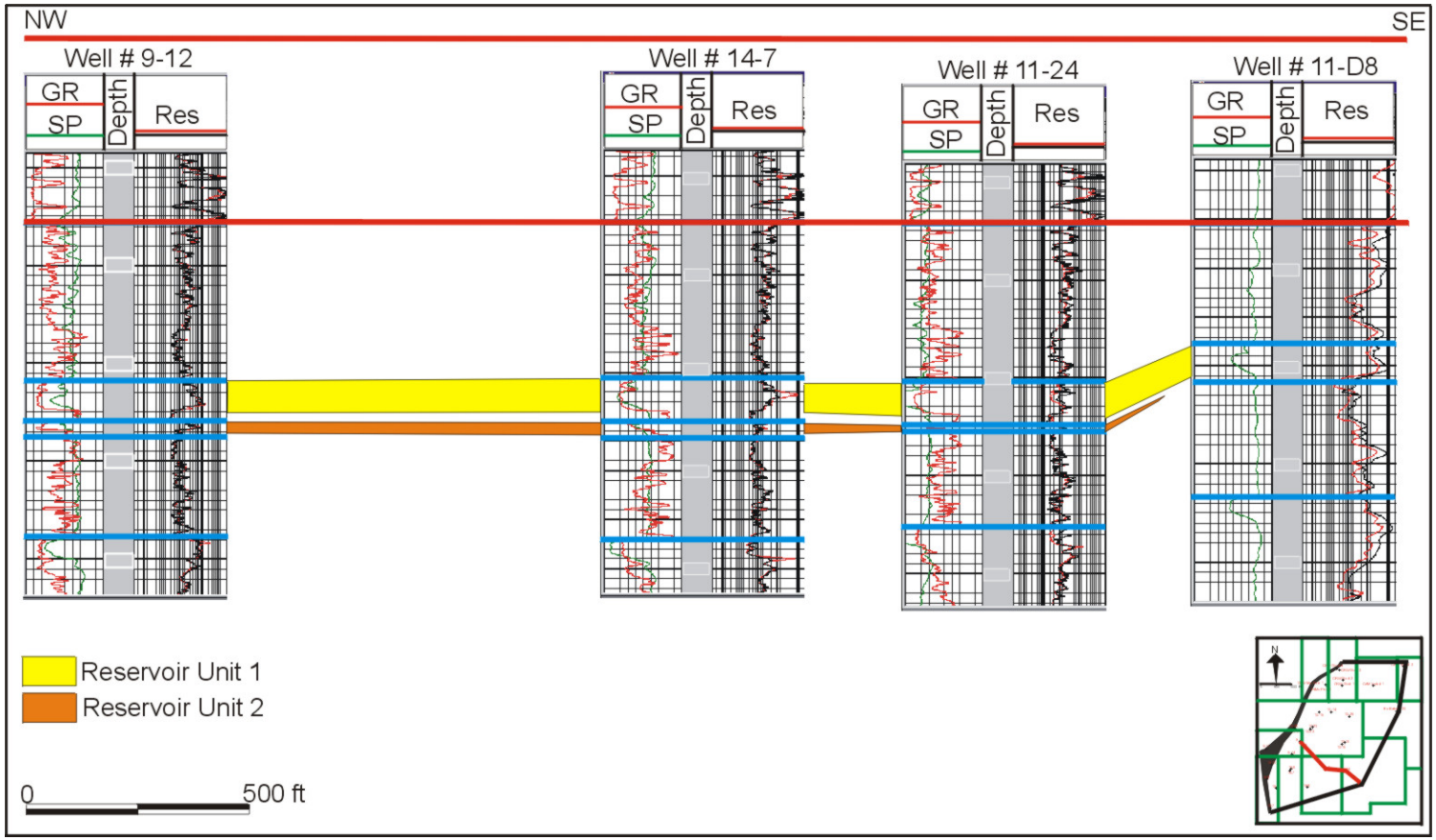

Figure 29. A northwest - southeast cross section illustrating the Van Field reservoir units. Note that the reservoir unit 2 thins to the east (datum is the base of the Ferry Lake Anhydrite).

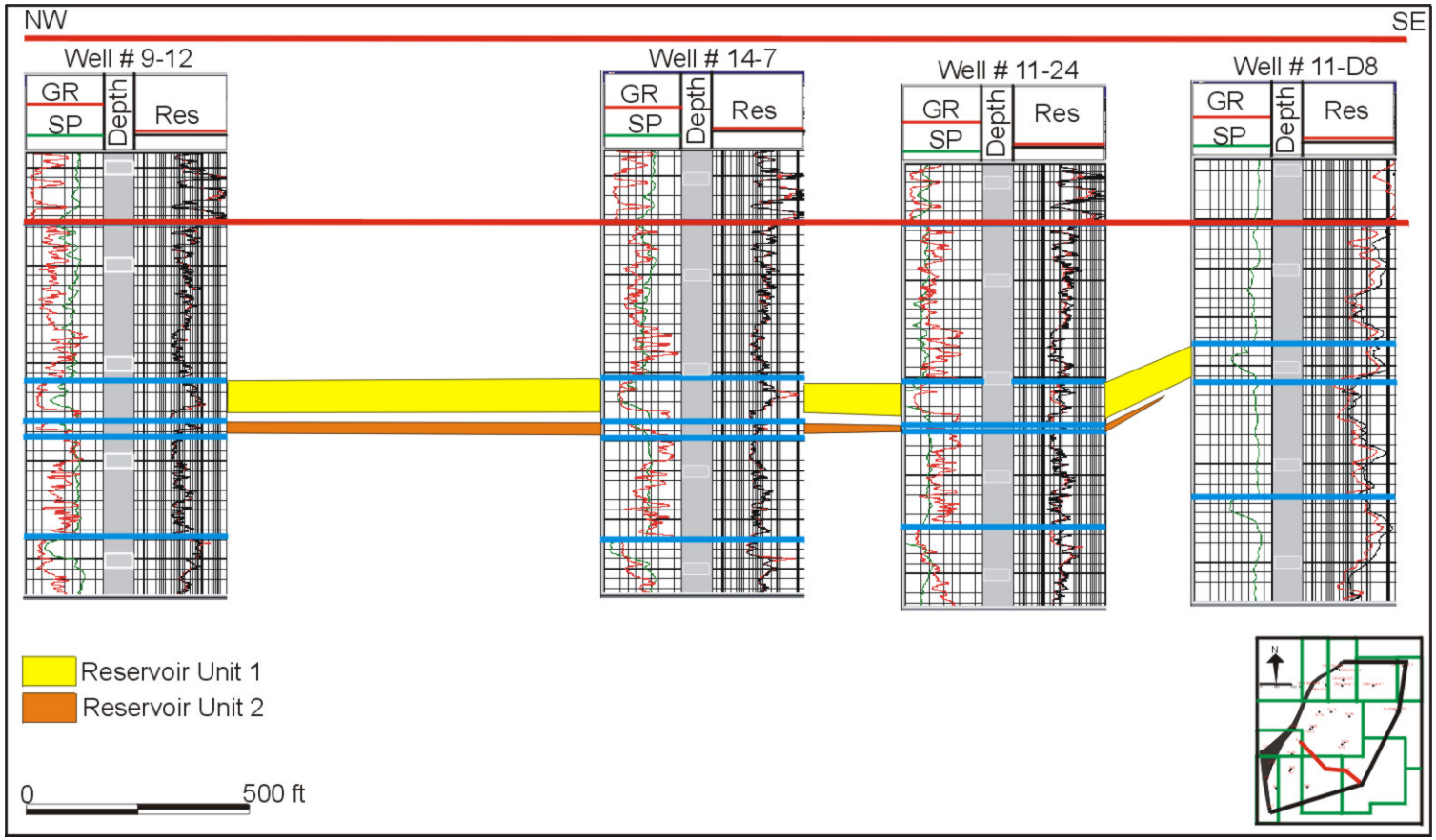

Figure 30. An east - west cross section illustrating the reservoir units across Van Field (datum is the base of the Ferry Lake Anhydrite).

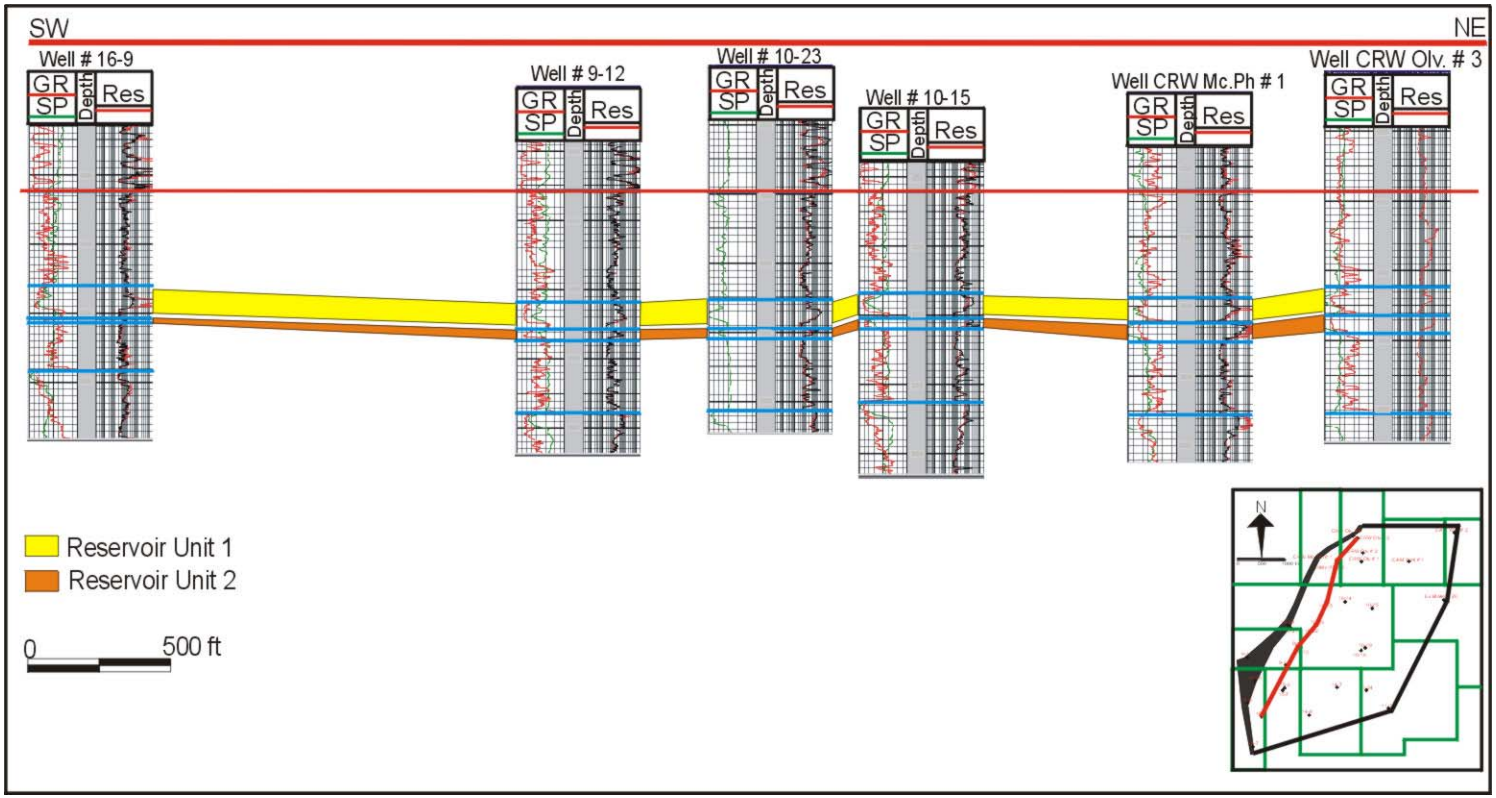

Figure 31. The southwest - northeast cross section illustrating the reservoir units across the field (datum is the base of the Ferry Lake Anhydrite).

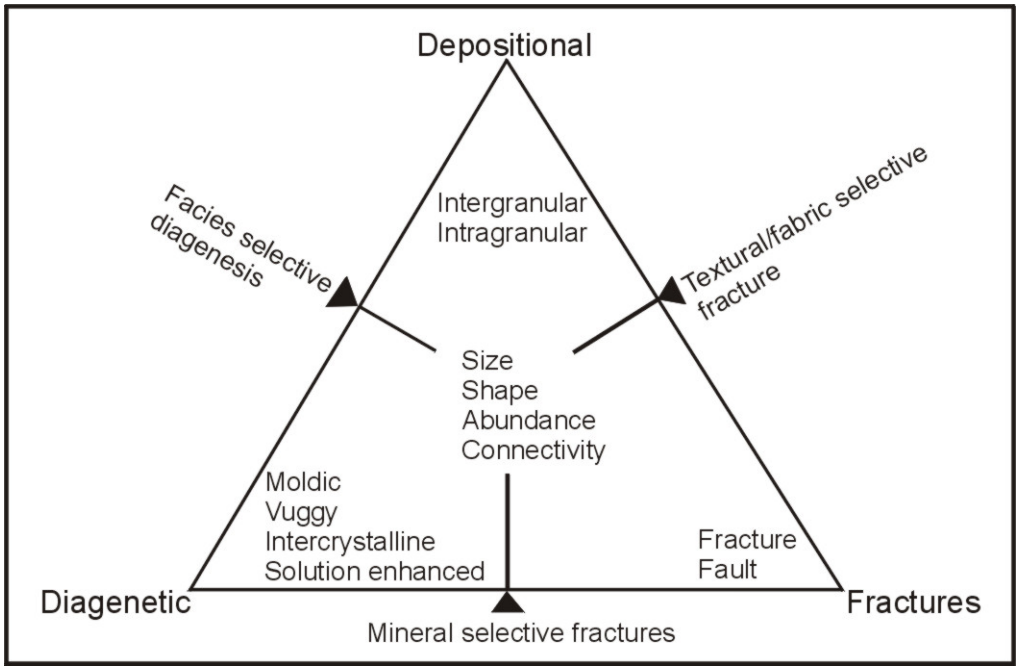

Figure 32. Porosity classifications for carbonate reservoir (modified from Ahr, 1995).

Petrophysical Analysis

Core-Log Integration

Permeability is arguably the most important characteristic in hydrocarbon reservoirs; therefore, it is particularly important to find methods for estimating permeability when measured values from cores are unavailable. Fortunately, one well in the study area had been cored and measured values of porosity and permeability were available from it. The measured values formed the basis for comparison with calculated porosities from wireline log data. Measured permeability is plotted as a function of measured porosity to determine the equation of a straight line. That equation is then used to estimate permeability from calculated porosity where cores are not available.

In order to insure that core and log depths coincide, depth shifting and averaging is necessary. This has been done in the Brawner 10-22 well to get a better relationship between core and borehole log parameters. In the 10-22, there are two kinds of electric log data available: gamma-ray (GR) and density porosity (PHID). The PHID log provides the necessary information to compute permeability estimates using the slope-intercept equation mentioned earlier. The core description and petrophysiscal parameters along with the log traces from the GR and PHID logs are shown in Figure 33. Petrophysical parameters for the reservoir are shown in figure 34.

The regression analysis applied in reservoir units 1 and 2 revealed a strong relationship between core porosity and core permeability ($R^2 = 0.944^2$), between density porosity and core porosity ($R^2 = 0.907^2$), and between density porosity and core permeability ($R^2 = 0.91^2$). All correlation above was compared with gamma ray value. The gamma ray correlated moderately with porosity and permeability. The discrepancy of gamma ray toward porosity and permeability might be caused by the presence of radioactive minerals such as potassium feldspar, micas, or glauconite that associated with the sandstones. Linear regression analyses of those petrophysical parameters are illustrated in Figure 35, 36, and 37. A straight line model was used with the linear regression calculations and has been used to obtain permeability estimates (pseudo-permeability) for the non-cored wells in the study area. The equation is:

$$y = 0.000048 \times 10^{32.444702x} \quad \ldots\ldots\ldots\ldots\ldots\ldots\ldots\ldots\ldots\ldots \; 5$$

where porosity is plotted on the x axis and permeability on the y axis.

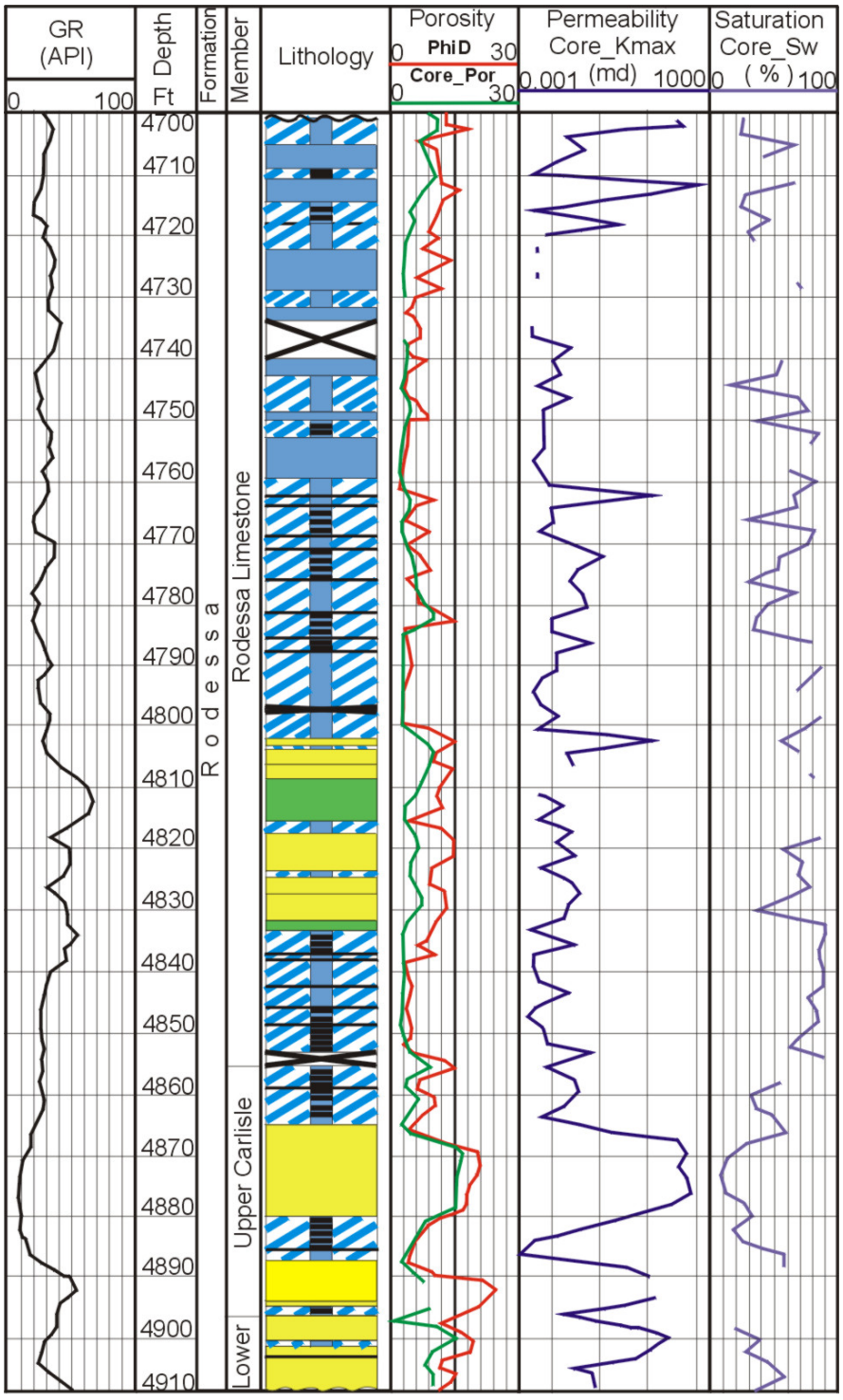

Figure 33. Core lithology, together with core permeability (core_k), core porosity (core_por), core water saturation (core_sw), and two wireline logs (gamma ray and density porosity).

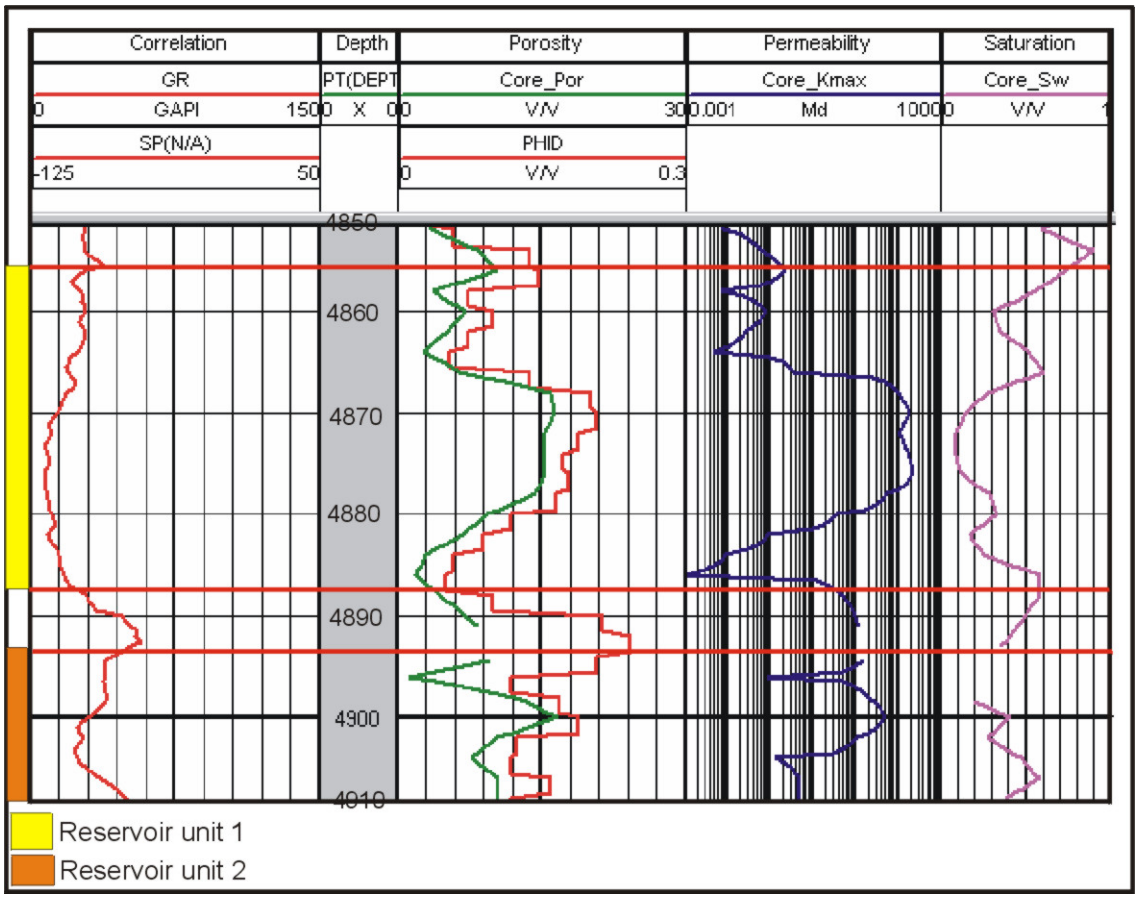

Figure 34. The petrophysical parameter of the interval of interest (reservoir units 1 and 2).

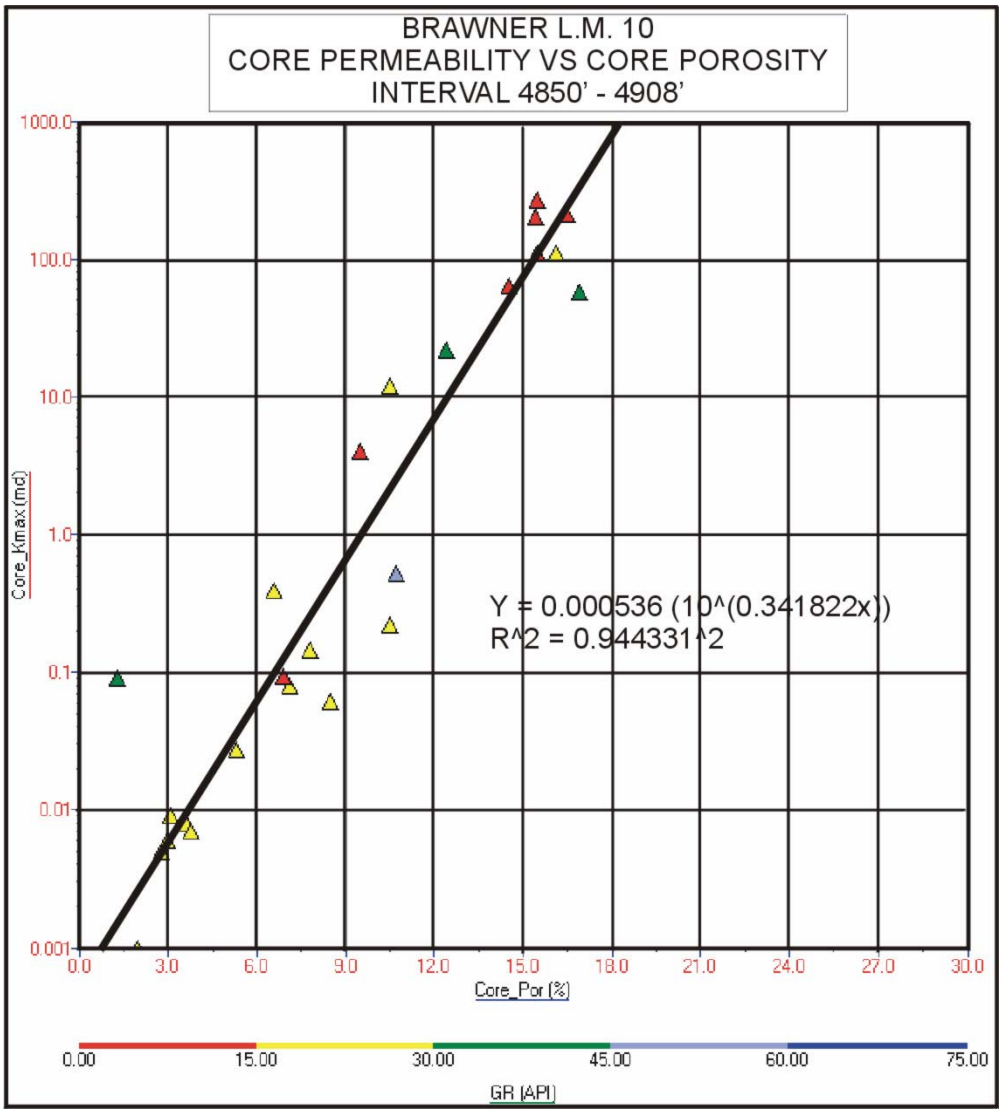

Figure 35. Cross plot of core permeability and core porosity compared with the gamma ray values in the interval of interest. The correlation coefficient, R^2, is 0.944^2.

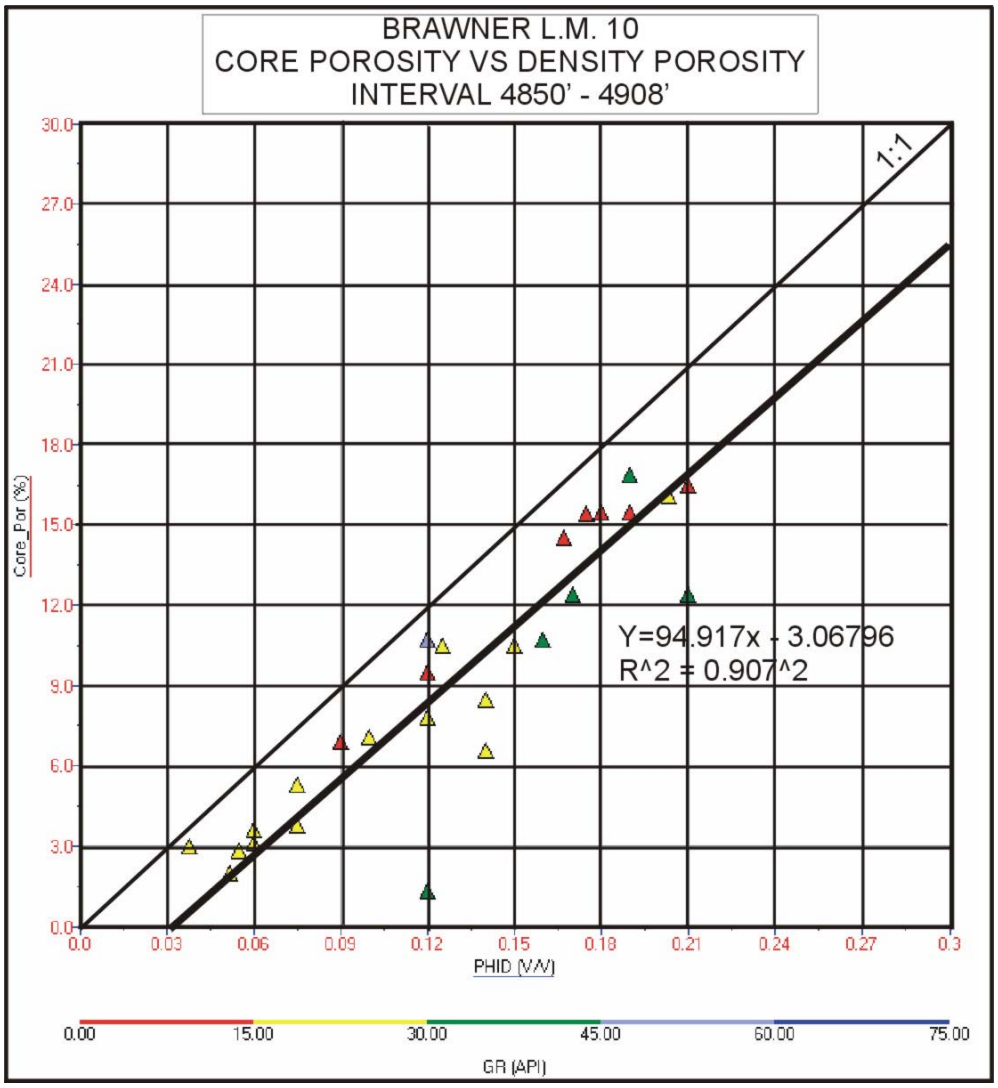

Figure 36. Cross plot of core porosity and density porosity compared with gamma ray values in the interval of interest. It shows a systematic different between core and log porosities of about 4 p.u; assumption of a limestone matrix is a possible cause. To get log porosity agree with core porosity, a change in matrix value is needed. The correlation coefficient, R^2, is 0.907^2.

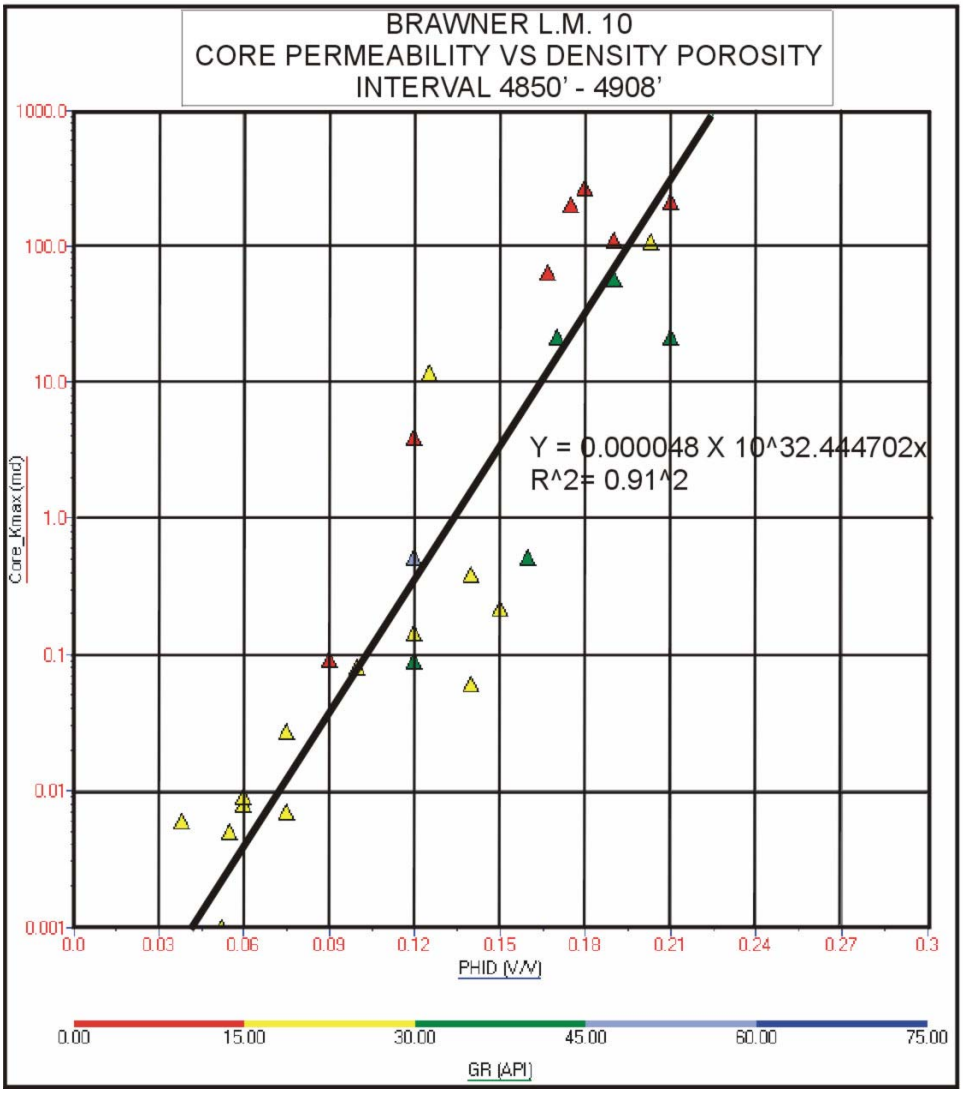

Figure 37. Cross plot of core permeability and density porosity compared with gamma ray values in the interval of interest. The correlation coefficient, R^2, is 0.91^2.

Spatial Distribution and Quality Ranking of Poroperm Values

"Slice maps" were made to represent the average values of porosity and permeability in the interval of interest (reservoir unit 1 and 2) over each 10 foot interval of depth from the top of the Carlisle downward. Porosity is grouped into classes following the qualitative classification by Archie (Ahr, 1995 after Archie, 1952) and permeability is grouped following the qualitative classification by North (Ahr, 1995 after North, 1985). Tables 2 and 3 show those qualitative classifications of porosity and permeability.

Table 2. Archie's porosity classification and qualitative description (modified from Ahr, 1995 after Archie, 1952)

Porosity range (%)	Qualitative description
5 or less	Poor
10	Fair
15	Good
> 20	Excellent

Table 3. North's permeability classification and qualitative description (modified from Ahr, 1995 after North, 1985)

Permeability range (md)	Qualitative description
<1.0 – 15	Poor to fair
15 – 50	Moderate
50 – 250	Good
250 – 1000	Very good
> 1000	Excellent

Based on the two classifications above, a reservoir quality ranking scheme has been developed for the study area. Quality is defined by identifying the highest combined porosity-permeability paired values. The reservoir ranking is then applied to each slice in the stack of slice maps for the interval of interest (reservoir unit 1 and 2). A color code was created to represent the different quality ranks. An example of the reservoir slice map is shown in Figure 38. The quality ranking for each reservoir unit is discussed below.

In reservoir unit 1, the reservoir thickness is almost uniform across the study area. It has an average porosity of about 8.5 percent and 46 millidarcies of permeability. The slice representing vertical depths of 10-20 feet below the top of the Carlisle shows that almost 60 percent of the north-central field area exhibits "good quality" reservoir poroperm values. Within reservoir unit 2, there is a "quality shift away" from the center of the field area toward the north. It has an average porosity and permeability values of about 10.7 percent and 896 millidarcies. By depths of 50-60 feet below the datum (top of Carlisle), the best reservoir quality zones appear around the CRW Olv. No. 1 and CRW Olv. No. 2 wells. The complete quality rankings for each depth slice are shown in Appendix B.

Relationship between Porosity-Permeability and Facies

Porosity-permeability data for the entire Rodessa Formation indicate a strong relationship between depositional lithofacies and poroperm pairs (Figure 39). The lithofacies dominated by skeletal constituents shows a broad range of porosity-

permeability, while non-skeletal rocks show a relatively narrow, more predictable range of porosity and permeability. Regardless of the effects of cementation, the broad range and less predictable values of porosity-permeability in the skeletal facies is probably related to bimodal (leached and non-leached) porosity. Less predictability in poroperm values also means less accuracy in estimating permeability with the linear equation. The most uniform and predictable reservoir is the Carlisle sandstone lithofacies, which has a narrow range and predictable relationship in porosity-permeability values. This is probably because the sandstones have only intergranular porosity and the pore-pore throat size relationship varies only within narrow limits as compared with the carbonate pores and pore throats in the Rodessa Limestone.

Water Saturation

Water saturation (Sw) is defined as the fraction of the pore space occupied by water. The water saturation in this study is been calculated using the Simandoux equation (Eq. 1), which has been chosen because of the high shale content of the sandstones in the study area. The presence of shale or clay minerals can cause erroneous values of water saturation and porosity derived from logs (Asquith, 1982). Some porosity logs, such as sonic and neutron, record anomalously high porosity levels when V_{shale} is high. Density logs normally are more accurate, as long as the shale density is equal to or greater than the matrix density of the reservoir. If the shale effect is ignored, the S_w calculated with the Archie equation will have a relatively higher value than the real value and will result in overestimation of hydrocarbon saturation.

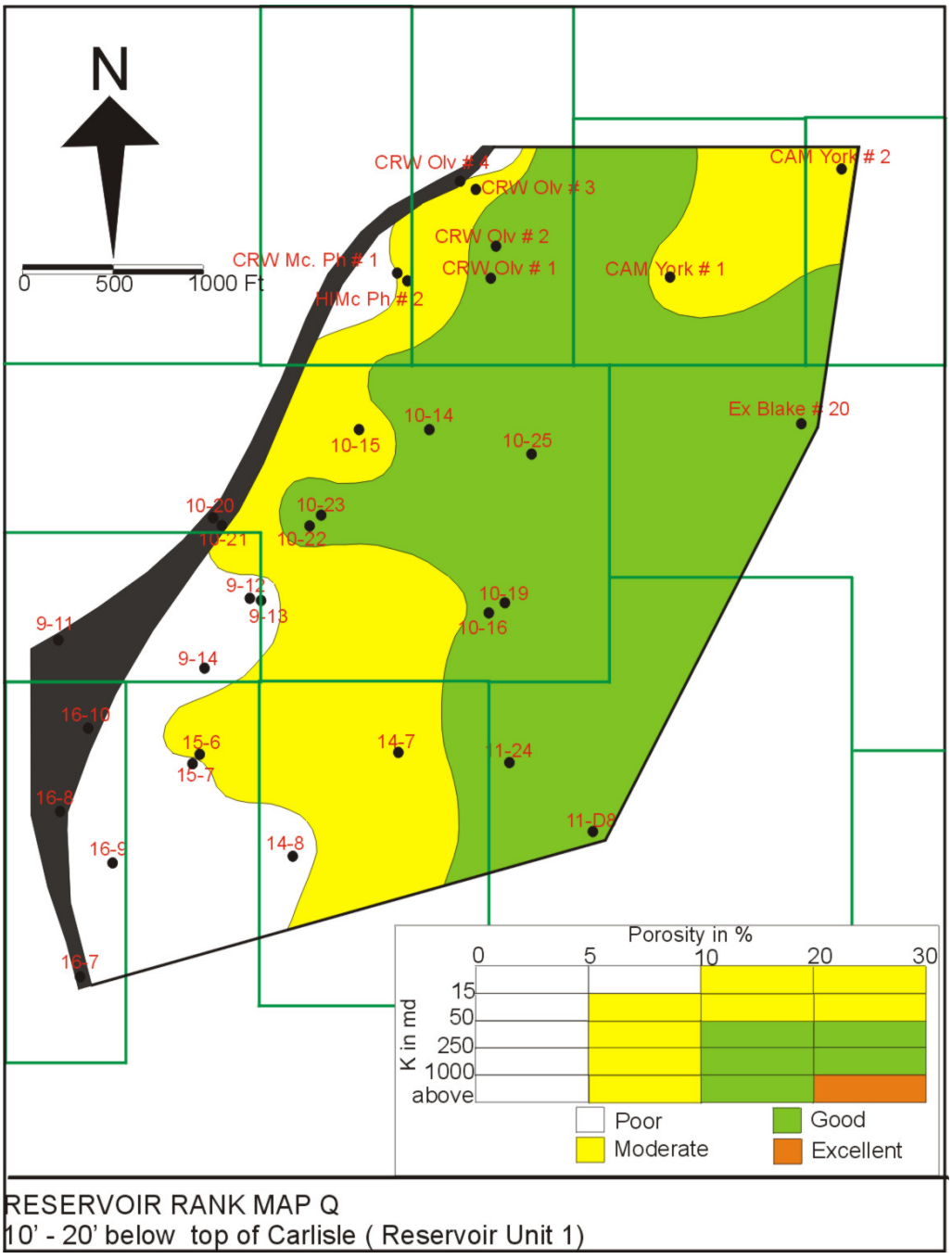

Figure 38. The slice map reservoir quality rank within the reservoir unit 1 at a depth of 10-20 feet below the top of Carlisle.

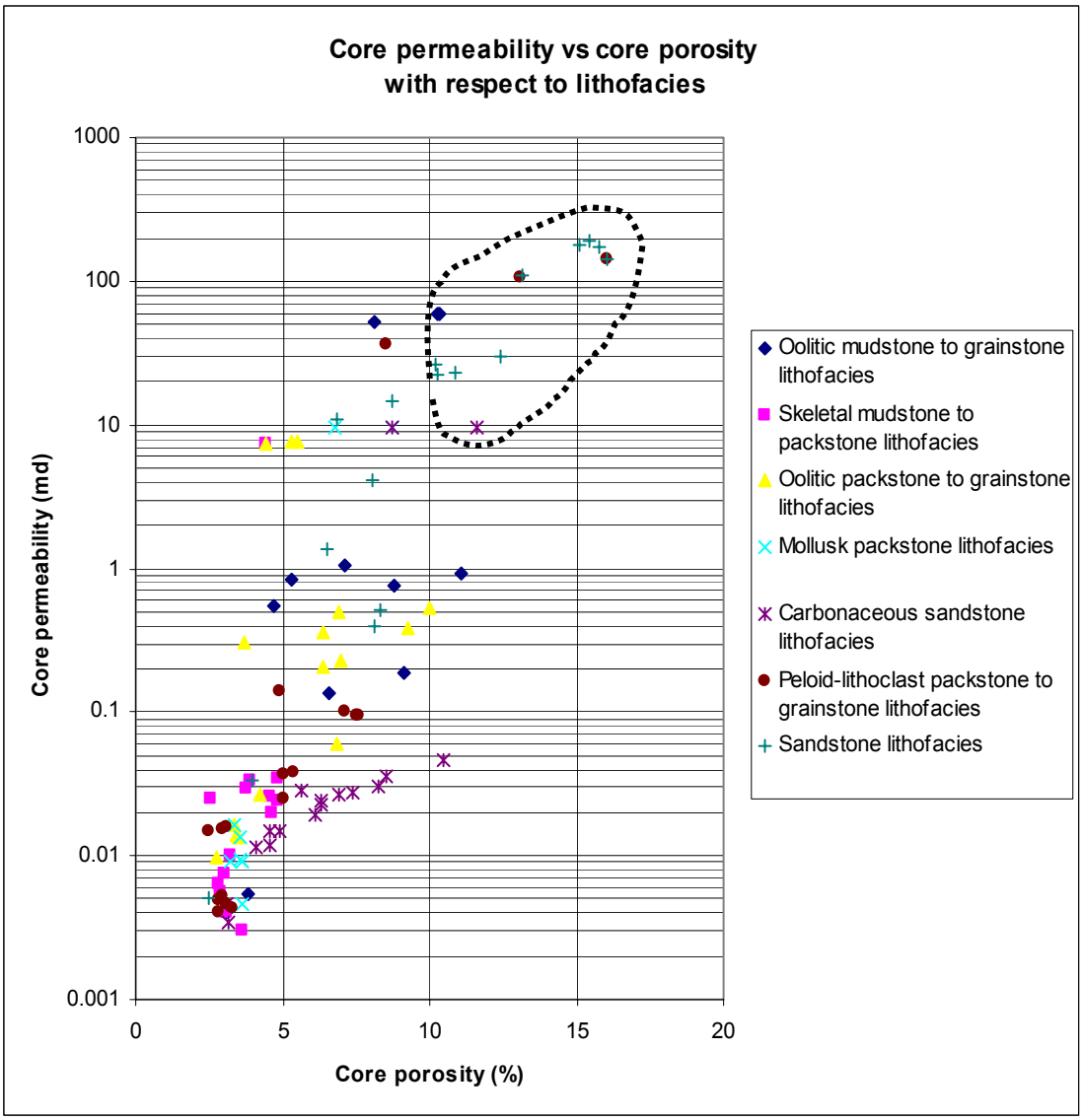

Figure 39. Cross plot core permeability and core porosity compared with lithofacies showing that sandstones comprise the best reservoir in the Rodessa Formation. Dashed line is representing the reservoir's lithofacies.

The Simandoux equation requires some preliminary calculations before going through the equation itself. The first step is determining the volume of shale (Vsh) from a gamma ray log. After that, the Vsh is applied to correct the porosity log for shale effects. After those steps, the Simandoux equation can be used. One variable used in the Simadoux equation is the water resistivity. The water resistivity was obtained by generating a Pickett plot. The Pickett plot (Figure 40) is a double logarithmic plot of a resistivity measurement on the x-axis versus a porosity measurement on the y-axis.

The water saturation analysis showed that hydrocarbon bearing zones are present in both reservoir units within the Carlisle sandstone. The water saturation in the reservoir unit 1 ranges from about 10 to 50 percent. In reservoir unit 2, water saturation ranges from about 10 to 60 percent. In the upper part of the Rodessa Limestones, the water saturation calculation shows value ranges from about 10 to 70 percent, but error is possible due to the presence of anhydrite. Anhydrite generally has high resistivity due to lack of fluid that transmit electric current. The presence of anhydrite within the formation can result in low calculations of water saturation. Thus, low water saturation in an anhydritic interval is not clearly representing hydrocarbon content. The example of petrophysical analysis is shown in Figure 41.

Average S_w values for each 10-foot core slice were calculated and plotted to generate field-scale water saturation distribution maps. Generally the low water saturations are located in the western part of the study area, stretching along the fault boundary. Water saturation increases gradually to the east. Although the oil - water

contact was not clear enough to identify for all reservoir units, it shows a southwest-northeast trend. The average field-scale water saturation map is illustrated in Figure 42.

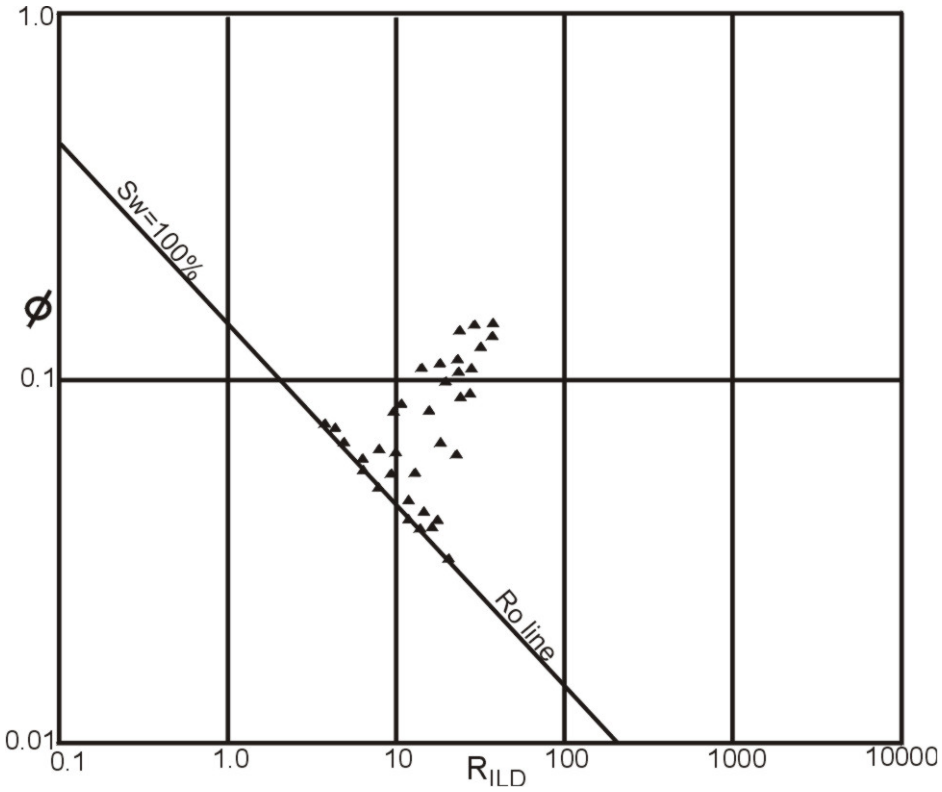

Figure 40. Example of a Pickett plot taken from well CRW Olv No. 4.

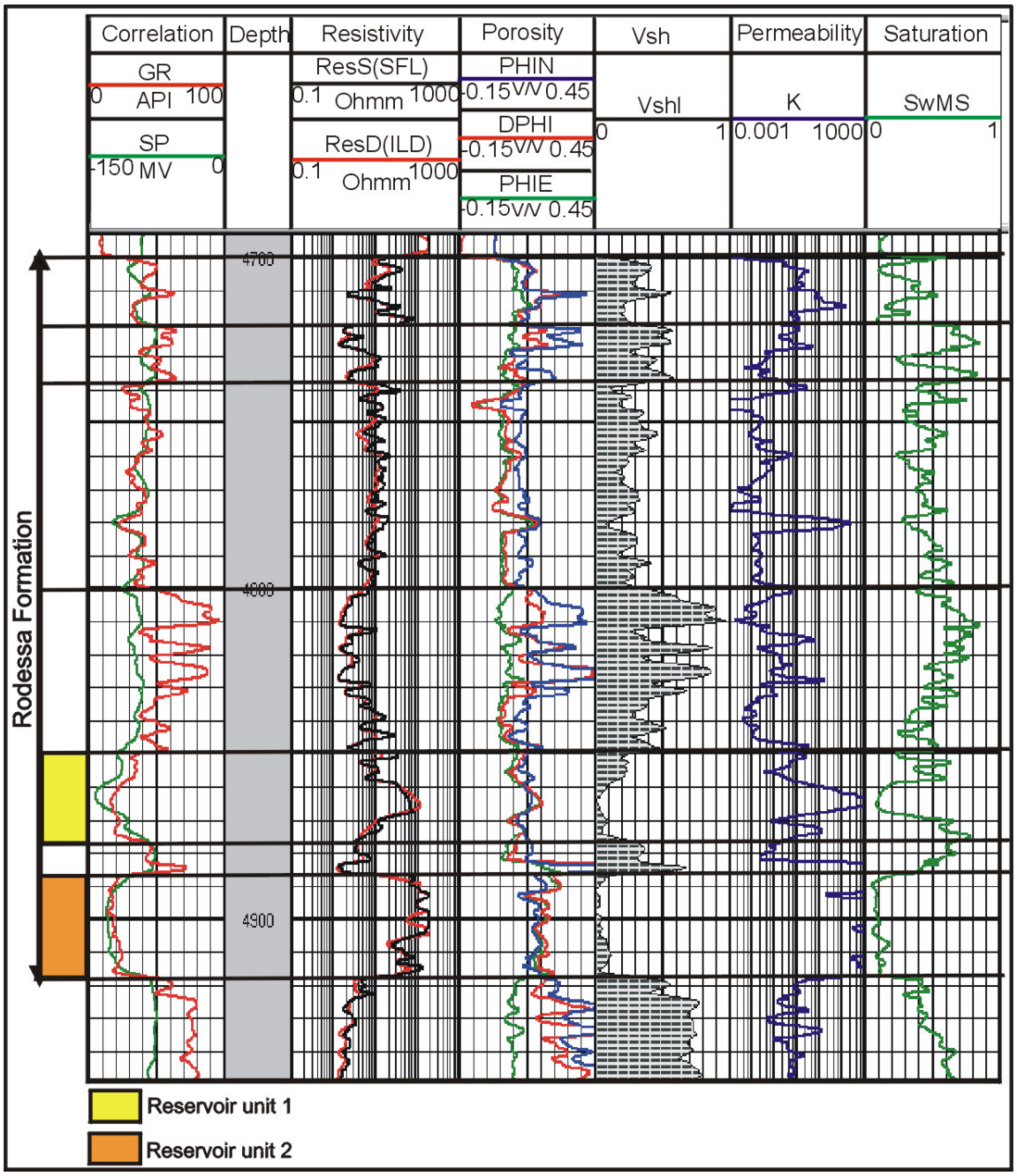

Figure 41. Well log analyses of the CRW Olv No. 2 for each reservoir unit. Good reservoirs with low water saturation are shown in reservoir unit 1 and 2.

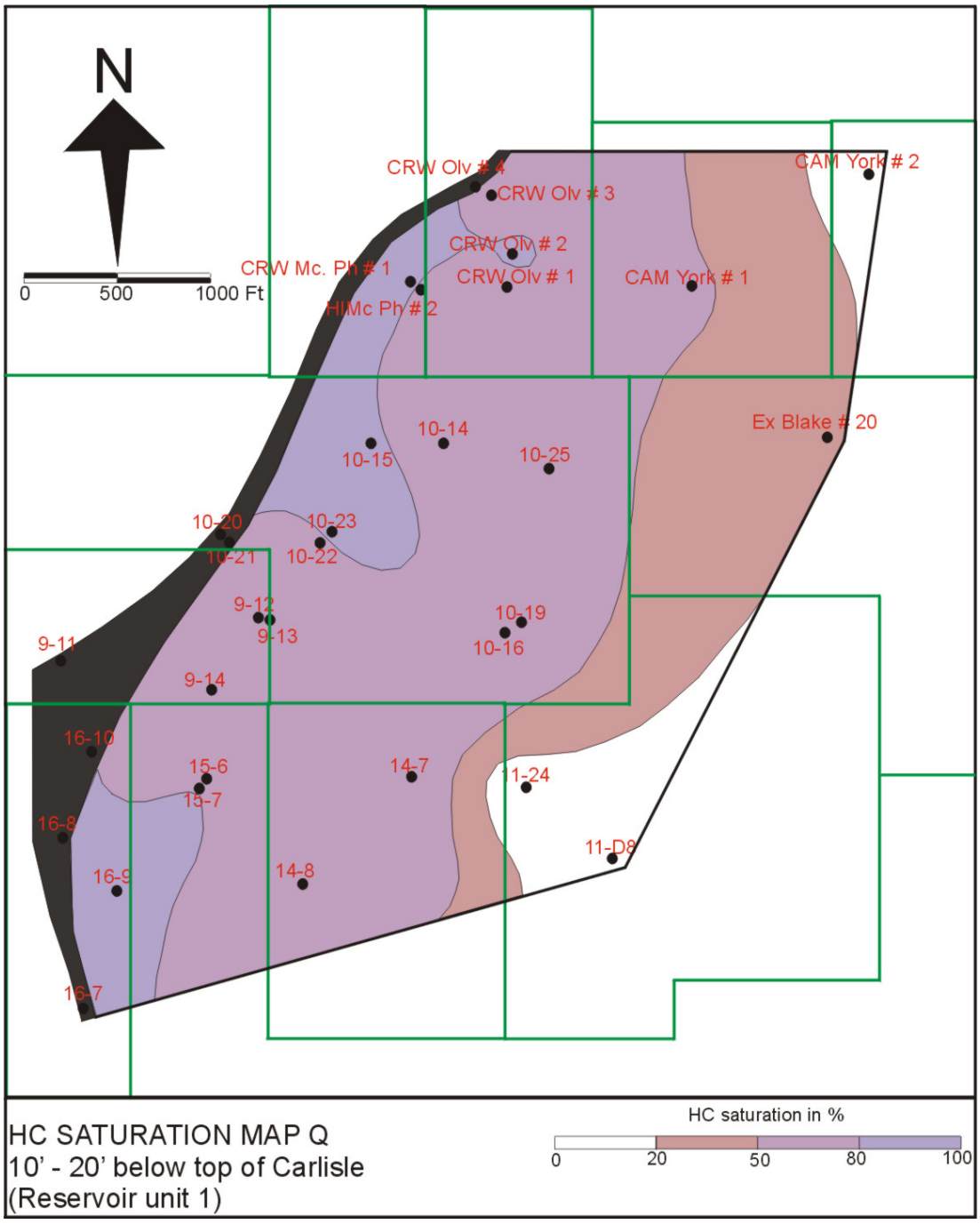

Figure 42. Field-scale average water saturation distribution map for the slice at a depth of 10-20 feet below the top of the Carlisle Sandstone, which is part of reservoir unit 1.

DISCUSSION

A single core from the Brawner 10-22 well in Van Field represents the entire Rodessa formation in the study area. Seven lithofacies were identified in the core; two of the seven are reservoir facies and five are non reservoir facies. The Rodessa Formation can be divided into two members; the Rodessa Limestone and the Carlisle Sandstone.

The complete core was examined and described in detail. The lithological changes in the core from bottom upward represent gradual changes in depositional regimes. Interval D, which is the lower part of the Rodessa interval, represents a high energy depositional system. Interval A is followed by the limestones dominated interval mixed with terrigenous clastics (Interval C). Fine grain carbonaceous sandstones are overlain by interval B. The top 104 feet of Rodessa Formation consist of interbedded skeletal and non skeletal limestones, which reflect broad shallow water environments varying from subtidal sand bar to lagoon to intertidal-sebkha. Field-scale depositional environments were identified using well log signatures. Subsequently, synthetic depositional models were developed from core and log information. Both the core derived and log derived depositional models reflect the shallowing upward depositional sequences that are interpreted to be typical of a tropical marine environment. It has been reported that shallowing-upward sequence are common in the Rodessa Formation (Bushaw, 1968, and Rainwater, 1970). Those workers explain the shallowing trend as a reflection of an overall regression.

Rodessa rocks exhibit abundant diagenetic alteration. Notably, five main types of alteration were noted in the study core. They are micritization, cementation, dissolution, neomorphism, and compaction. Dissolution is the main factor that enhanced porosity, while cementation reduced it. In short, porosity is depositional in origin, but diagenesis affected it, so the most common pore type in Van Field is fabric/texture-selective diagenetically altered porosity. Although the diagenetic sequence in the Rodessa Formation is complex because of fluctuating sea level during the cretaceous period, a general diagenetic history for the Rodessa Formation in Van Field is interpreted as beginning in the marine phreatic and passing through fresh water meteoric and shallow burial (subphreatic) environments. No evidence of hydrothermal mineralization or other types of deep burial diagenesis were detected.

Two reservoir units can be identified in Van Field. Reservoir unit 1 corresponds with lithofacies 6 (peloid-lithoclast packstone to grainstone lithofacies) and the upper part of lithofacies 7 (sandstone lithofacies). Reservoir unit 2 corresponds with the lower part of lithofacies 7. The best quality reservoir occurs in unit 2, the coarse sandstone zone in the Carlisle member of Rodessa Formation. Studies of water saturation in the field show that reservoir unit 2 is a hydrocarbon bearing zone. The distribution of reservoir quality in this zone conforms nicely with the synthetic depositional environment derived mainly from interpretation of log signatures. It is possible to generate an “electrofacies map” in the Carlisle sandstones, but it is not possible to do so in the Rodessa Limestones.

CONCLUSIONS

1. The Rodessa Formation consists of limestones and sandstones that were deposited on a broad, restricted, shallow marine platform. Depositional facies are dominated by shallowing-upward sequences interpreted to be lagoonal, subtidal, and intertidal.
2. Diagenesis, including micritization, cementation, dissolution, neomorphism, and compaction has extensively altered rocks in the study area. Porosity and permeability were enhanced by dissolution and reduced by cementation and compaction. Diagenesis is interpreted to have begun in the marine phreatic environment and continued through the fresh water phreatic and shallow burial environments
3. Rodessa reservoir rocks exhibit intergranular, intragranular, vuggy, and moldic porosity of depositional origin with a diagenetic overprint.
4. Two reservoir units can be identified from core and well log interpretation. Based on core measurements in Brawner 10-22 well, from the top to the bottom they are: Reservoir unit 1 has an average porosity and permeability of about 9 percent and 27 millidarcies, respectively. This reservoir unit consists of pelloidal grainstones and sandstones (lithofacies 6 and 7). In cored well, reservoir unit 2 has an average porosity and permeability of about 11 percent and 53 millidarcies. Core study reveals that unit 2 consists of coarse, siliciclastic sandstones (lower part of lithofacies 7). Based on well log calculation for all wells in the study area, the reservoir unit 1 has an average of porosity and permeability values of about 8.5 percent and 46

millidarcies, respectively. Reservoir unit 2 averages 10.7 percent porosity and 896 millidarcies permeability.

5. The reservoir units extend more or less evenly across the field, but the best reservoir quality zones exist in unit 2 in the north-central part of Van field.
6. Both units 1 and 2 are hydrocarbon bearing with S_{hc} values varying from 40 to 90 percent.
7. Field-scale S_w maps show that the lower saturation values exist in the western part of study area, they are elongate parallel to the Mexia-Talco fault zone that borders the study area, and saturation then increase toward the east in the study area.

REFERENCES CITED

Adams, A. E., and W. S. MacKenzie, 1998, A color atlas of carbonate sediments and rocks under the microscope: London, Mason.

Ahr, W. M., 1995, Unpublished lecture notes from "Carbonate Reservoir:" College Station, Texas A&M University.

Archie, G. E., 1952, Classification of carbonate reservoir rock and petrophysical considerations: AAPG Bulletin, v. 36, no. 2, p. 278-298.

Asquith, G. B., and C. Gibson, 1982, Basic well log analysis for geologists: Tulsa, AAPG, 216 p.

Asquith, G. B., and A. D. Jacka, 1992, Petrophysics of bimodal porosity: Lower Cretaceous Rodessa Limestones, Running Field, Houston County, Texas: Gulf Coast Association of Geological Societies Transactions, v. 42, p. 1-12.

Bebout, D. G., and R. G. Loucks, 1977, Cretaceous carbonate of Texas and Mexico: application to subsurface exploration: Bureau of Economic Geology, The University of Texas at Austin.

Burgess, J. D., 1990, Correlation of Cretaceous and Jurassic oil from Hunt and Kaufman Counties, Notheast Texas: Society of Economic Paleontologist and Mineralogist Publication 9 , p. 69-75.

Bushaw, D. J., 1968, Environmental synthesis of the East Texas Lower Cretaceous: Gulf Coast Association of Geological Societies Transactions, v. 18, p. 416- 438.

Dunham, R. J., 1962, Classification of carbonate rock according to depositional texture: *in* W. E. Ham, ed., Classification of carbonate rocks: AAPG Memoir 1, p. 108-121.

Forgotson, J. M., 1957, Stratigraphy of Comanchean Cretaceous Trinity group: AAPG Bulletin, v. 41, p. 2328–2368.

Jackson, M. P. A., and S. J. Seni, 1983, Evolution of salt structure, East Texas diapir province: AAPG Bulletin, v. 67, p. 1219–1274.

Keith, B. D., and E. D. Pittman, 1983, Bimodal porosity in oolitic reservoir: Effect on productivity and log response, Rodessa Limestones (Lower Cretaceous), East Texas Basin: AAPG Bulletin, v. 67, p. 1391–1399.

Longman, M. W., 1980, Carbonate diagenetic textures from near surface diagenetic environments: AAPG Bulletin, v. 64, p. 461–487.

Lowe, J. T., and D. B. Carington, 1990, Occurrence of oil in the Austin Chalk at Van Field, Van Zandt County, Texas: A unique geological setting: AAPG Bulletin, v. 74, p. 1502.

Lucia, F. J., 1992, Carbonate reservoir models: Facies, diagenesis, and flow characterization: AAPG Special Publication 95, p. 269–274.

Perkins, B. F., 1974, Geoscience and man: Aspect of Trinity division geology: Baton Rouge, School of Geoscience, Louisiana State University.

Pindell, J., and J. F. Dewey, 1982, Permo-Triassic reconstruction of western Pangea and the evolution of the Gulf of Mexico/Caribbean region: Tectonics, v. 1, p. 179-211.

Rainwater, E. H., 1970, Regional stratigraphy and petroleum potential of Gulf Coast Lower Cretaceous: Gulf Coast Association of Geological Societies Transactions, v. 20, p. 145–157.

Roberts, J. L., and B. E. Lock, 1988, The Rodessa Formation in Bossier Parish, Louisiana: Lithofacies analysis of hydrocarbon-productive shallow water clastic-carbonate sequence: Gulf Coast Association of Geological Societies Transactions, v. 38, p. 103–111.

Schlumberger, 1989, Log interpretation principles and applications: Houston, Schlumberger Educational Service, 244 p.

Sellers, P. B., Jr., and R. C. Phillips, Jr., 1979, Fiftieth anniversary of a model oil field: SPE Paper 8273, p. 1-9.

Swanson, R. G., 1981, Sample examination manual: AAPG Special Publication 92, p. 1-35.

Turner, J. R., 1993, A model for evolution of salt diapirs and salt dome canopy, East Texas Basin: Gulf Coast Association of Geological Societies Transactions, v. 43, p. 421– 430.

Wescott, W. A., and W. C. Hood, 1994, Hydrocarbon generation and migration routes in the East Texas Basin: AAPG Bulletin, v. 78, p. 287–306.

Wilson, J. L., 1975, Carbonate facies in geologic history: Berlin, Springer-Verlag.

APPENDIX A

CORE DESCRIPTION

Interval 4690' - 4760'

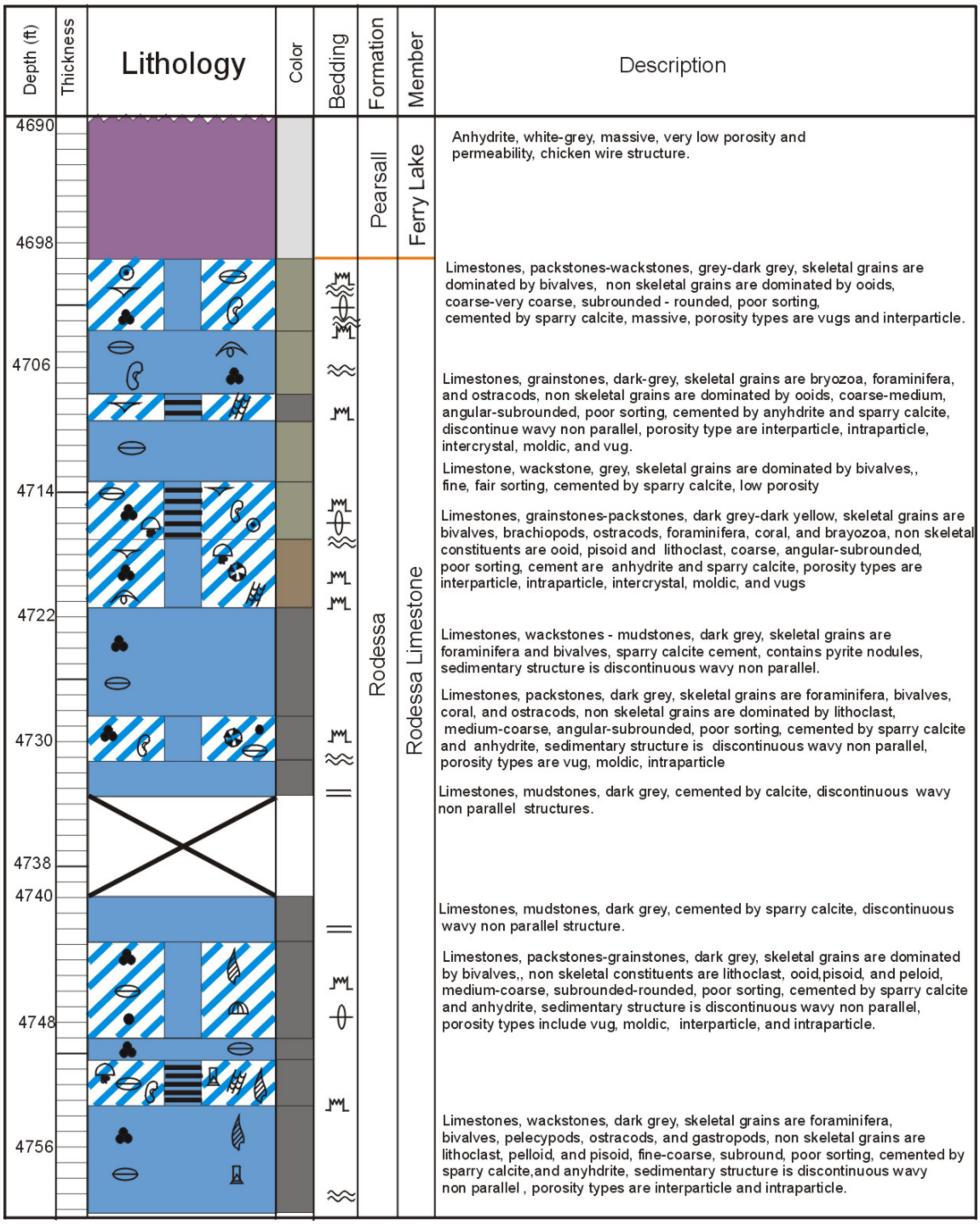

Interval 4760' - 4837'

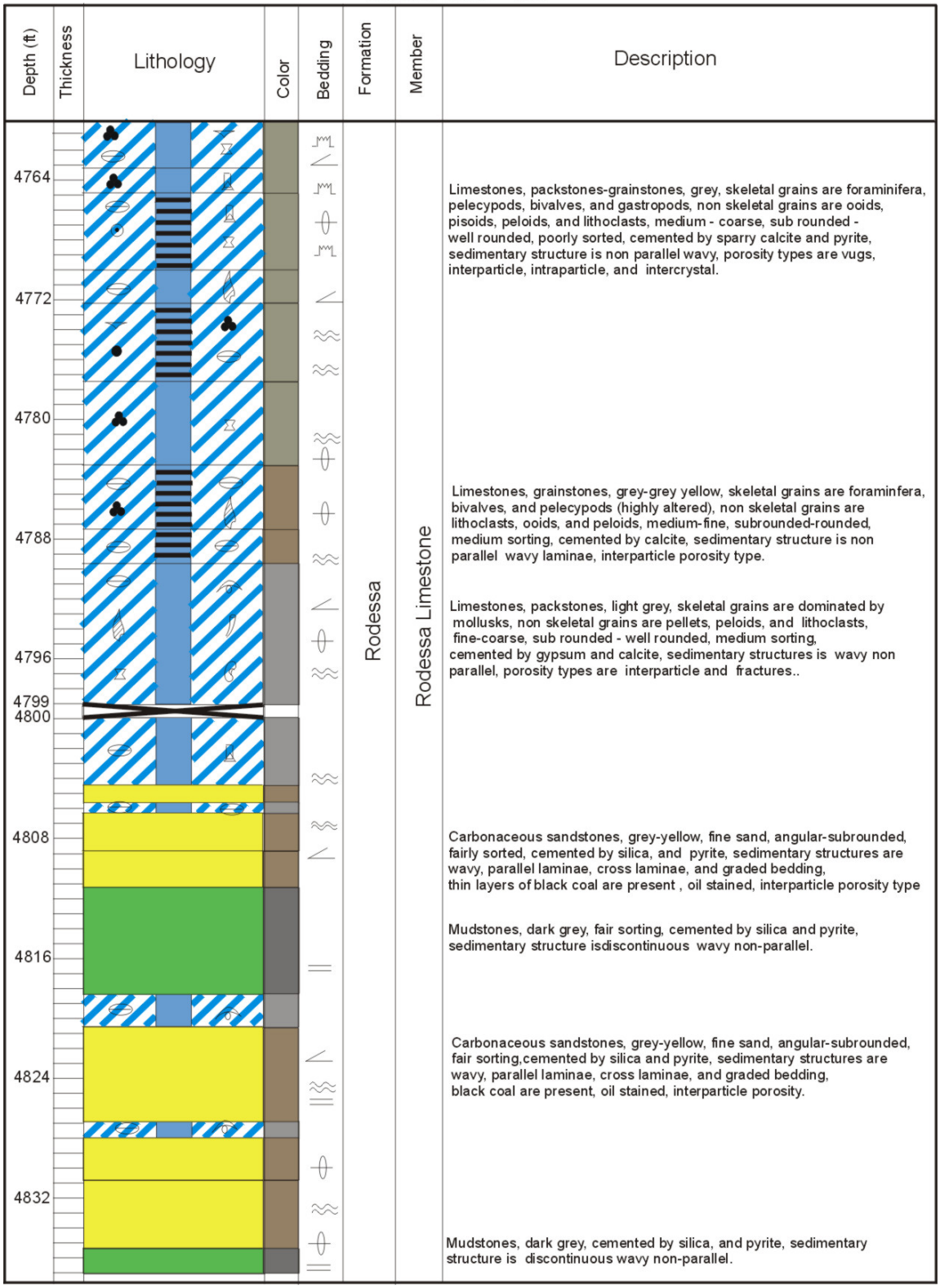

Interval 4837' - 4915'

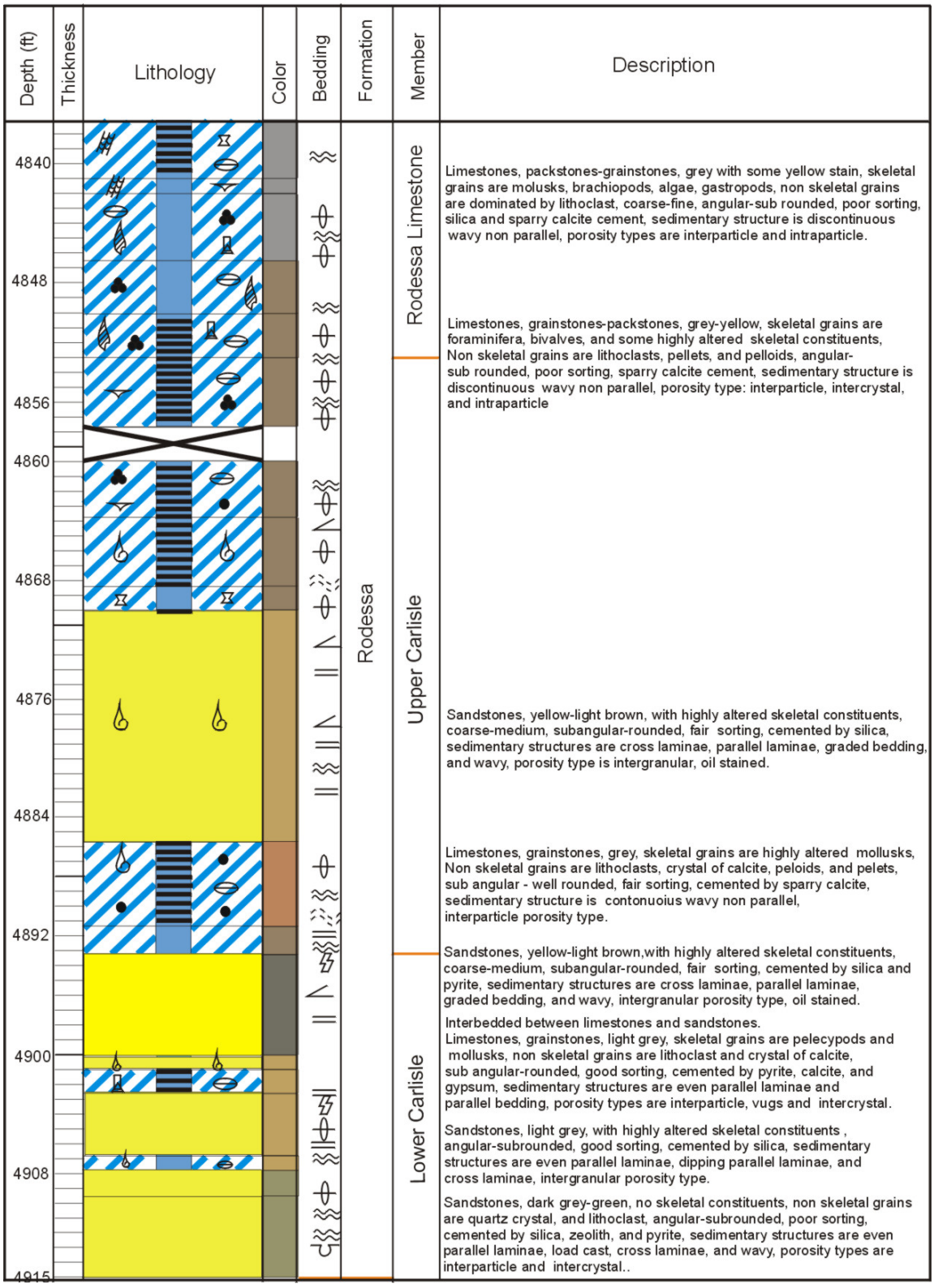

APPENDIX B

ISOPACH MAP OF RESERVOIR UNITS

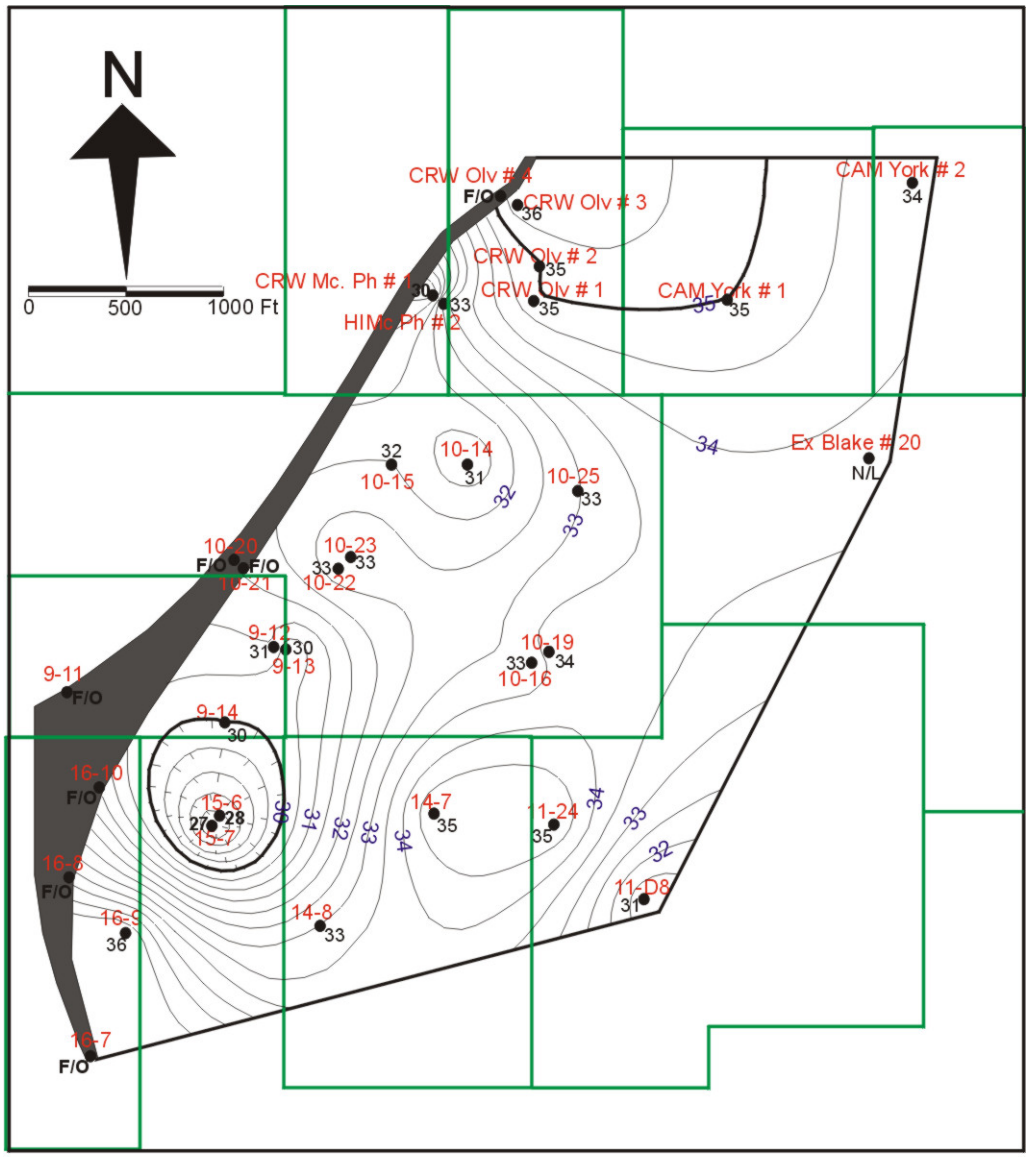

ISOPACH OF RESERVOIR UNIT 1 (in feet)

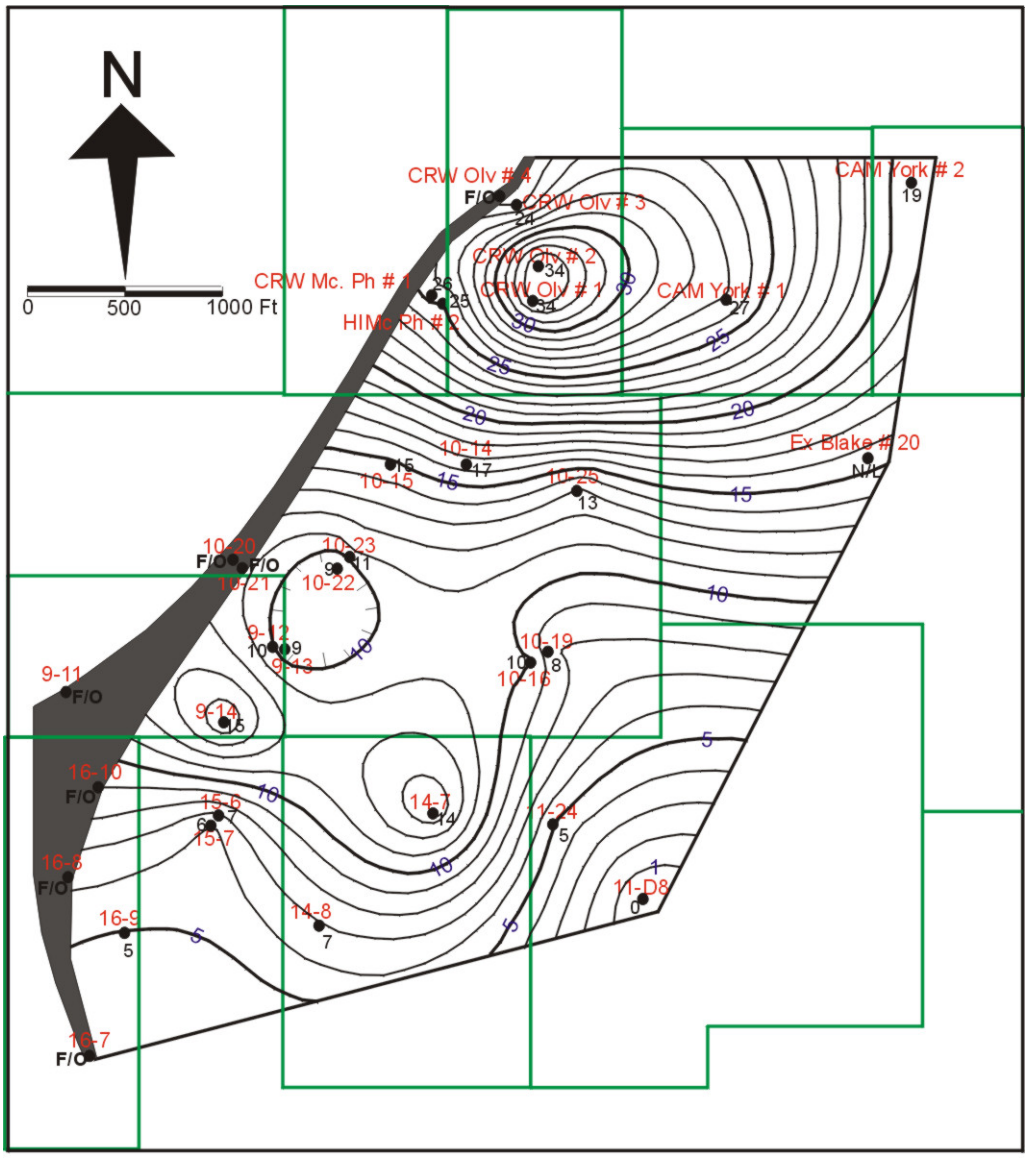

ISOPACH OF RESERVOIR UNIT 2 (in feet)

APPENDIX C

RESERVOIR RANK DISTRIBUTION (SELECTED SLICE MAPS)

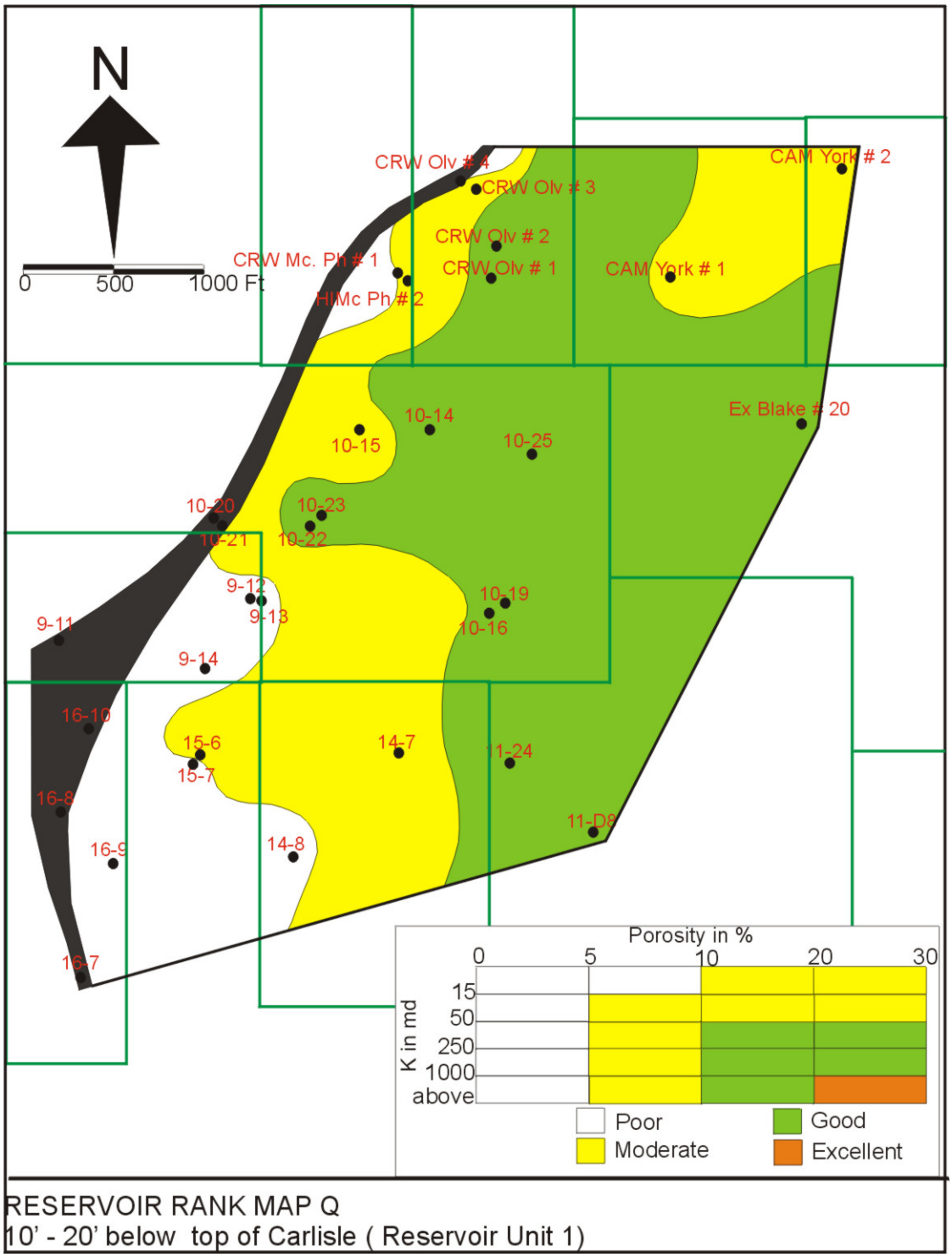

RESERVOIR RANK MAP Q
10' - 20' below top of Carlisle (Reservoir Unit 1)

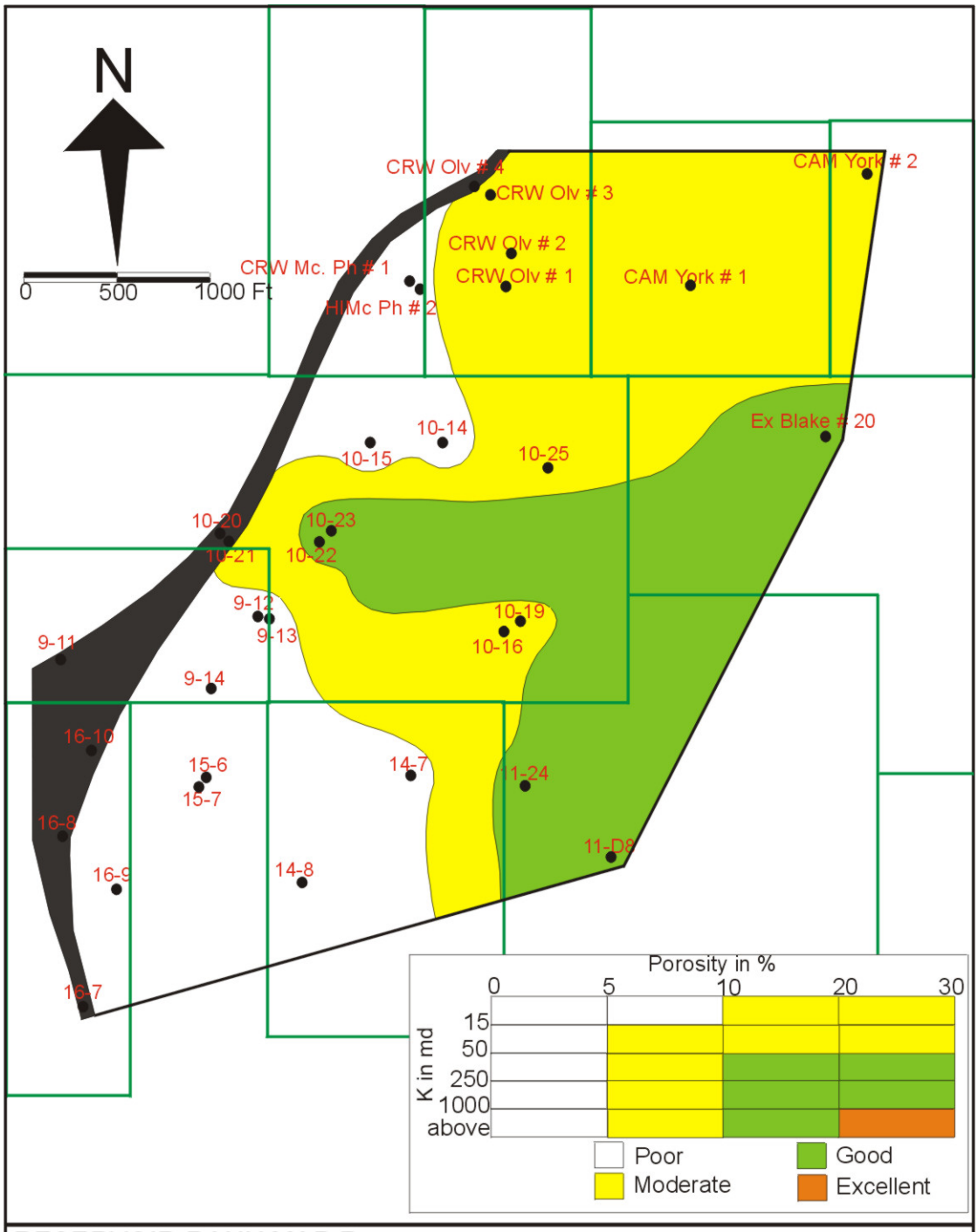

RESERVOIR RANK MAP R
20' - 30' below top of Carlisle (Reservoir Unit 1)

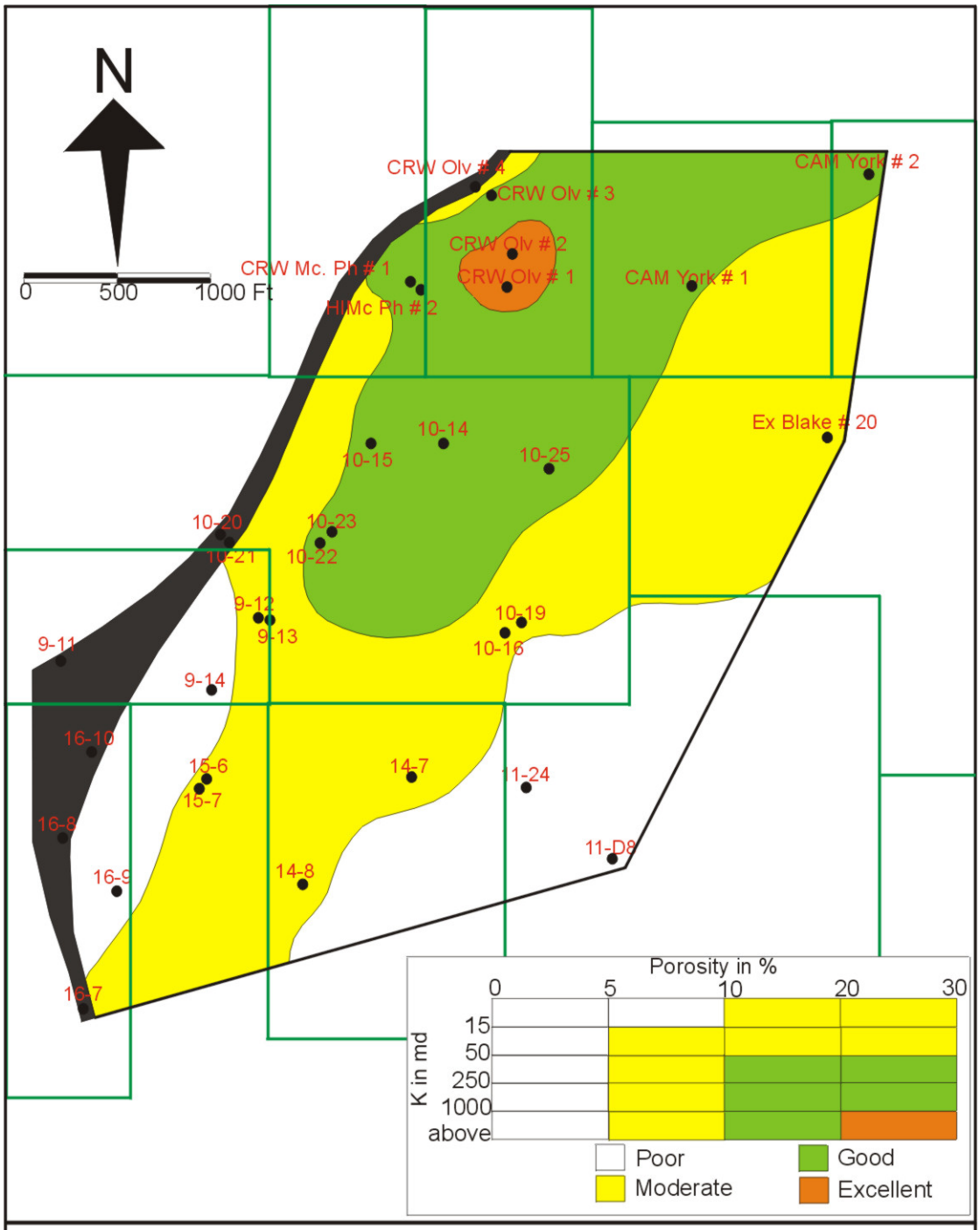

RESERVOIR RANK MAP T
40' - 50' below top of Carlisle (Reservoir Unit 2)

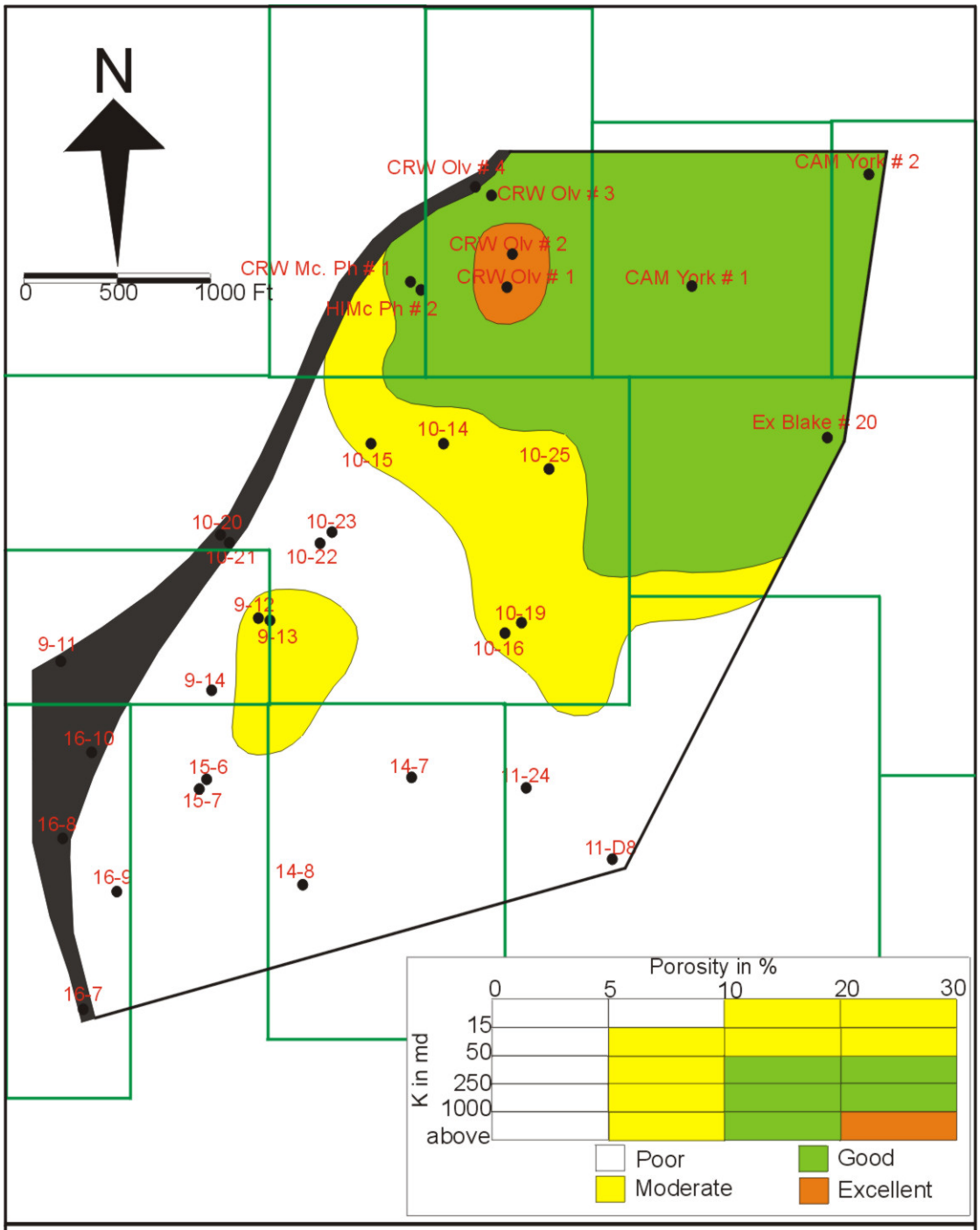

RESERVOIR RANK MAP U
50' - 60' below top of Carlisle (Reservoir Unit 2)

APPENDIX D

HYDROCARBON SATURATION DISTRIBUTION (SELECTED SLICE MAPS)

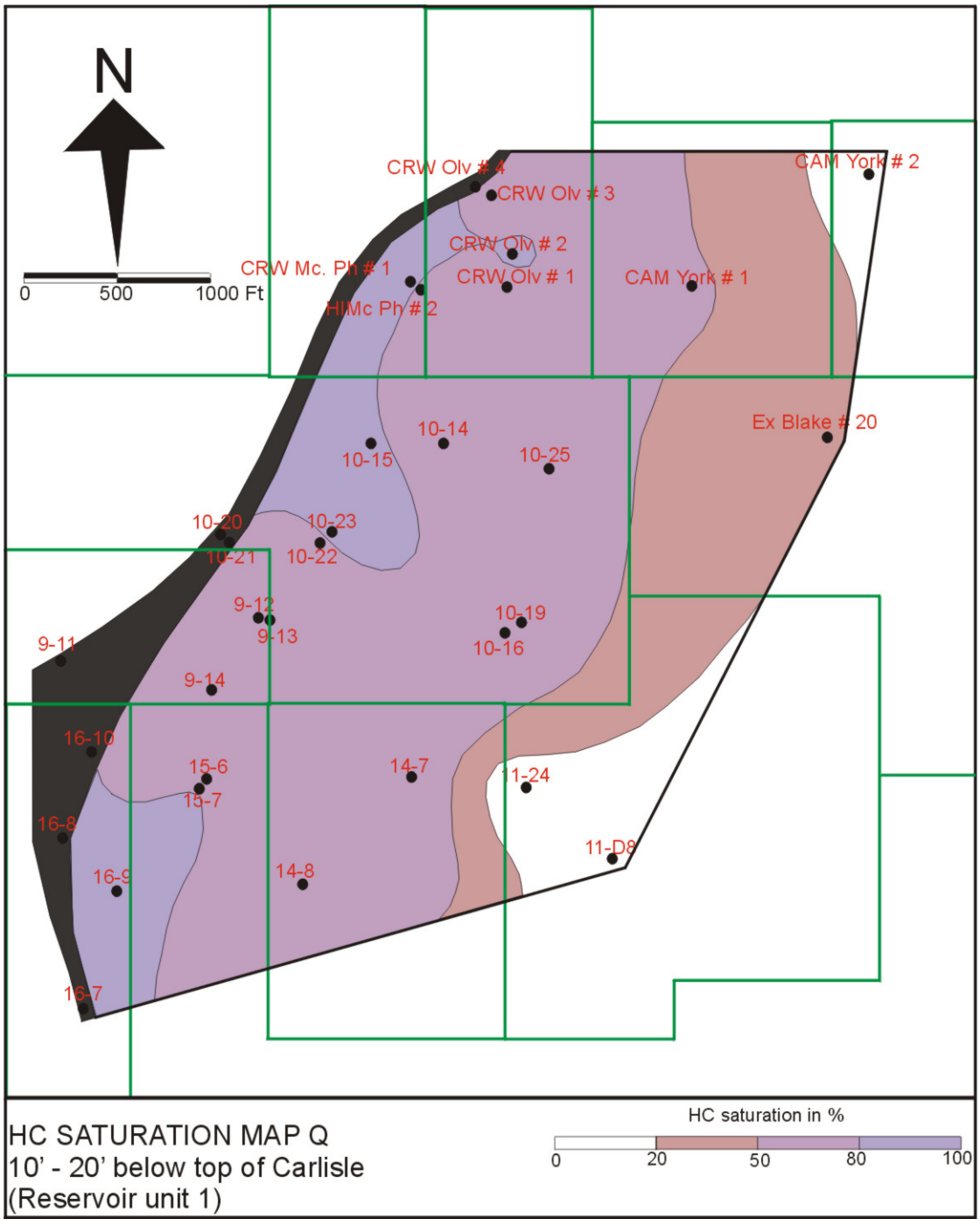
N
0
500
1000 Ft
CRW Olv # 4
CRW Olv # 3
CRW Olv # 2
CRW Olv # 1
CRW Mc. Ph # 1
HIMc Ph # 2
CAM York # 1
CAM York # 2
Ex Blake # 20
10-14
10-15
10-25
10-20
10-23
10-21
10-22
9-12
9-13
10-19
10-16
9-11
9-14
16-10
15-6
15-7
14-7
11-24
16-8
11-D8
16-9
14-8
16-7
HC SATURATION MAP Q
10' - 20' below top of Carlisle
(Reservoir unit 1)
HC saturation in %
0
20
50
80
100

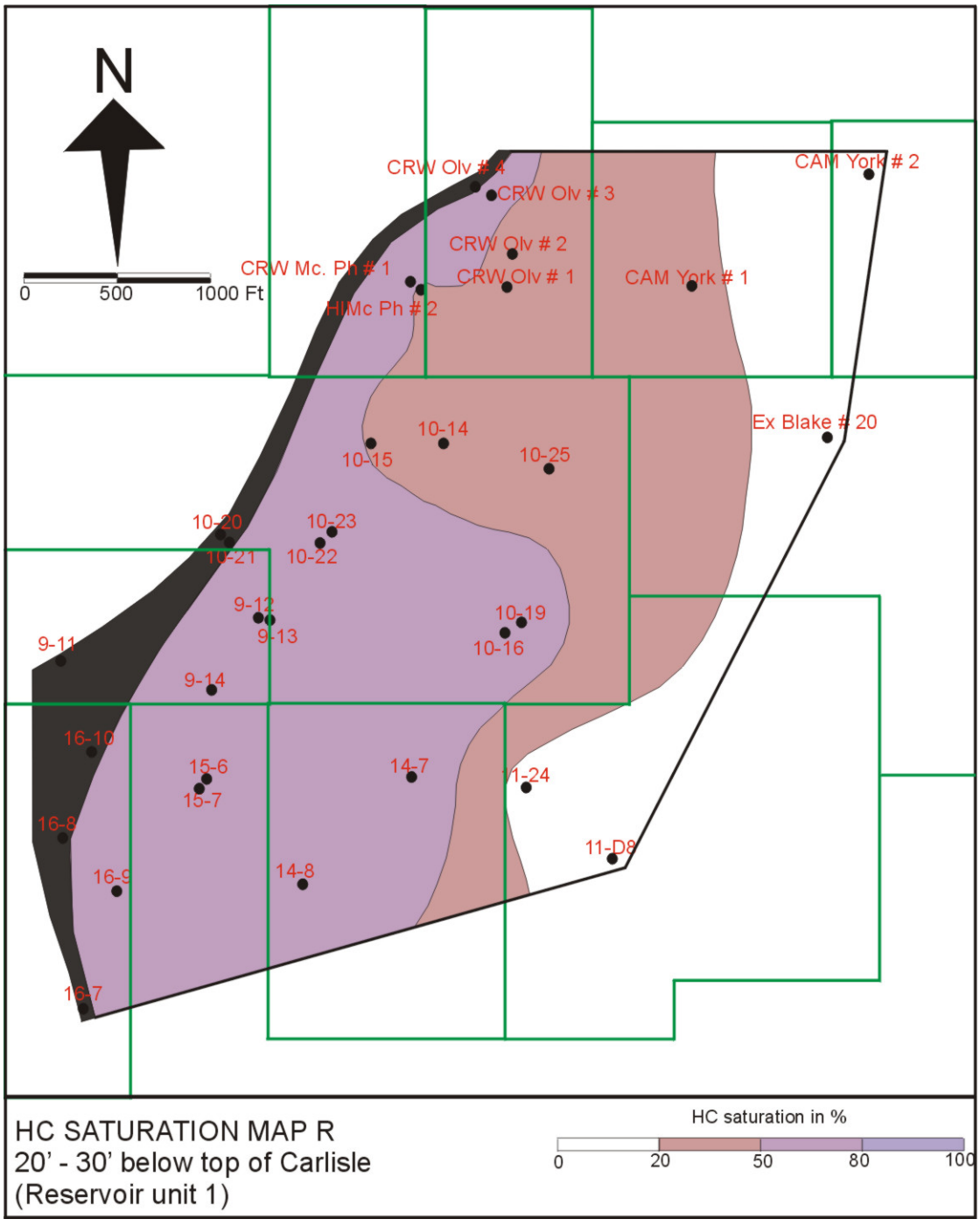
N
0
500
1000 Ft
CRW Olv # 4
CRW Olv # 3
CRW Olv # 2
CRW Olv # 1
CRW Mc. Ph # 1
HIMc Ph # 2
CAM York # 1
CAM York # 2
Ex Blake # 20
10-14
10-15
10-25
10-20
10-23
10-21
10-22
9-12
9-13
9-11
9-14
10-19
10-16
16-10
15-6
15-7
14-7
1-24
16-8
16-9
14-8
11-D8
16-7
HC SATURATION MAP R
20' - 30' below top of Carlisle
(Reservoir unit 1)
HC saturation in %
0
20
50
80
100

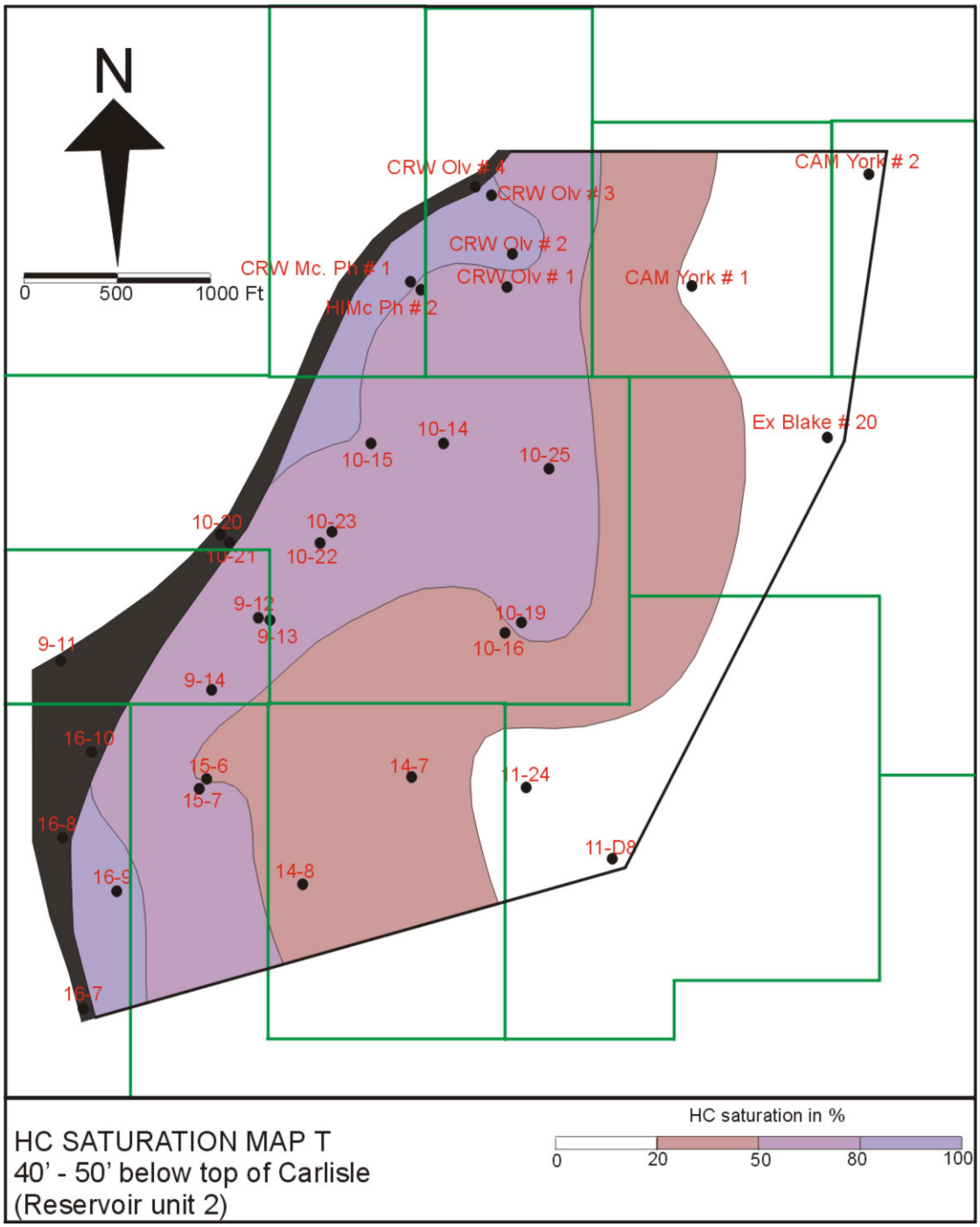
N
0
500
1000 Ft
CRW Olv # 4
CRW Olv # 3
CRW Olv # 2
CRW Olv # 1
CRW Mc. Ph # 1
HMc Ph # 2
CAM York # 2
CAM York # 1
Ex Blake # 20
10-14
10-15
10-25
10-20
10-23
10-21
10-22
9-12
9-13
10-19
10-16
9-11
9-14
16-10
15-6
15-7
14-7
11-24
16-8
11-D8
16-9
14-8
16-7
HC SATURATION MAP T
40' - 50' below top of Carlisle
(Reservoir unit 2)
HC saturation in %
0
20
50
80
100

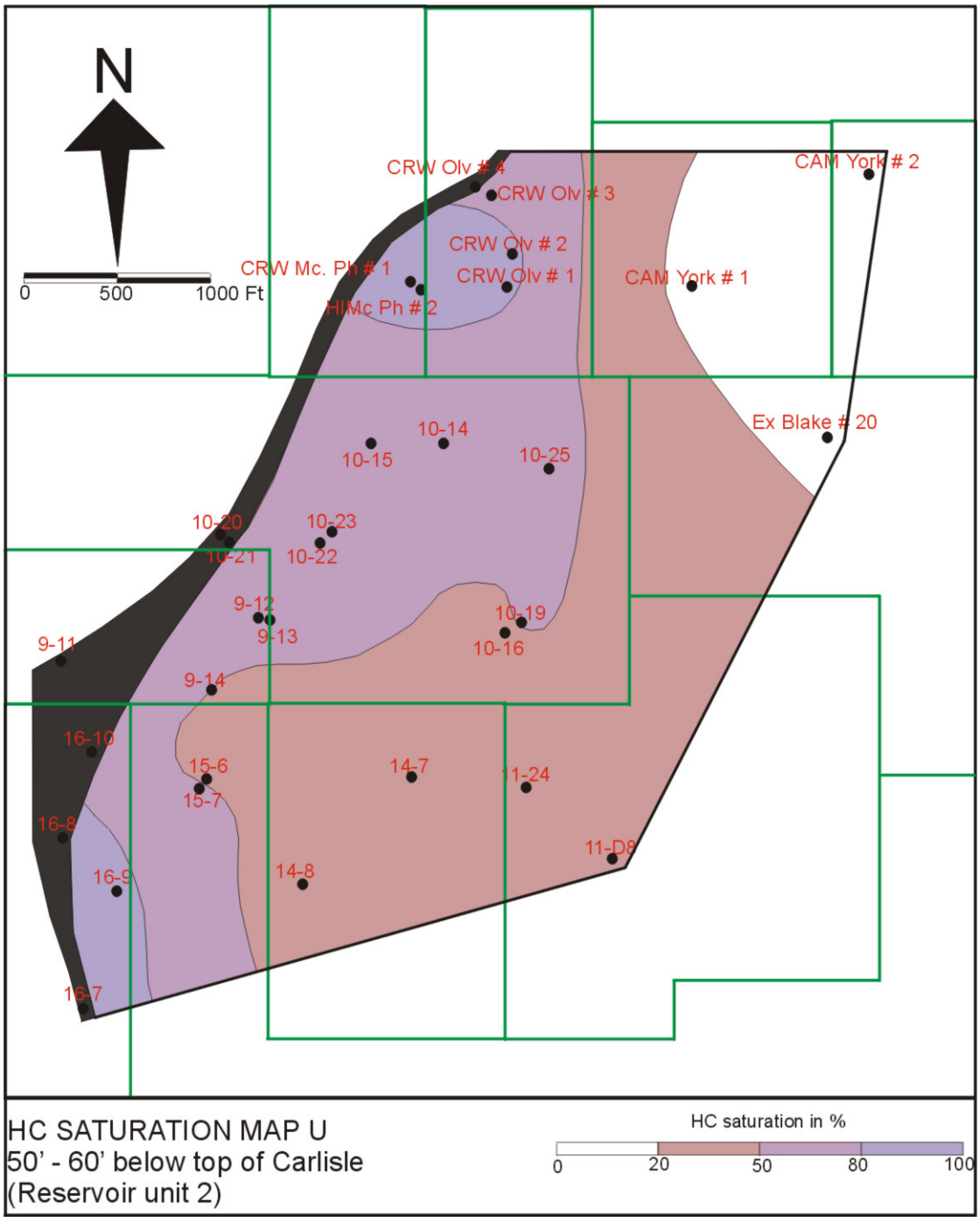
N
0
500
1000 Ft
CRW Olv # 4
CRW Olv # 3
CRW Olv # 2
CRW Olv # 1
CRW Mc. Ph # 1
HMc Ph # 2
CAM York # 2
CAM York # 1
Ex Blake # 20
10-14
10-15
10-25
10-20
10-23
10-21
10-22
9-12
9-13
10-19
10-16
9-11
9-14
16-10
15-6
15-7
14-7
1-24
16-8
11-D8
16-9
14-8
16-7
HC SATURATION MAP U
50' - 60' below top of Carlisle
(Reservoir unit 2)
HC saturation in %
0
20
50
80
100

VITA

NAME	Yanyan Triyana
EDUCATION	Padjadjaran University Bandung, Indonesia B.S., Geology, 1999 Texas A&M University College Station, Texas M.S., Geology, 2003
PROFESSIONAL EXPERIENCE	Junior geologist, Unocal 76, Sugar Land, Texas May – August, 2001
PROFESSIONAL MEMBERSHIP	American Association of Petroleum Geologist Society of Petroleum Engineer Society for Sedimentary Geology
BUSINESS ADDRESS	Unocal Indonesia Company Pasir Ridge, Balikpapan 76102, Indonesia P.O. Box 276
PERMANENT ADDRESS	Jl. Sambung Jaya no 64, Kawalu Tasikmalaya 46181 Jawa Barat, Indonesia